PROBABILISTIC SEISMIC HAZARD MAP OF INDIA

FINAL REPORT

TECHNICAL REPORT

INDIAN INSTITUTE OF TECHNOLOGY MADRAS

NATIONAL DISATER MANAGEMENT AUTHORITY

GOVT. OF INDIA, NEW DELHI

PREFACE

A Memorandum of understanding was signed by NDMA and Bureau of Indian Standards (BIS) and IIT Madras on April 2019 and the project titled "R &D on Probabilistic Seismic Hazard Map (PSHM)" of India was awarded to IIT Madras. NDMA provided the funds and project was monitored by both NDMA and committee members of the BIS including CED 39. The present document reports the technical results of the PSHA project carried out by the IIT Madras for NDMA. The basic frame work of PSHA is well documented in the literature. The methodology of PSHA has been developed as suggested by the maps subcommittee CED 39:4 The methodology adopted for the present study is given below:

- The database will consist of all known earthquakes of magnitude 4 and above recorded in and around India in the last 500 years.
- All magnitude values will be expressed in terms of moment magnitude Mw. The maximum magnitude to be considered will be 0.5 units above the recorded or estimated past value for the region.
- Recurrence parameters will be found by studying for completeness as per established statistical analysis as suggested by Kijko, Sellvol, Weichert and others.
- All faults identified by official agencies such as Geological Survey of India (GSI), India Meteorological Department (IMD), CSIR-National Geophysical Research Institute (NGRI) will be included in PSHA.
- The shear wave velocity profiles for B, C and D-type site condition available for India will be collected from GSI, NGRI, IMD and published journal articles.
- Ground motion equations for B-type rock will be developed using the strong motion data
- Multiple ground motion relations will be used in logic tree to include epistemic uncertainty
- The hazard will be computed by considering a circular region of 500 km around each sample point.
- PSHA result will be presented for different return periods as contours on a grid of $0.1^0 \times 0.1^0$.

The final results will be presented here refer to engineering bed rock conditions corresponding to B-type rock site (V30 = 760 m/s). Strong motion data required for the work has been collected from IITR, NCS and NGRI. Several individuals have contributed to the successful completion of the project. Notable among these are Dr. ID Gupta (Chairman CED 39:4), Dr. CVR Murty (Chairman CED 39) and Dr. D. Srinagesh (NGRI). They have extended directly all possible support for the technical and administrative work involved in bringing the PSHA mapping work to its final stage. Members of the CED 39:4 have been a source of strength for carrying out the PSHA work which in some parts involved expert judgment. The present document is the Final Report of IITM submitted to NDMA.

Prof. S T G Raghukanth
Principal Investigator
Dept. of Civil Engineering
IIT Madras, Chennai.

PROJECT TEAM

Prof. S T G RAGHUKANTH

SREEJAYA K P

Dr. DHANYA J

ABSTRACT

KEYWORDS: Probabilistic seismic hazard; Recurrence; GMPE; India

Success of earthquake disaster mitigation strategy depends on how well the stakeholders are sensitized to the necessity of reducing the vulnerability of built up structures. Past experience in seismic hazard management has highlighted the importance of having a well planned vulnerability reduction program built into the larger policy framework of sustainable development. The vulnerability of Indian habitat was dramatically demonstrated by the Kutch earthquake of 26th January 2001, which did not belong to the more frequent Himalayan sources. The looming seismic risk to our cities can be perceived in the backdrop of active faults in the Himalayas, North-Eastern India and in the Indo-Gangetic plain. Even in the less active peninsular region infrequent earthquakes can cause considerable damage. The principal cause for loss of life and damage is due to collapse of built infrastructure and resultant discontinuity in economic and social activity. While the financial loss in absolute terms is a function of the state of development, initial investment and cost of living indices, seismic vulnerability is closely dependent on the social and economic condition of the population. Prognosis of seismic hazard plays key role in planning and protecting buildings, life lines, industries and other safety sensitive structures. This necessitates estimation and quantification of future ground vibration. This motion lasting a few seconds is due to the sudden release of energy stored for centuries at the fault level influenced by the path and local soil conditions.

The present report highlights how surface level hazard at rock sites (B-type) can be estimated to develop charts and tables that can be used by government agencies, architects, engineers and other interested groups. All known data about past earthquakes and mapped faults are considered to characterize the seismic activity of the thirty-three source zones of the country. State-of-art probabilistic hazard analysis is carried out covering the whole country on a grid size of 0.1° x 0.1°. New attenuation equations are derived for the regions incorporating known recorded information or correction factors, suitably incorporated in a hybrid framework. Well

established probabilistic analysis procedure is adopted to compute the prevalent hazard in terms of peak acceleration (PA), short period (0.2 s) and long period (1 s) spectral accelerations for different return periods.

A brief introduction highlighting the concept of return period along with a brief review of past PSHA efforts for estimating seismic hazard in India is presented in **Chapter 1**. The tectonic setting of the country, the fault map, catalogue preparation (till 2019 for Mw$\geq$3), completeness and recurrence characteristics (fault based and spatial smoothening based) are discussed in **Chapter 2**. In **Chapter 3**, a hybrid attenuation relation is proposed for active regions in India combining the limited instrumental data with a more comprehensive database. Furthermore, correction factors for the existing GMPEs for become applicable for stable continental region is also derived based on regional seismological model parameters. Additionally, a discussion on Indian and global GMPEs which can find its suitable application for the region of interest is also discussed in the chapter. The estimated region specific parameters are suitably incorporated in standard Probabilistic Seismic Hazard Analysis (PSHA) procedures and all India Hazard maps are prepared and presented in **Chapter 4**. The results presented can be directly used on B-type rock sites. For other site classes, corrections have to be applied in terms of approximation prescribed in standard codes or by carrying out local geotechnical studies. The results presented in the report can be used further in city level microzonation, vulnerability analysis and risk evaluation. Table presents the existing hazard in major cities for varying return periods. The results are not direct indications for safety of the habitat, rather the corresponding assessment can be made by combining the result with the vulnerability of the built up infrastructure. Numerical results presented here are subject to minor variations as and when new earthquake and fault data get accumulated.

TABLE OF CONTENTS

LIST OF TABLES

LIST OF FIGURES

ABBREVIATIONS

ARS	Acceleration Response Spectra
ANN	Artificial Neural Network
CC	Correlation Coefficient
CI	Central India
CIGN	Central Indo-Gangetic Network
CESMD	Center for Engineering Strong Motion Data
COSMOS	Consortium of Organizations for Strong Motion Observation Systems
CMT	Centroid Moment Tensor
DSHA	Deterministic Seismic Hazard Analysis
DBE	Design Basis Earthquake
EW	East-West
EDR	Euclidean Distance based Ranking
FAS	Fourier Amplitude Spectra
GPS	Global Positioning System
GSI	Geological Society of India
GMPE	Ground Motion Prediction Equation
GMMs	Ground Motion Models
GNSS	Global Navigation Satellite System
GRD	Ground Residual Displacement
G-R	Gutenberg Richter
GSN	Global Seismic Network
HC	Hazard Curve
IBC	International Building Code
IGP	Indo-Gangetic Plain
IMD	Indian Meteorological Department
IGCAR	Indira Gandhi Centre for Atomic Research
ISC	International Seismological Centre
KW	Koyna-Warna
LH	Likelihood
LLH	Log Likelihood
MBT	Main Boundary Thrust
MCT	Main Central Thrust
MCE	Maximum Credible Earthquake
MDF	Mahendragarh Dehradun Fault
MDE	Modified Euclidean Distance
MFT	Main Frontal Thrust
MKT	Main Karakoram Thrust
MMT	Main Mantle Thrust

MSE	Mean Squared Error
NDMA	National Disaster Management Authority
NEI	North Eastern India
NGA	Next Generation Attenuation
NS	North-South
PEER	Pacific Earthquake Engineering Research Center
PESMOS	Program for Excellence in Strong Motion Studies
PA	Peak Acceleration
PGV	Peak Ground Velocity
PGD	Peak Ground Displacement
PI	Peninsular India
PMD	Pakistan Meteorological Department
PGRD	Peak Ground Residual Displacement
PSHA	Probabilistic Seismic Hazard Analysis
RP	Return Period
Sa	Spectral Acceleration
S.A	Site Amplification
SPECFEM	Spectral Finite Element Method
SZ	Seismogenic Zones
UHRS	Uniform Hazard Response Spectrum
USGS	U.S. Geological Survey
WH	Western Himalayas

NOTATION

General

$E(.)$	Expectation operator
$P(.)$	Probability
$\forall$	For all
$\in$	Is member of
$\sum$	Addition operator
$\overline{(.)}$	Average
ln	Natural logarithm
log_{10}	Logarithm to the base 10

Report Specific

R	Distance
z	Z-score
A	Area of rupture
M_w	Moment magnitude of earthquake
M_b	Body-Wave Magnitude
M_s	Surface Wave Magnitude
M_L	Local Magnitude
M_0	Seismic moment
μ	Shear modulus
$\phi\ \delta\ \lambda$	Strike, Dip and Rake
ρ	Density
λ and μ	Lame's Constants
w	Arbitrary vector
V_{s30}	Shear wave velocity upto 30m
μ_{y^*}	mean annual rate of exceedance
K	number of probable sources
ν	Value corresponding to bin
μ	Mean
σ	Standard deviation
ϵ	Error or residue
V_s	S-wave velocity
V_p	P-wave velocity
ρ	Density
Q	Quality factor
t_r	Rise time

R_{jb}	Joyner-Boore Distance
R_{rup}	Closest distance to fault
R_{epi}	Epicentral Distance
R_{hyp}	Hypocentral Distance
F_{mech}	Fault Mechanism
F_{loc}	Regional Flag
a and b	Guttenberg-Richter parameter
$\lambda(m)$	Recurrence parameter
ν	Poisson's Ratio
W and $biases$	Weights and biases in network
η_i and ε_{ij}	Inter and Intra event residue
τ and σ	Inter and Intra event standard deviations
f_1 and f_2	Transfer Function

CHAPTER 1

Literature review

1.1 Introduction

India faces threats from a variety of natural hazards such as floods, droughts, landslips, cyclones, earthquakes and tsunamis. The spate of earthquakes in the recent past, causing extensive damage has heightened the sensitivity of administrators, engineers and the general public to the looming hazard due to future earthquakes occurring near densely populated Indian cities. Strong earthquakes are rare events, rarer than cyclones, windstorms and tidal waves. Nevertheless, India has seen quite a few earthquakes in the recent past. Earthquakes have occurred from pre-historic times, more or less in the same regions, where they are presently felt. The present heightened awareness towards earthquake disaster mitigation in the country is attributable to a large loss of life and property suffered during the Khillari (30th September 1993), Jabalpur (22nd May 1997), Chamoli (29th March 1999), Bhuj (26th January 2001) and Nepal (25th April 2015) earthquakes. The seismic hazard or the potential of a site to experience ground motion due to an earthquake cannot be altered. The risk faced by human habitat due to earthquakes can be reduced by making man-made systems and structures less vulnerable and more robust to withstand the ground motion. Seismic risk has a character to increase with time if continuous mitigating actions are not taken. This fact may be appreciated by recognizing that increasing population puts greater demands on the housing, energy, water and transport needs of the society. In turn, these needs have to be met by increased construction activity of buildings, dams, reservoirs, bridges, power plants etc. Thus, even in areas of low seismic activity, the loss due to unexpected earthquakes may be high purely due to heavy infrastructure development, unless the built-up structures are engineered and maintained to withstand future earthquakes.

As we take up the question of safety of man-made constructions, subtle issues crop up. It is not just new constructions that have to be made earthquake resistant. Engineers are called upon to protect existing cities, monuments and other structures built at a time when knowledge about

earthquakes was limited. Moreover, all types of construction may not be equally important, particularly so, when available financial resources are limited. In addition, earthquakes are low probability events with extremely high risks to society. Damaging earthquakes are rare with their recurrence periods being of the order of several decades or centuries. But once they occur, much of the structural damage takes place within a few seconds, directly attributable to ground vibration. Hence engineers usually characterize seismic hazard in terms of the ground motion that can be experienced at the construction site. This way the dynamic response of structures can be studied to foresee where they may fail and for what level of seismic forces. This in turn helps in site selection, design and retrofitting strategies. The point to be noted here is that the quantification of hazard is needed for unpredictable future events. The nature and amplitude of ground motion at a site can be described in a probabilistic sense by combining past information with engineering methods of risk estimation.

1.1.1 Return Period

The most sought-after ground motion descriptor is the response spectrum, which engineers use to find the most probable extra force, due to all possible future earthquakes, that a structure has to withstand in its expected life period. The life expectancy of a structure depends on socio-economic factors and hence engineering designs are not meant to assure 100% safety against every type of earthquake, for all times to come. A residential building may be expected to remain robust for a period of 50-100 years, where as a monumental structure may be envisioned to perform for 1000 years or more. Some amount of subjectivity is unavoidable here, but a consensus can be arrived at by public debate moderated by specialist opinion. Thus, one may like to know with high level of confidence what could be the foreseen peak acceleration (PA) and design response spectrum (Sa) in an interval of say 50, 100, or 1000 years. The level of confidence itself can be stated as a probability or percentage. At present, the popular way of describing hazard for building design is to specify that value of Sa that will be exceeded with only a 2% chance in 50 years (IBC, 2015). This is closely linked with the concept of return period T_r, which is the average time between consecutive occurrences of the same event in a time series. The event we are interested in here is the ground motion exceeding a value y^* at the chosen site, due to rupture of any fault in a wide region around the site. A given event of

return period Tr is equally likely to occur in any year during the design life of N_d years. Hence, the annual probability of exceedance of y^* is $p = 1/T_r$. For large T_r and N_d, it can be shown that

$$P[PA\ or\ Sa > y^*\ in\ N_d\ years] = N_d/T_r \tag{1.1}$$

If N_d = 50 years, it follows T_r is nearly 2500 years. In other words the hazard to a design period of 50 years with the confidence of 98% has to correspond to a return period of ≈2500 years. If we are willing to reduce the confidence level to 90%, the probability of annual exceedance will be set at 0.1. This would mean we are designing for seismic hazard corresponding to 500 year return period. This is not same as postulating an earthquake that occurs once in 500 years or once in 2500 years. Actually, all possible magnitudes and hypo-central distances are to be rationally combined to estimate the future ground motion to be experienced by the building during its projected life of 50 years. For safety-sensitive installations such as large dams and nuclear power plants one may need still longer 5000- and 10,000-year return period ground motion values. With the above points in view, the present study aims at mapping the existing seismic hazard in terms of PA and response spectrum corresponding to 5% damping for several return periods. Considering the sub-continental scales involved and the spatial variations to be addressed the Indian land mass is discretized into grids of $0.1^\circ \times 0.1^\circ$ size. Each corner of such a grid is treated as a site for computing the hazard.

1.2 Source, Path, Site

The standard paradigm in hazard studies is the source, path, site triplet. The causative seismic sources are first identified. Here, these are taken as known mapped faults in source zones that can be associated with past earthquake activity. The quantification of the seismic potential of the sources is carried out by assembling a catalogue of past events of M w $\geq$ 3 in the respective seismogenic zones. The catalogue is statistically analyzed to characterize the identified zones in terms of the Gutenberg-Richter (G-R) recurrence relation and the maximum expected earthquake magnitude (M_{max}). The attributes of the zone are further apportioned to the line sources within the zone depending on their capacity for rupture and historical activity. A given site

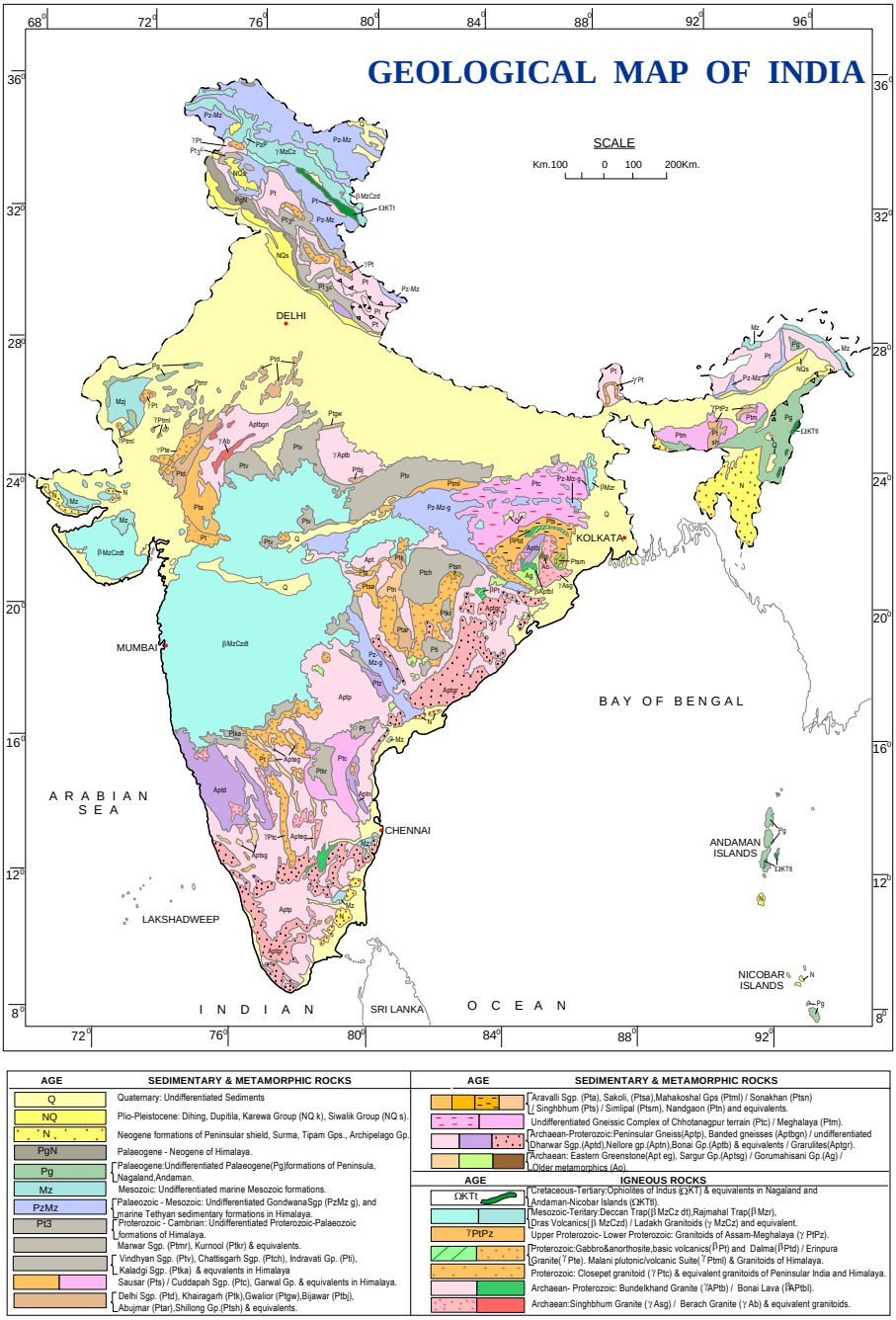

Figure 1.1: Geological provinces in India (GSI, 2000)

responds to all possible future events emanating from any of the fault in the range of influence of 300 km radius. Here the hypocentral distance and the path properties control the attenuation of ground motion depending on the quality factor of the intervening rock medium. The site is ideally a point on the surface after removing the top 1-2 m of debris or deposits. The position

of the site can be geometrically fixed up with respect to every fault rupture. The subsurface geological and geotechnical condition at the site can be described in terms of the depth wise variation of material density and shear wave velocity. The prominent geological map of India is illustrated in Figure 1.1. Since geotechnical properties of the subsurface soil can vary drastically over short distances the national level hazard map has to be for a common type of site. The effect of local soil layers can be accounted by investigations specific to a given site. Here the reference site condition is taken as the B-type rock site which has its average shear wave velocity in the top thirty meters to be approximately 760 m/s.

1.3 Uncertainties

Computation of seismic hazard is beset with unknowns and uncertainties. Two broad categories of uncertainties can be recognized. First is the epistemic or model related uncertainty. With the present knowledge of the subject we are committing ourselves to certain models which may in future get changed with better scientific knowledge. One can get a range for this uncertainty if we can use alternate models for source description and methods of statistical analysis. It is known that with more data, variance in the error estimates of the parameters can be reduced. The second type called aleatory uncertainty is inherent to the natural process under observation. This can not be reduced with more data or knowledge. For example, magnitude values of earthquakes with their sources and fault rupture lengths that will affect a particular site will remain uncertain. Probabilistic seismic hazard analysis (PSHA) can address both the types of uncertainties by adopting different source models and attenuation relations following the logic tree approach. Hence in present work different hazard estimation techniques and the suitable global GMPEs are appropriately implemented in a probabilistic hazard framework. Further, the final hazard values are derived based on judgments and weights estimated from instrumental data or regional characteristics.

1.4 Ground Motion Prediction Equations

The ground motion prediction for regions lacking dense set of database can be performed based on a mechanistic model or using empirical methods like attenuation relations, stochastic models, etc. However, mechanistic approaches are often computationally expensive, for performing analysis corresponding to a suit of events essential in reliable quantification of hazards. Hence, for performing hazard analysis, a more simple empirical Ground motion prediction equations (GMPE) form an essential component. Over the years there are numerous GMPEs developed across the world for both global and regional basis (Douglas, 2016). For the regions with sufficient ground motion records, these recorded data itself can be used to develop GMPEs. In the absence of such recorded data, GMPEs could be built based on the synthetic databases generated using different empirical, numerical, analytical or hybrid techniques. A typical GMPE is a relation connecting the ground motion parameter (Y) with the variables relating to source, medium, site etc. such that

$$log(Y) = f(M_w, R, V_{s30}, F, z, ...) + \epsilon \tag{1.2}$$

where, M_w is the seismic moment, R is the source to site distance,V_{s30} is the shear wave velocity, F represents various flags associated with region, site, mechanism, etc., z represents depth and ϵ is the residue between prediction and data from the modeling. In general, GMPEs can be broadly divided into parametric models and non-parametric models. The parametric models are formulated based on a fixed functional form derived based on the observed ground motion characteristics. One of the preliminary GMPEs is derived by Esteva and Rosenblueth (1964) using a very simple exponential functional form to predict peak acceleration (PA). Later,McGuire (1974) developed a model for spectral acceleration, but the application of the model is restricted to the near-field. For regions with sparse recorded data, Herrmann and Goertz (1981), De Natale *et al.* (1988), Atkinson (2001) etc. used synthetic data generated from empirical and stochastic methods to develop prediction equations. In subsequent years, the functional forms of GMPEs underwent numerous modifications to incorporate the amplification, attenuation, mechanism of faulting, damping, and uncertainties exhibited by the ground motions. These modifications lead to very complex functional forms. Some of the latest GMPEs are

that of Ancheta *et al.* (2014), Boore *et al.* (2014), Campbell and Bozorgnia (2014) and Chiou and Youngs (2014) developed based on updated NGA west2 database, Zhao *et al.* (2016) using Knet-Kik-net database etc. One of the major setbacks of such kinds of parametric models is that it requires a predefined functional form. The capability of the formulated functional form to accurately predict the ground motion characteristics is also a matter of concern. In such situations, one can resort to non-parametric analysis, where the model is mostly data-driven without any predefined closed-form equation. Schnabel and Bolton Seed (1973) proposed the first GMPE based on the non-parametric method for PA at rock type sites in the western United States. Further, Anderson (1997) using the data from the Guerrero network developed a non-parametric interpolation function to predict PA. Recently, advanced non-parametric models such as machine learning algorithms, Artificial Neural networks (ANN), fuzzy logic, etc. found their application in earthquake engineering. In that direction, Ahmad *et al.* (2008) used ANN to develop attenuation relation for PA, peak ground velocity (PGV), and peak ground displacement (PGD) for Europe using 358 ground motion records. Güllü and Erçelebi (2007), Günaydın and Günaydın (2008), etc. predicted PA, using neural network algorithms on selected strong motion data of the earthquakes in Turkey. Recently, Alavi and Gandomi (2011) and Thomas *et al.* (2016) proposed hybrid simulated annealing-ANN technique and randomized adaptive neuro-fuzzy interface system respectively to predict PA, PGV, and PGD using 2815 data records in NGA west database. The main limitation of non-parametric models based on fuzzy logic and machine learning algorithms is in understanding the physical interpretation of the functional form. Further, the applicability of the non-parametric method beyond the range of data points used to develop the model is restricted. Nevertheless, it can be noticed that though it is difficult to interpret the model, the non-parametric model can capture the complex earthquake characteristics intuitively. Hence the possible applications of the method in ground motion prediction should be explored more extensively. It is known that the spectral characteristics of the ground motion are essential for the design of structures at the site. Tezcan and Cheng (2012) attempted to predict response spectra for 13 periods between T = 0s and 4s with 1482 data records from the NGA database, using support vector regressions (SVR). But, the SVR method uses just the combination of vectors with weights whose size is not pre-determinable. Further, the SVR algorithm has no physical meaning and can even become computationally expensive for large datasets. On the other hand, in the case of ANN, the model architecture

can be fixed, and an estimate on the number of unknowns could be attained beforehand. Derras *et al.* (2014) has attempted to formulate a ground motion model using ANN for Europe, using 1088 records from 320 earthquakes in the reference database for Seismic ground-motion prediction in Europe (RESORCE) database. Later, Derras *et al.* (2016) used the same technique on 16446 recordings from 318 earthquakes in the NGA West2 database to model the variability with respect to site conditions. These are some of the global GMPEs. Indian context various researchers have attempted to develop region specific GMPEs. Most of the GMPEs developed for India are based on parametric modelling. Some of the recent studies are from Singh *et al.* (2017) developed GMPW S_a in Indo Gangetic Basin, Gupta and Trifunac (2018a,b) developed GMPE for Fourier amplitude spectra and Pseudo spectral Velocity for Himalayas and North Eastern India, Bajaj and Anbazhagan (2019) developed GMPE for S_a at A type soil class based on calibrated seismological model.

1.5 Ground Motion Databases

The ground motion at a site is characterized best from the recorded data. These are several networks installed across the globe, data from which is routinely used for various studied which include source identification and modelling, quantifying medium characteristics, understanding the geological structure of a region, ground motion prediction models etc.

Some of the global ground motion databases include PEER-NGA for shallow crustal regions, IRIS broad-band database, COSMOS and CESMD centers of earthquake strong motion database, K-Net-KiK-net network of Japan, European Strong-Motion (ESM) database, etc. Among these, one of the most widely used database for ground motion prediction is that from PEER-NGA. The database constitute of two parts: NGA-West2 which includes a very large set of ground motions recorded in worldwide shallow crustal earthquakes in active tectonic regimes and NGA-East for the Central and Eastern North-American (CENA) region. The NGA-West2 database constitutes of 21540 records from 599 earthquakes in the magnitude range 3-7.9 occurred from 1935 to 2011.

In India, seismograph networks include PESMOS, IGCAR broadband stations and CIGN network. The PESMOS database is a nationwide network for strong motion records in In-

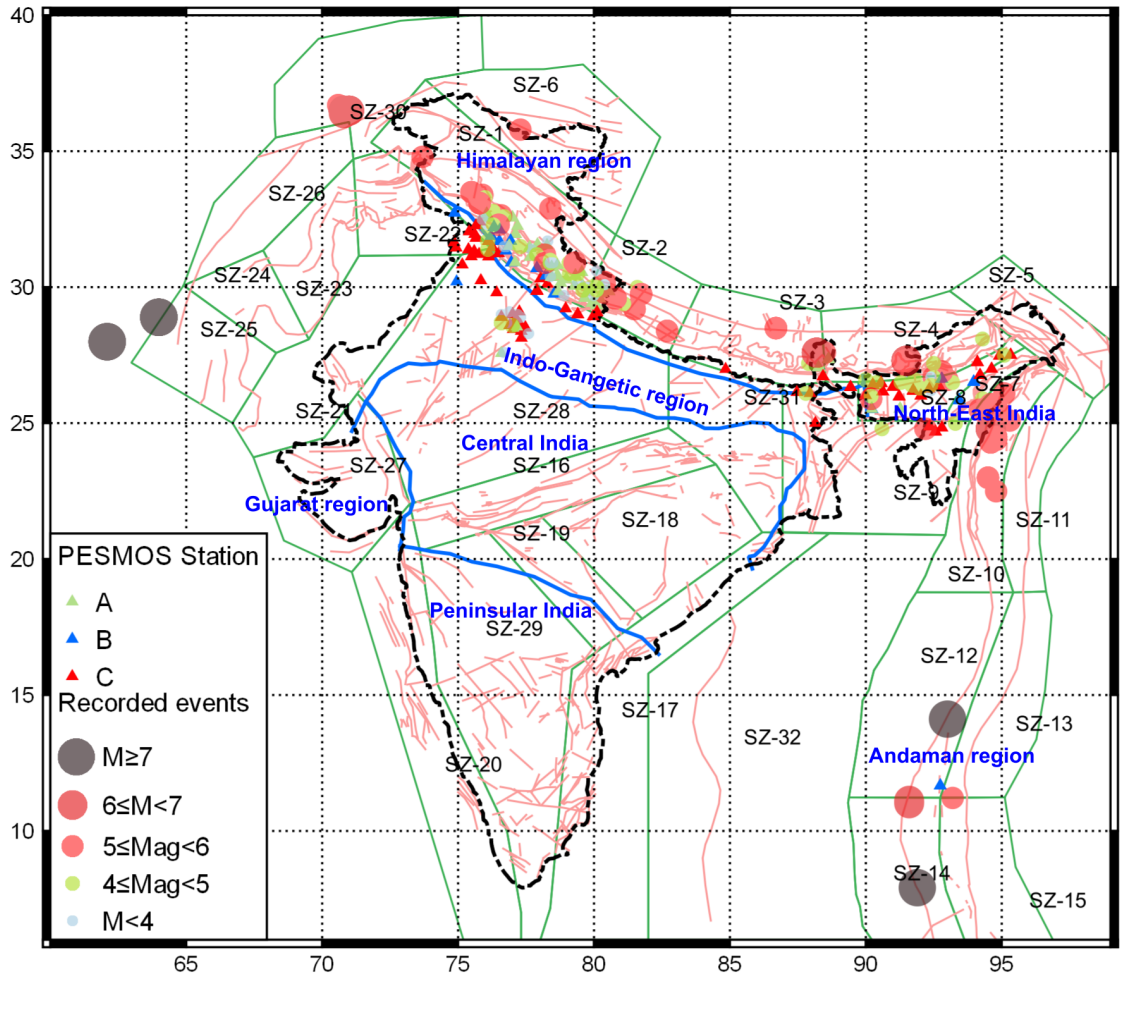

Figure 1.2: Distribution of epicenters of earthquakes and recording stations in PESMOS network. Along witht the fault map of India as per Geological Survey of India (GSI) (2000) and major geological regions in India

dia, which is maintained and operated by Indian Institute of Technology, Roorkey (IITR).The database contains information from 294 strong motion accelerographs have been installed Himalayas, Northeast India and Indo-gangetic region. Figure 1.2 shows the distribution of epicentres of earthquakes along with the recording stations in the network. A total of 267 groundmotion records from 65 earthquakes, over a magnitude range of 4 to 7 from for Western Himalayan region and 277 records from 65 earthquakes over a magnitude range of for North East India from 1986 to 2015 are available from the network. The hypocentral depth of the available records ranges between 2km to 484km for Western Himalaya(WH) and 20km to 484km for North East India(NE). In October 2012, Central Indo-Gangetic Plain Network (CIGN) with 26

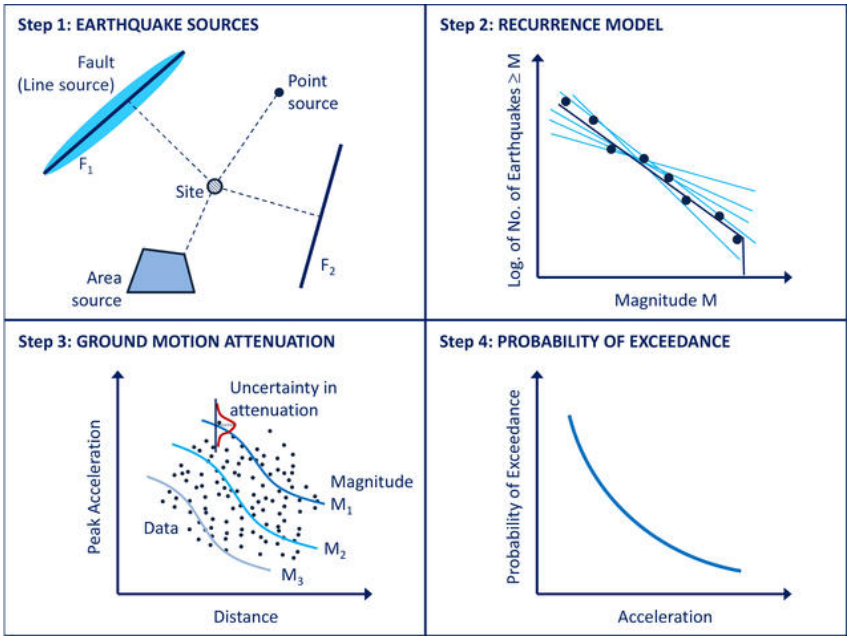

Figure 1.3: Probablistic Seismic Hazard Analysis (PSHA) framework (Kramer, 1996)

recoding stations got commissioned across Indo-Gangetic basin region. Two major records in the network are those for 2014 M_w 6.1 Bay of Bengal earthquake and 2015 M_w7.86 Nepal earthquake. The data from these networks are very useful in understanding regional characteristics and in the validation of the models developed for the region.

1.6 Probabilistic seismic hazard analysis

Probabilistic seismic hazard analysis is important for the seismically safe design of structures. The design spectra proposed in several design codes are often based on such seismic hazard analysis. The first seismic hazard map for a region is that developed by Esteva (1963). Later, Cornell (1968) established the fundamental concepts of probabilistic quantification of seismic risk. Kiureghian and Ang (1977) improved Cornell's assumption of point-source mechanism to consider finite sources. Furthermore, the concept of hazard deaggregation to find the critical source and magnitude for a site is proposed by McGuire (1974). A Typical framework for performing PSHA is shown in Figure 1.3. Accordingly, the first step toward quantifying the hazard level at a site is to identify all the potential sources in the region. Then identify the uncertainties associated with the seismicity levels and ground motion prediction. A proper

assessment of the uncertainties involved in the region is essential in hazard estimation. The two broad classes of uncertainty are aleatory uncertainty associated with the data models used for estimation and epistemic uncertainty arising due to the lack of knowledge. The widely adopted classical Cornell-McGuire probabilistic seismic hazard analysis (PSHA) procedure is briefly discussed further.

Probabilistic seismic hazard analysis estimates the probability of exceedance of the ground motion parameter at a site due to all possible future earthquakes as visualized by the previous hazard scenario. Assuming that the number of earthquakes occurring on a fault follows a stationary Poisson process, the probability that the control variable Y exceeds level y^*, in a time window of T years, is given by

$$P(Y > y^* \; in \; T \; years) = 1 - e^{-\mu_{y^*} T} \tag{1.3}$$

Here, μ_{y^*} indicates the mean annual rate of exceedance of the ground motion measure y^* (reciprocal of μ_{y^*} denotes return period RP) at a site due to all probable earthquakes caused by all probable sources. If there were 'K' number of probable sources in the region whose seismicity is known, then μ_{y^*} in Equation 1.3can be computed as

$$\mu(y) = \sum_{i=1}^{N_s} N_i(m_0) \int_{m_0}^{m_u} \int_{r_0}^{r_u} P\left[Y > y|m, r\right] P_{R|M}(r|m) P_M(m) \; \partial r \; \partial m \tag{1.4}$$

where m_0 and m_u indicate the minimum and the maximum threshold magnitude observed at the source; r_0 and r_u are the minimum and maximum site distances from the source. $P_M(m)$ is the probability density function of the exponentially distributed magnitude which can be obtained through the G-R relationship. $p_{R|M}(r|m)$ is the conditional probability density function of hypocentral distance which can be obtained numerically for the identified probable sources. $P[Y > y|m, r]$ denotes the conditional probability that the chosen ground motion intensity level is exceeded for a given magnitude and distance which can be determined using the ground motion relationship. The corresponding value is obtained as a lognormal random variable with the mean value given by the ground-motion prediction equation (GMPE) and the standard deviation given by the error term '$ln(\varepsilon)$'. Though the methodology is straightforward, implementation of the same is challenging in many regions due to the lack of knowledge on the source, seismicity,

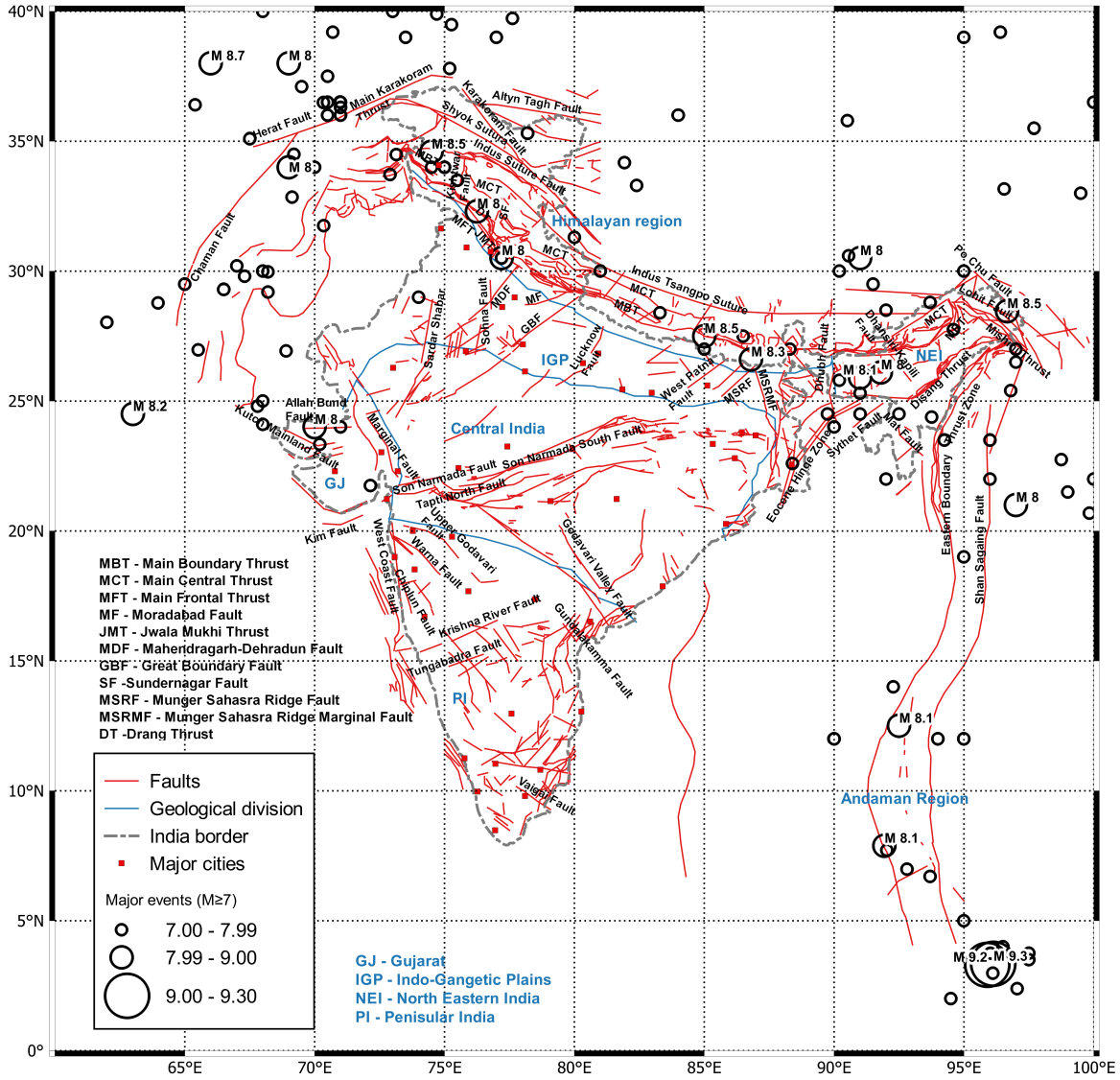

Figure 1.4: Tectonic fault map of India GSI (2000)

and medium characteristics. The seismotectonic atlas of India GSI (2000) has compiled the major linear-faults in India. The corresponding tectonic fault map is shown in Figure 1.4. The recurrence characteristics of each of these faults can be estimated provided all the earthquakes associated with the fault are known. However, currently available information on the seismicity is not sufficient to estimate fault level recurrence directly. Hence, a convenient method adopted in literature is to identify possible earthquake zones. Alternatively, Iyengar and Ghosh (2004*b*) and NDMA (2010) postulated an approach to estimate the magnitude-recurrence characteristics of the fault from zonal values. The fault map delineated for the study region is shown in Figure

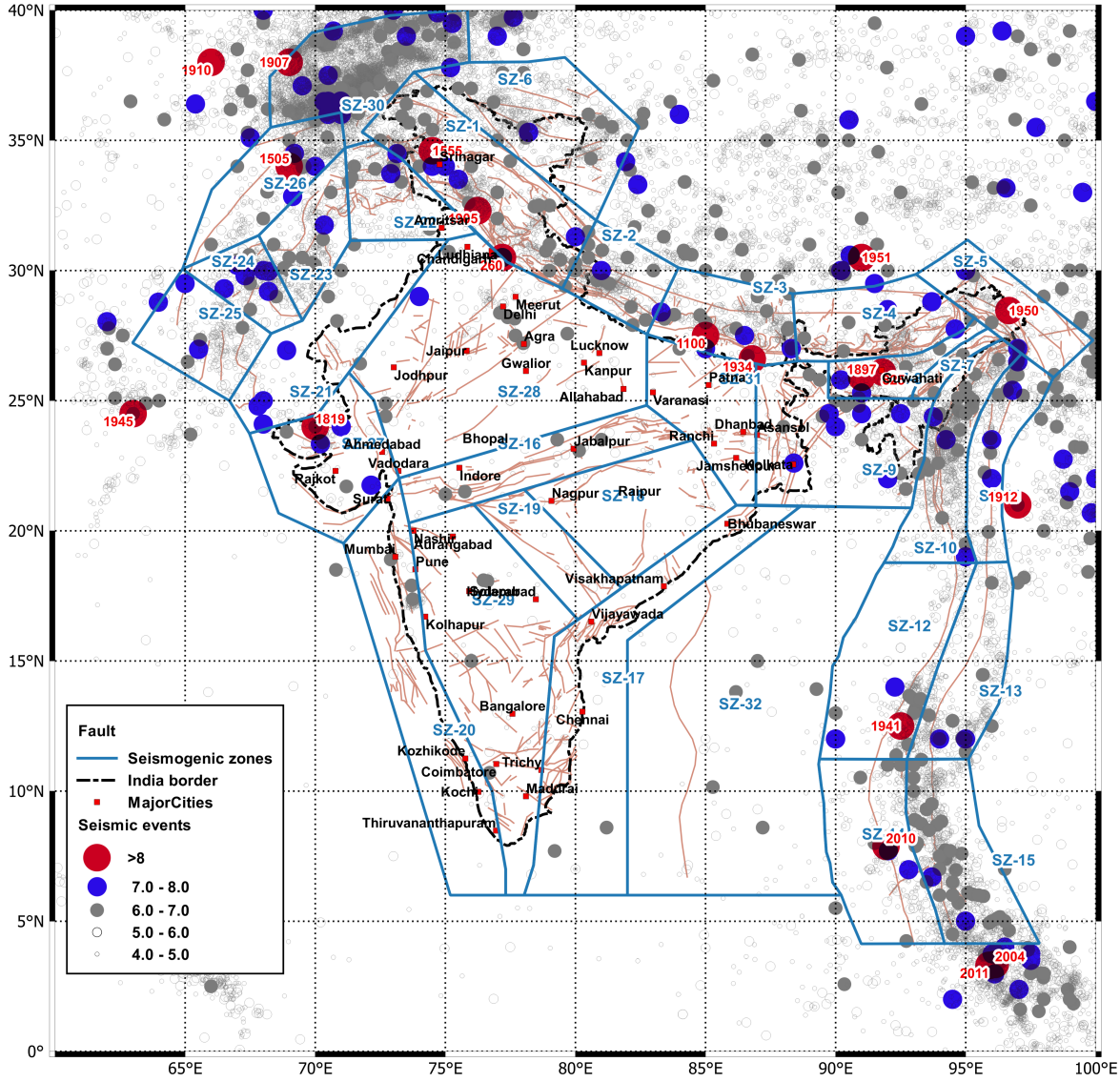

Figure 1.5: The 32 Seismogenic zones identified for India according to NDMA (2010) along with the seismicity and fault map.

1.4. The NDMA (2010) demarcated India into 32 seismogenic zones. The regions constituted by each of these zones is shown in Figure 1.5. These zonal parameters are then disaggregated to each individual faults based on their past seismic activity and their fault length. Inherently, the PSHA estimations become more reliable when the source, seismicity, and ground-motion models can be improved as and when more data becomes available.

1.7 Seismic Hazard Analysis

1.7.1 Global

A brief look into the various recent global seismic hazard analysis models are described further. Petersen *et al.* (2015) developed seismic-hazard maps for the United States. The maps were prepared by combining the hazard derived from spatially smoothed historical seismicity with the hazard from fault-specific sources. The reference site condition is firm rock (B Type soil class with V_s30 760m/s). A maximum hazard Around 22 ground motion models were used in the analysis. In the neighbouring regions of India; Ram and Wang (2013) performed hazard analysis of Nepal with twenty-three seismic source zones, each one is assumed to be seismically homogenous so that every point within them is assumed to have an equal possibility of occurrence of an earthquake in future. The estimated hazard following CEA (2005), gave a maximum PA of 1.08g for 2475years return period for rock type soil class. Recently, Rahman and Bai (2018) performed a probabilistic seismic hazard for the Nepal region. The estimations are derived based on areal, linear and gridded seismic source models. Around 10 GMPEs from similar tectonic regime is combined into a suitable logic tree to estimate the final hazard. A maximum value of 1.02g is reported for PA corresponding to 2475 years return period. Similarly, Waseem *et al.* (2018) performed an analysis for Northern Pakistan such that shallow seismic provinces and deep provinces are recognized based on similar geology, tectonics and seismicity characteristics. shallow and deep area zones are differentiated based on the focal depths of the earthquakes. The seismic hazard estimations are reported for China predominantly following the spatial smoothened seismic activity as can be seen in Xu (2019). A maximum value of $\approx$0.4g for PA is been reported for the region corresponding to 475 years return period for rock type soil class. Similar studies for other regions like Thailand, Bangladesh, Afghanistan, Myanmmar, Italy and many other regions in the world can be seen in literature (Ornthammarath *et al.*, 2011; Somsa-Ard and Pailoplee, 2013; Zuccolo *et al.*, 2013; Carlton *et al.*, 2018; Waseem *et al.*, 2019).

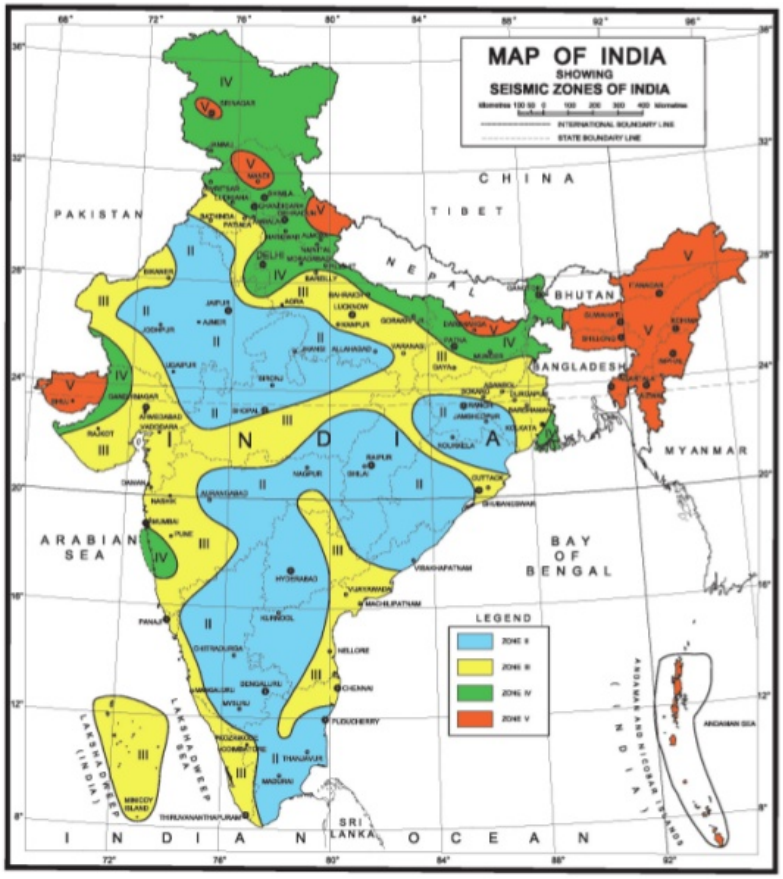

Figure 1.6: Seismic Zone map according to IS:1893-1 (2016)

1.7.2 India

The history of several catastrophic earthquakes has motivated several researchers to estimate the seismic hazard of India using either deterministic or probabilistic approaches. The current seismic zonation map of India (Figure 1.6) prescribed by the Indian code IS:1893-1 (2016) is estimated based damages after an earthquake and the uncertainties with respect to the occurrence, magnitude, distance, etc. are not considered for the categorization. Further, deterministic maps of India have been given by Parvez *et al.* (2003) developed for PA, PGV and PGD and Kolathayar *et al.* (2012) for PA, Sa (0.1s) and Sa(1s). It should be noted that the estimates based in DSHA, do not account for the uncertainties associated with the future event related to their occurrence. However, as explained earlier, PSHA accounts for the uncertainties associated with the seismic events in terms of their size, location, path, etc. Several hazard maps have been developed for India using this approach. The earliest of those hazard maps are from

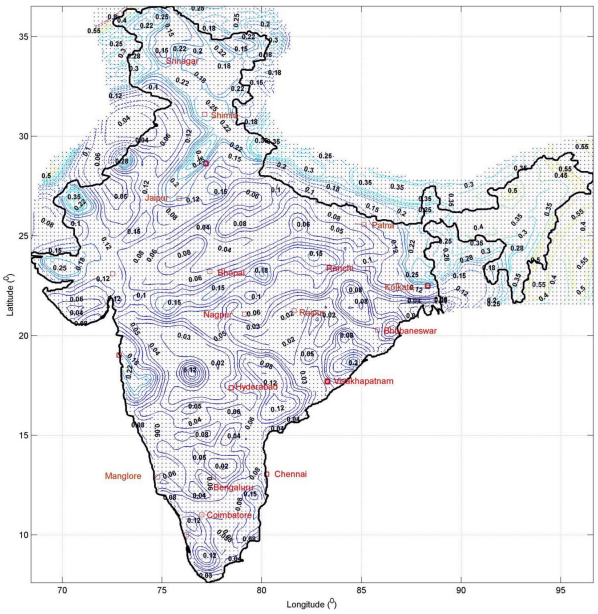

(a) NDMA (2010)(PA)

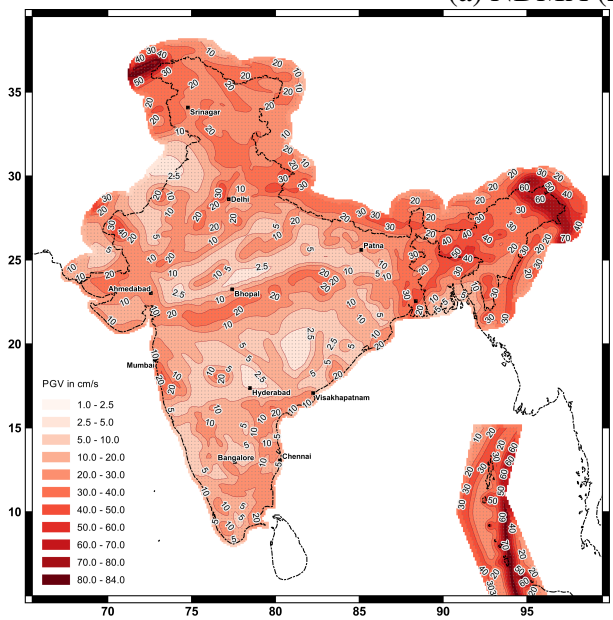

(b) Raghukanth *et al.* (2017)(PGV)

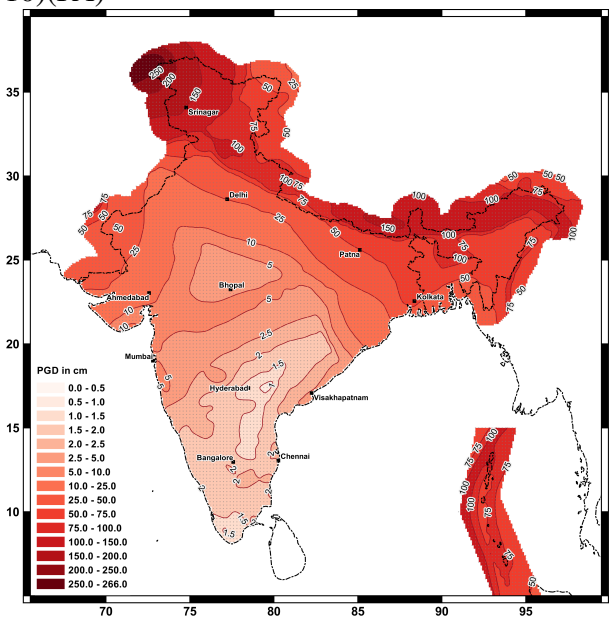

(c) Raghukanth *et al.* (2017)(PGD)

Figure 1.7: Contour map corresponding to 2500yrs return period for PA provided in NDMA (2010), PGV and PGD estimated by Raghukanth *et al.* (2017)

Basu and Nigam (1977)and Khattri *et al.* (1984*a*). These works used GMPEs from the literature without addressing the uncertainty associated with regional differences. Recently, NDMA (2010) developed regional GMPEs and utilized them for estimating the hazard in terms of S_a at 0, 0.2, and 1s for very hard rock sites or A-Type conditions.

Apart from the above studies, numerous studies have been carried out to estimate the hazard for smaller provinces. A few of the recent models includes the estimated by Rout *et al.* (2015) for North-West Himalaya, Sil and Sitharam (2015) for North-East Himalaya, Maiti *et al.* (2016) for West Bengal, Ashish *et al.* (2016) for Peninsular India, Desai and Choudhury (2014) for Mumbai and Pallav *et al.* (2012) Manipur. Some of the hazard maps for India reported based on gridded seismicity can be seen Jaiswal and Sinha (2007), Nath and Thingbaijam (2012) and Sitharam and Kolathayar (2012). However, most of the hazard maps developed for the country are based on spectral accelerations. On the other hand, for the design of long periods important structures like pipelines, nuclear reactors, transmission towers, dams, bridges, etc. hazard values corresponding to long-period ground motion characteristics like those related to velocity and displacements (Tromans, 2004; Bommer and Alarcon, 2006). Recently, understanding the importance of these characteristics on the design of the structure, seismic hazard estimates corresponding to PGV and PGD for India is estimated in Raghukanth *et al.* (2017). The estimates are performed with the region-specific GMPEs developed based on the synthetic database. Thus Figure 1.7 shows a few of the hazard maps available for India. These maps form the useful basis of the design of structures at various sites in the region. It should be noted that most of the hazard analysis is performed for A type soil class. Moreover, the hazard analysis based on fault lines alone is not appropriate as the epicentres of events are not closely correlated to the known faults and as all faults are not known. Thus a consideration on to the area sources of diffused seismicity based on spatial averaging of past seismicity is essential.

1.8 Summary

This chapter highlights the importance of performing probabilistic seismic hazard analysis for a region. Further, the basic explanation on to the key aspects in hazard in terms of return period, source, site, path and uncertainties involved are also discussed. A gist on to the various ground motion prediction models available and those developed globally and nationally are also described. Furthermore, a briefing on to the different ground motion recording instrumentations available are also provided. Additionally, the probabilistic seismic hazard analysis procedure along with some of the regional and global hazard estimations are also described in this chapter.

The present study aims at developing All India PSHA map avoiding the major limitations of the previous studies briefly reviewed above. This exercise is presented in this report under the following heads.

Chapter 2: Seismogenic zones, Catalogue and Recurrence relations

Chapter 3: Ground Motion Prediction Equation

Chapter 4: Probabilistic Seismic Hazard Maps

Appendix I: Earthquake Catalogue

Appendix II: Effects due to lack of instrumental data

CHAPTER 2

Seismogenic zones, Catalogue and Recurrence relations

2.1 Introduction

In the previous chapter we have performed we have described the recent estimation procedure for seismic hazards. Accordingly, the importance is stated for the identification of all potential seismic source and the activity rate based on event epicentres. Thus In this chapter, an effort to identify the potential source, assimilation of a comprehensive catalogue and the corresponding recurrence characteristics will be discussed. The analysis will be primarily based on the 32 seismogenic zones identified for the study region by NDMA (2010). These are the regions with concentration of faults and also past epicentres. Here, a quantification the seismic activity in these source zones are derived by developing the Gutenberg-Richter recurrence relations. A comprehensive database of location, date and magnitude of past earthquakes is required, for deriving such recurrence relations. Generally, it is known that accurate data is available for events that have happened in the last 50-100 years only. Since damage causing earthquakes are rare the length of the catalogue (sample size) influences our conclusions on the occurrence of strong earthquakes. This situation is common in countries that started sophisticated instrumentation in the middle of the 20 th Century. In India after 1964 reliable information on instrumental magnitudes and locations are available (Chandra, 1992; Guha and Basu, 1993). Prior to this period damage reports and historical records are the major sources for building up a database. In the past several investigators attempted to prepare earthquake catalogues for the Indian subcontinent. Notable efforts are by Oldham (1883*b*); Chandra (1977, 1992); Bapat *et al.* (1983); Rao (2005) and IMD. There have been efforts to derive earthquake recurrence relationships for some special regions of India by combining data from several sources (Kaila *et al.*, 1972; Khattri *et al.*, 1984*b*; Seeber *et al.*, 1999; Shanker and Sharma, 1998; Iyengar and Ghosh, 2004*b*; Raghukanth and Iyengar, 2007; Jaiswal and Sinha, 2007; NDMA, 2010; Raghukanth, 2010). All these studies provide valuable information on Indian seismic parameters for further work

and comparison. However, it may be noted here that comprehensive quantification of seismic activity inclusive of fault based as well as epicentre location based spatial smoothening for the whole country has not yet been attempted. This provides the impetus to develop an All India catalogue of past earthquakes. The collected earthquake data is naturally assigned to the thirty-two source zones of the previous chapter. The methodology proposed by Kijko and Graham (1998) and Weichert (1980) combining prehistoric, historic and instrumental data is used to estimate the potential maximum magnitude (M_{max}) and the (a, b) values in the recurrence relation. The primary sources for earthquake data are the national repository with the India Meteorological Department (IMD) and the reports of the Geological Survey of India (GSI). Instrumental magnitude and location of recent earthquakes are presently available on the internet also. In the present study, the earthquake catalogue for the region $(0^\circ N - 40^\circ N, 65^\circ E - 100^\circ E)$ has been assembled. The considered region overlaps with parts of Afghanistan, Bhutan, Burma, Nepal, Pakistan, and Sri Lanka. Hence special efforts have been made to collect instrumental, historical and paleo-earthquake data from diverse sources.

2.2 Seismo-Tectonic Setting of India

2.2.1 Source characteristics

The Indian sub-continent has experienced several moderate to large earthquakes owing to the active subduction of the Indian plate against the slow-moving Eurasian plate. This collision has resulted in several major tectonic faults in the Indian sub-continental region. Since these faults are fractured zones, having a higher rupture potential to generate seismic events at a rate depending on the amount of build-up stresses. The identification of these potential rupture areas is very important for the assessment of the probabilistic seismic hazard for the sites in the study region. The Seismotectonic Atlas of India (Geological Survey of India (GSI), 2000) has delineated the faults identified in India and its adjoining region and has been used to construct a fault map of India. Furthermore, the faults reported by Styron *et al.* (2010) for Himalayan and Tibetan regions are also included in this study region. After removing duplicate faults, the region with 1838 faults is illustrated in Figure 2.1. It is evident that Himalayan arc borders the entire northern part formed due to the continental collision. Some of the major fault systems that

are identified along the range are, namely, Indus Suture Thrust, Main Frontal Thrust (MFT), Main Central Thrust (MCT), and Main Boundary Thrust (MBT). These fault systems of the Himalayan range have caused several devastating earthquakes such as the 1905M_w7.8 Kangra, 1934 M_w8 Bihar-Nepal,1991 M_w6.8 Uttarkashi, 1999 M_w6.8 Chamoli, 2011 M_w6.9 Sikkim and 2015 M_w7.9 Nepal earthquakes. High seismicity is also observed at syntaxis regions of the Himalayan range. The prominant fault in the western syntaxis region are Main Karakoram Thrust (MKT) and Main Mantle Thrust (MMT). Further to the west, Hindukush-Pamir region is seismically very active experiencing several major earthquakes which include 2005 M_w7.6 Kashmir earthquake. To the south of the Hindukush region, Chaman fault marks the western plate boundary. The eastern end of the Himalayan arc is identified as Assam syntaxis. This region also suffers very high seismicity and has produced several major earthquakes, namely, 1897 M_w8.1 Assam earthquake, 1950 M_w 8.6 Assam-Tibet earthquake, etc. The N-S trending Burmese-Andaman arc marks the eastern plate boundary and runs southward from the Assam syntaxis to the Andaman-Nicobar archipelago. The Sagaing fault, Eastern Boundary Thrust Zone, etc. are some of the major fault systems that are present here. Several subduction events have been recorded in this region, notably, the 2004 M_w9.3 tsunamigenic Andaman-Sumatra earthquake.

Apart from the above regions, the stable continental region has also experienced numerous large magnitude intraplate events such as 1967 M_w6.5 Koyna earthquake, 1993 M_w6.2 Killari Earthquake. 1997 M_w6 Jabalpur Earthquake, 2001 M_w7.6 Bhuj earthquake, etc. The Himalayan region and the peninsular India are separated by the sedimental plains of Indo-Gangetic foredeep with very low seismicity. However, extensive damage witnessed during 1934 M_w8 Bihar-Nepal and 2015 M_w7.9 Nepal earthquakes indicates that these sedimental plains can cause significant amplification of the ground motion due to major events that occur in the lower Himalayas. Furthermore, the seismicity of India over the fault map is illustrated in Figure 2.2.It becomes clear that the regions coinciding with the boundary of the Indian tectonic plate exhibit higher levels of seismic activity, namely, the Hindukush-Pamir region in the North West, Himalayan arc in the North and the Burmese-Andaman arc in the East. Based on the activity pattern regional seismotectonic and geology, NDMA (2010) has identified 32 seismogenic zones. In the present work, a 33rd seismogenic zone is also appended to the existing ones. This zone corresponds to the Tibetan Region. Each of the seismogenic zones 8,27 and 28 are subdivided into two sepa-

rate zones as per the suggestions from the map committee. The resulting fault based database consisted of a total of 856 fault segments from NDMA (2010), 42 fault segment from Gamage and Venkatesan (2019) 940 fault segments from Styron *et al.* (2010) and 33 seismogenic zones (SZ) is shown in Figure 2.1 [Note: Duplicating faults are removed hence the total number of faults for the region is 1875]. Among 33 seismogenic zones, the active zones are SZ: 1 to 4 (Himalayan range), SZ: 5 and 8 (North-eastern India region), SZ: 10 to 15 (Andaman region), SZ: 21 to 26 (Chaman fault), SZ: 27 (Kutch), SZ: 30 (Hindukush-Pamir), and SZ: 33 (Tibetan Region). The seismic characterizations of these source zones, as well as faults, require complete information about their past seismic activity. The following section briefly discusses the process of collecting and compiling a database of size and occurrence time of past earthquakes.

2.3 Updated earthquake catalogue of India

To get an insight into the seismicity pattern of the study region, the preliminary step lies in assembling a comprehensive database of past seismic records into an “Earthquake Catalogue" which contains information on the magnitude, spatial, and temporal occurrence of the events. These data are sourced from available records (instrumented or examining historic transcriptions) or by paleoseismic studies. The reliable information of the instrumental earthquake data for the study region can be collected from the those provided by Indian Meteorological Department (IMD), United States Geological survey (USGS), International Seismological Centre (ISC-GEM), National Seismological Center (NSC) Nepal and Pakistan Meteorological Department (PMD). Some of the earlier historical events that occured in the region can be infered from the reports of Oldham (1883*a*); Milne (1911); Quittmeyer and Jacob (1979) and Bilham (2019). The information on some of the large magnitude having a recurrence period over 100 years is assessed from the paleoseismic investigations conducted on the geomorphologic evidence. Recently, the seismic catalogue of India has been assembled by Raghukanth (2010) having a total of 23,077 events, later updated in NDMA (2010) having a total of 38,860 events for a period up to 31 December 2008. The data in this catalogue are composite derived from three sources, namely, instrumental data, historical data retrieved from government archives

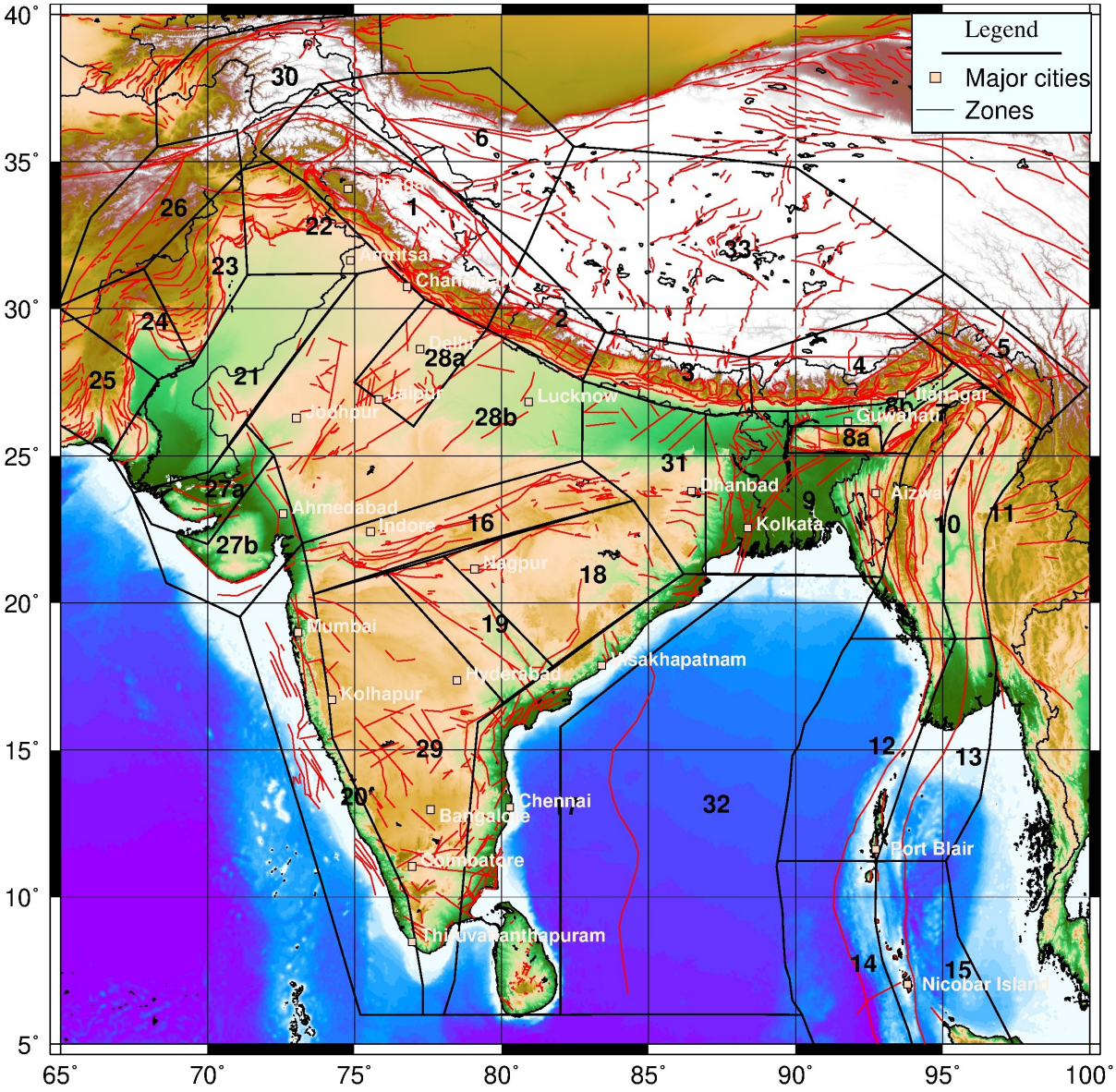

Figure 2.1: Fault map of India and adjoined regions (Geological Survey of India (GSI), 2000; Balakrishnan *et al.*, 2009; Gamage and Venkatesan, 2019; Styron *et al.*, 2010). The 32 Seismogenic Zones according to NDMA (2010) and a 33rd Zone for Tibetan region. Some of the major cities with population exceeding 1 million people are also indicated. [Note: "MBT"-Main Boundary Thrust,"MFT"-Main Frontal Thrust, "MCT"-Main Central Thrust, "MKT"-Main Karakoram Thrust, "MDF'-Mahendragarh-Dehradun Fault, "MF"-Moradabad Fault, "GBF"-Great Boundary Fault, "ADF"-Aravalli-Delhi Fault, "LF"-Lucknow Fault, "MSRF"-Munger Sahasra Ridge Fault, "MSRMF"-Munger Sahasra Ridge Marginal Fault, "UGF"-Upper Godavari Fault, "KMF"- Kutch Mainland Fault, "GF"- Gundlakkamma Fault, "KGF"-Kinnerasani Godavari Fault]

and data gathered from paleoseismic investigations. It should be noted that more than a decade passed since this catalogue is updated. Hence, in this article, the above catalogue for the study

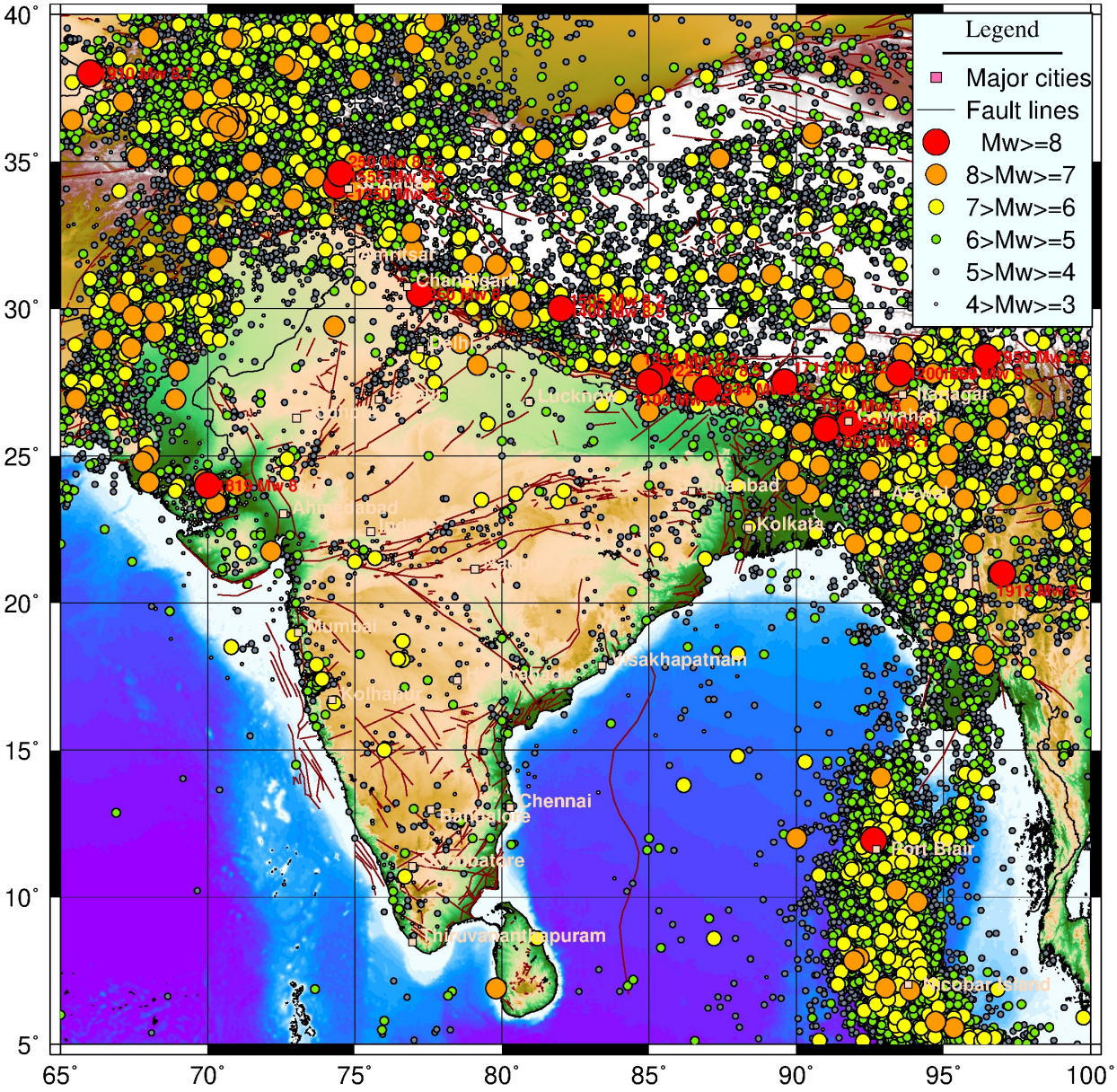

Figure 2.2: Seismic events considered in the homogenized catalogue with events dating from 2600 BCE until 2018 CE. The seismogenic zones of India are also indicated. Some of the major cities with a population exceeding 1 million people are also shown.

region (Latitude $0°N - 40°N$ and Longitude $65°E - 100°E$) has been updated by appending the events of magnitude $M_w \geq 3$ reported in the region till 31 December 2019. These additional events are collected from catalogues available at the earthquake databases of the International Seismological Centre (ISC-GEM) (`http://www.isc.ac.uk/iscgem/`), the US Geological Survey (USGS) (`http://earthquake.usgs.gov/earthquakes`), Indian Meteorological Department (IMD) and National Seismological Center (NSC), Nepal `http://seismonepal.gov.np/earthquakes`. Furthermore, the events reported by Raghukanth

and Iyengar (2006) is used to update the catalogue inclusive of small events in Koyna region. The historic catalogue is updated based on that reported by Rao and Rao (1984); Iyengar *et al.* (1999); Ambraseys and Jackson (2003); Ambraseys and Bilham (2003); Rao (2015); Bilham (2019). Thus the catalogue assembled for the study region ($0°N - 40°N, 65°E - 100°E$) contains a total of 68016 events up to a period of 31st December 2019. The earliest known earthquake in the updated catalogue is 2600BCE M_w 7.7 Kalibangan earthquake as reported in Rao (2015). The magnitude reported as body waves and surface wave magnitudes of the additional data has been converted to the moment magnitude based on the conversion relations of Scordilis (2006). The magnitudes reported as local magnitude is converted using the relation proposed by Baruah *et al.* (2012) and that reported as duration magnitude using Yenier *et al.* (2008). Some of the significant seismic events reported for the region is summarized in Table 2.1. Furthermore, the reported events with maximum magnitude in each of the 33 seismogenic zones are summarized in Table 2.2. It can be noted that the zone belonging to the active region has maximum magnitude of M_w>7.8. The SZ-18 (Mahanandi Graben & Eastern Craton) has the lowest Maximum recorded event (M_w6.1). This updated homogeneous catalogue has been declustered and forms the basis for estimating the seismicity parameters of the considered seismic sources shown in Figure 2.2. A detailed description of the de-clustering algorithm and the completeness test on the assimilated catalogue is discussed further.

Table 2.1: Great earthquakes observed within the study region

Long.	**Lat.**	**Year**	**Month**	**Date**	**Mw**	**Depth**	**Hr.**	**Min.**	**Sec.**	**Ref**
74.37	34.18	-1250	0	0	8.5	0	0	0	0	Iyengar *et al.* (1999)
74.50	34.60	250	0	0	8.5	0	0	0	0	Iyengar *et al.* (1999)
77.20	30.50	260	0	0	8.0	0	0	0	0	Kumar *et al.* (2001)
91.80	26.10	825	0	0	8.0	0	0	0	0	Rajendran *et al.* (2004)
85.00	27.50	1100	0	0	8.5	0	0	0	0	Lavé *et al.* (2005)
93.50	27.80	1200	0	0	8.0	0	0	0	0	Rao (2015)
85.30	27.70	1225	6	7	8.5	0	0	0	0	Bilham (2019)
85.30	27.70	1344	9	14	8.2	0	0	0	0	Bilham (2019)
82.00	30.00	1400	0	0	8.5	0	0	0	0	Bilham (2019)
82.00	30.00	1505	6	6	8.2	0	0	0	0	Bilham (2019)
74.50	34.60	1555	2	1	8.5	0	0	0	0	Iyengar *et al.* (1999)
91.00	26.00	1664	2	15	8.0	0	0	0	0	Rao (2015)
89.60	27.50	1714	5	4	8.2	0	0	0	0	Bilham (2019)
70.00	24.00	1819	6	16	8.0	0	0	0	0	IMD
91.00	25.90	1897	6	12	8.1	0	11	6	0	IMD
66.00	38.00	1910	7	12	8.7	0	7	36	0	IMD
97.00	21.00	1912	4	25	8.0	0	2	24	0	IMD
86.94	27.28	1934	1	15	8.3	0	8	43	0	ISCGEM
92.63	11.94	1941	6	26	8.0	20	11	52	3.67	ISCGEM
63.68	24.98	1945	11	27	8.1	15	21	56	53.73	ISCGEM
96.45	28.36	1950	8	15	8.6	15	14	9	34.65	ISCGEM
95.95	3.33	2004	12	26	9.3	30	0	58	53.72	ISCGEM
97.11	2.10	2005	3	28	8.4	0	16	9	0	ISCGEM
92.42	0.75	2012	4	11	8.3	20	10	43	10.29	ISCGEM
93.05	2.27	2012	4	11	8.6	20	8	38	36.76	ISCGEM

Table 2.2: Zonewise events with Maximum Reported magnitude

Zone	Zone Name	Long.	Lat.	Year	Month	Date	Mw	Depth	Hr.	Min.	Sec.	Ref
SZ-1	Western Himalaya	74.37	34.18	-1250	0	0	8.5	0	0	0	0	Iyengar *et al.* (1999)
		74.5	34.6	250	0	0	8.5	0	0	0	0	Iyengar *et al.* (1999)
		74.5	34.6	1555	2	1	8.5	0	0	0	0	Iyengar *et al.* (1999)
SZ-2	Central Himalaya-I	82	30	1400	0	0	8.5	0	0	0	0	Bilham (2019)
SZ-3	Central Himalaya-II	85	27.5	1100	0	0	8.5	0	0	0	0	Lavé *et al.* (2005)
		85.3	27.7	1225	6	7	8.5	0	0	0	0	Bilham (2019)
SZ-4	Eastern Himalaya	89.6	27.5	1714	5	4	8.2	0	0	0	0	Bilham (2019)
SZ-5	Mishmi Block	96.445	28.363	1950	8	15	8.6	15	14	9	34.65	ISCGEM
SZ-6	Altya Tegh & Karakoram	81.431	35.425	2008	3	20	7.1	15	22	32	59.76	ISCGEM
SZ-7	Naga Thrust	94.522	26.228	1906	5	12	6.5	35	5	48	44.32	ISCGEM
SZ-8	Shillong Plateau & Assam valley	91	25.9	1897	6	12	8.1	0	11	6	0	IMD
SZ-9	Bengal Basin	87.7	22.9	1669	6	4	8	0	0	0	0	Rao (2015)
SZ-10	Indo-Burmese Arc	95	19	1858	8	24	7.5	0	19	8	0	IMD
SZ-11	Shan-Sagaing Fault	96	22	1839	3	23	7.8	0	0	0	0	IMD
SZ-12	West Andaman-I	92.626	11.94	1941	6	26	8	20	11	52	3.67	ISCGEM
SZ-13	East Andaman-I	93.603	12.993	1983	1	24	6.8	75	23	9	22.31	ISCGEM
SZ-14	West Andaman-II	91.406	7.037	1973	4	7	6.6	20	3	0	59.24	ISCGEM
SZ-15	East Andaman-II	93.4	10.25	1847	10	21	7	0	0	0	0	Rao (2015)
		96.406	4.381	1935	8	3	7	25	1	10	5.87	ISCGEM
SZ-16	SONATA	79.3	23.5	1846	5	27	6.5	0	0	0	0	IMD
		75	21.4	1847	5	27	6.5	0	0	0	0	IMD
		82.1	23.8	1927	1	2	6.5	35	0	0	0	Rao (2015)
SZ-17	Eastern Passive Margin	79.8	6.9	1615	4	14	7	0	0	0	0	Rao (2015)
SZ-18	Mahanandi Graben & Eastern Craton	85.27	21.81	1995	6	21	6.1	0	0	0	0	NSC
SZ-19	Godavari Graben	80.775	17.747	1969	4	13	5.7	20	15	24	55.92	ISCGEM
SZ-20	Western Passive Margin	72.9	18.9	1618	5	26	6.9	0	0	0	0	Rao (2015)
SZ-21	Sindh-Punjab	67.8	24.8	894	0	0	7.7	0	0	0	0	PMD
SZ-22	Upper Punjab	72.9	33.72	25	0	0	7.5	0	0	0	0	PMD
SZ-23	Koh-e-Sulaiman	71	34	1505	7	6	7.9	0	0	0	0	Bilham (2019)
SZ-24	Quetta-Sibi	66.436	28.958	1935	5	30	7.6	25	21	32	57.11	ISCGEM
SZ-25	Southern Baluchistan	65.526	26.92	2013	9	24	7.8	12.8	11	29	47.8	ISCGEM
SZ-26	Eastern Afghanistan	69.2	34.5	1874	10	18	7.8	0	0	0	0	IMD
SZ-27	Gujarat Region	70	24	1819	6	16	8	0	0	0	0	IMD
SZ-28	Aravali-Bundelkhand	78.58	28.83	1833	8	26	7.8	0	0	0	0	Bilham (2019)
SZ-29	Southern Craton	76.47	18.1	110	0	0	6.5	0	0	0	0	Sukhija *et al.* (2006)
SZ-30	Hindukush and Pamirs	70.676	36.199	1921	11	15	7.8	240	20	36	43.33	ISCGEM
SZ-31	Gangetic region	85	26.5	1408	0	0	7	0	0	0	0	Rao (2015)
SZ-32	Bay of Bengal	87.2	8.6	1882	0	0	6.3	0	0	0	0	Oldham (1883*b*)
SZ-33	Tibetan	90.2	30	1411	9	29	7.7	0	0	0	0	Ambraseys and Jackson (2003)
		91.261	31.056	1951	11	18	7.7	30	9	35	54.68	ISCGEM

Table 2.3: Input parameters for the different de-clustering methods

Declustering Method	Paramter	Value		
Gardner and Knopoff (1974)	Window	Distance (km)		Time (days)
	Uhrhammer (1986)	$e^{-1.024+0.804M_w}$		$e^{-2.87+1.235M_w}$
	Gruenthal	$e^{1.77+(0.037+1.02M_w)^2}$		$e^{-3.95+(0.62+17.32M_w)^2}$; if $M_w > 6.5$ $10^{2.8+0.024M_w}$; otherwise
Reasenberg (1985)	Parameter	Standard	Minimum	Maximum
	τ_{min}	1	0.5	2.5
	τ_{max}	10	3	15
	p_1	0.95	0.9	0.99
	x_k	0.5	0	1
	x_{meff}	1.5	1.6	1.8
	r_{fact}	10	5	20

2.3.1 Declustering

Once the catalog is compiled, the next step is to separate the catalog in to independent and dependent events. This is done to make sure that the earthquake catalog follows Poisson distribution which is a prerequisite for the hazard estimation. Here, it should be noted that the seismicity parameters are highly sensitive to the number of independent events separated after the declustering process. The developed catalog of India in the present study is compiled from various sources in the literature. In such situation, where the catalog has been compiled from a large number of sources, the use of proper declustering algorithm becomes important. Also, it can be noted that, there are no previous studies in literature that describe the declustering space and time window for Indian events. There are several declustering algorithms available in the literature. The first declustering algorithm has been introduced by Knopoff (1964), using a ten days window for analysing the clustered data. Later Gardner and Knopoff (1974) introduced specific space-time window as a function of magnitude. The chances of secondary and higher order aftershocks are ignored in this study. Apart from the window suggested by Gardner and Knopoff (1974), there are other windows proposed by Uhrhammer (1986) and Gruenthal, which are commonly used in the literature. These windows are shown in Table 2.3.

It is observed that, Urhammer window spans over larger distances for events with magnitude >6.5, and for smaller magnitude events, Gruenthal window gives higher value. Similarly, for events of magnitude less than 6.5, the time window from Gruenthal approach is more and it gets saturated to 1000 days after a magnitude value of 6.5.

Another approach proposed by Reasenberg (1985) considers the aftershock triggering within a cluster and the space time distance is based on Omori law. The default parameters and their range for the Reasenberg (1985) method is tabulated in Table 2.3. It can be noted that the algorithms by Gardner and Knopoff (1974) and Reasenberg (1985) are developed based on the earthquake sequences in Southern California and Northern California respectively. Hence, an understanding of how well these methods can be used for Indian earthquakes is to be investigated. For this, proper details of the aftershocks recorded for a particular event is required. It can be noted that, a detailed description of the aftershocks of 25th April 2015 M_w7.9, Nepal event, which extended for almost 45 days from the main shock is reported in Adhikari *et al.* (2015) and the catalog is available through `http://seismonepal.gov.np/ckfinder/userfiles/files/CATALOGUE_NSC45DAYS.txt`. This well-recorded data can be utilized to test the applicability of Gardner and Knopoff (1974) algorithm with Uhrhammer (1986) window, Gruenthal window and Reasenberg (1985) algorithm in removing the aftershock of 2015 M_w 7.9 Nepal Earthquake. Figure 1 shows the aftershocks obtained using all these methods. It can be seen that the Gardner and Knopoff (1974) algorithm with Uhrhammer (1986) window is able to separate almost all the aftershocks. However, the 12th May 2015 M_w 5.7 event, which is reported as the aftershock of 25th April 2015 M_w 7.9 event Adhikari *et al.* (2015), has not identified as an aftershock by this method. Also, the Gardner-Knopoff-Gruenthal method was able to separate 551 aftershocks out of 553 events and the independent events obtained are 2nd May 2015 M_w 4.4 event and 12th May 2015 M_w 7 event. Further, the evaluation of the catalog using Reasenberg (1985) method is shown in Figure 2.3 (Bottom panel). A set of parameters namely τ_{min}, τ_{max}, p_1, x_{meff}, x_k, r_{fact} are varied here to find the sensitivity of the algorithm. As per Van Stiphout *et al.* (2012), the minimum, maximum and standard values of these parameters are used for the analysis (Table 2.3). It can be noted that the standard values of the parameters are derived for Northern California and the minimum and maximum values correspond to the range for parameters based on χ^2 goodness of fit test of the same data. Here, the results show that the algorithm with

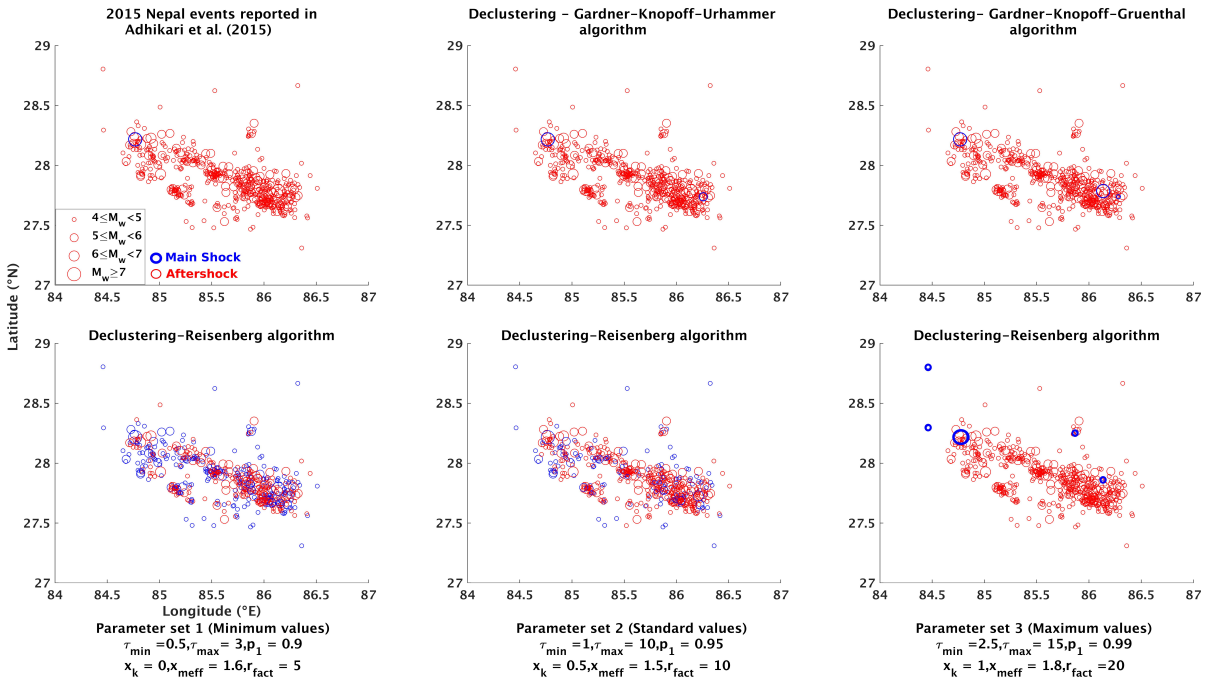

Figure 2.3: Declustering the catalog of 2015 M_w 7.9 Nepal event and its aftershocks by various methods. [Note: Blue colour indicate mainshocks and red colour indicate aftershocks]. The declustering window parameters for each of the methods is tabulated in Table 2.3

minimum and standard parameter values are not efficient in separating the aftershocks from the catalog. However, when the parameters are increased and the parameter set of maximum values is used for the evaluation, better separation of aftershocks is observed. In this case, the method was able to identify 549 aftershocks out of 553. Since, the aftershock separation is dependent on the parameters used, it can be noted that the method can only be used with a modified parameter set. However, the earlier approach of Gardner-Knopoff-Urhammer is able to remove well the aftershocks from the catalog with the fixed window itself. Hence, in this study, Gardner Knopoff-Urhammer approach is used for declustering the catalog. Thus, employing the corresponding algorithm on the assimilated 68016 events resulted in the removal of 40147 fore-shocks and after-shocks. Thus the final declustered catalogue contains a total of 27869 independent events of magnitude $M_w \geq 3$ and the corresponding spatial distribution is shown in Figure 2.4 and the temporal distribution is shown in Figure 2.5.

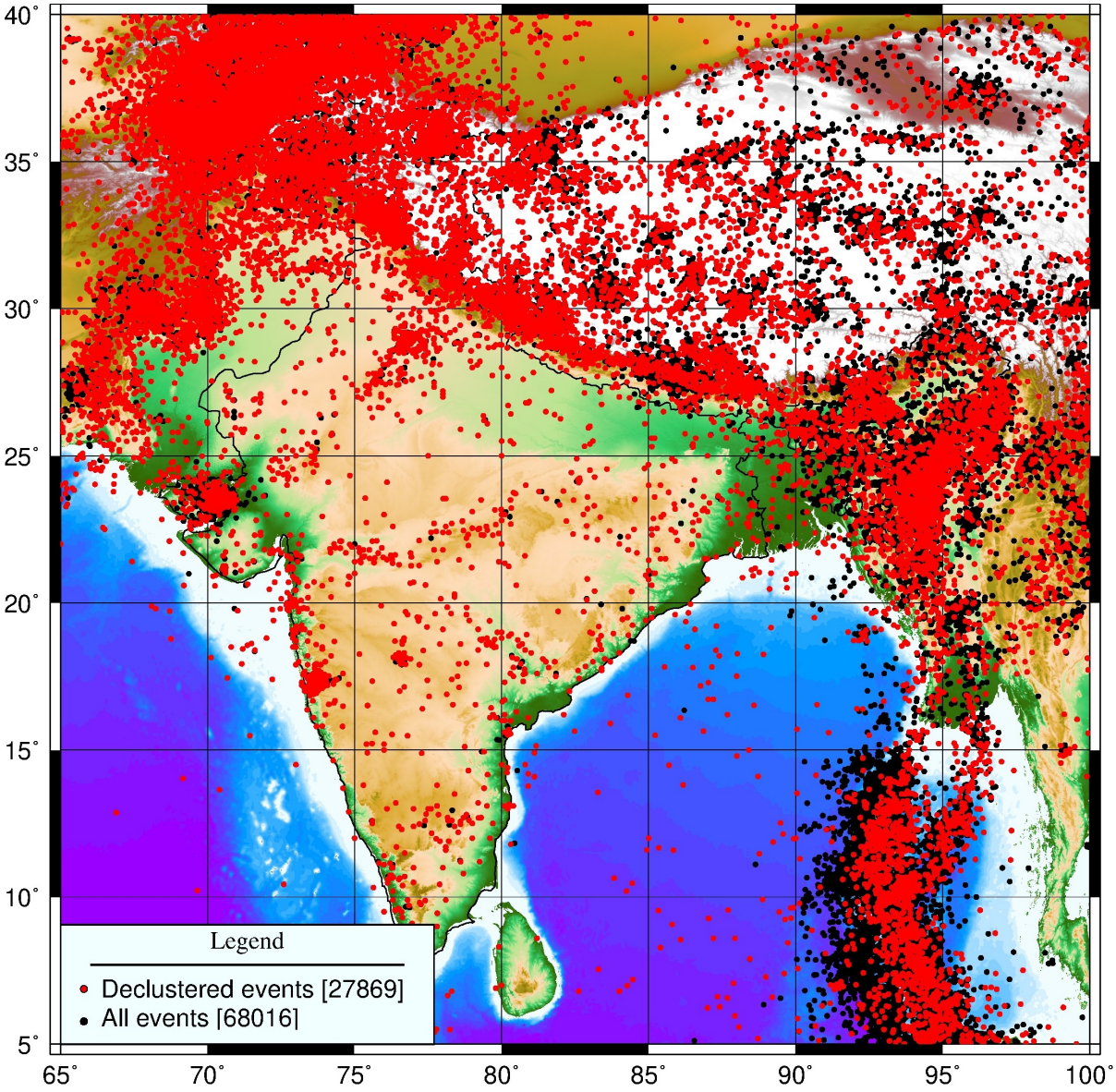

Figure 2.4: Seismic events in the catalog before (black cross) and after declustering (red cross) using Gardner-Knopoff-Uhrhammer algorithm. The total events are indicated within the brackets.

2.3.2 Completeness check

The time depended distribution of the earthquake magnitudes in the de-clustered catalogue illustrated in Figure 2.5 points to two concerns on the catalogue. First, the events with small magnitude are reliably recorded only in the last few decades, whereas information on larger events are available for a border temporal period. These differences in the information availability necessitate the estimation of the completeness period for each magnitude interval for the assembled catalogue. Furthermore, the reliable estimation of the seismicity recurrence charac-

teristics of the region can be suitably ascertained from the complete part of the catalogue. In the present work, catalogue has been checked for completeness by using the widely practiced visual approaches of Stepp (1972) and Tinti and Mulargia (1985) to demarcate the complete and historic parts for each magnitude intervals. In Stepp method, the annual event occurrence rates for each magnitude ranges are arrived by dividing the events in to several time windows (10 years, 20 years and so on) extending backward from the latest catalogue period which in present catalogue is 2018CE. The standard deviation of mean exceedance rate (denoted as $\sigma(\lambda)$) of each magnitude bin is estimated for varying time window length 'T'. A typical completeness interval check of the current catalogue data taken together is shown in Figure 2.6. It should be noted that as long as the data is complete it follows a constant standard deviation of $1/\sqrt{T}$. Thus the completeness interval can be visually identified for each magnitude class based on the point at which the standard deviation of mean occurrence departs from the constant line as illustrated in Figure 2.6. In Tinti and Mulargia (1985) method, the events which are divided into each magnitude class are further represented as the cumulative number for events with time. The completeness period is identified visually where the trend in the data stabilizes to a straight line (Figure 2.6). The corresponding complete part is demarcated from the historic catalogue for the present catalogue from both the approaches with downward arrows and shown in Figure 2.6. Thus, the completeness intervals for the all India catalogue are estimated using Stepp (1972) methods is to be 59 years (1960-2019) for magnitudes $4 \leq M_w < 5$; 75 years (1944-2019) for magnitudes $5 \leq M_w <_w 6$; 125 years (1894-2019) for magnitudes$6 \leq M_w < 7$; 200 years (1819-2019) for magnitudes $7 \leq M_w < 8$ and that using Tinti and Mulargia (1985) is 59 years (1960-2019) for magnitudes $4 \leq M_w < 5$; 77 years (1942-2019) for magnitudes $5 \leq M_w < 6$; 125 years (1894-2019) for magnitudes$6 \leq M_w < 7$; 210 years (1809-2019) for magnitudes $7 \leq M_w < 8$. The complete period for magnitudes $M_w \geq 8$ is taken to be the entire available range. It is noted that for the present catalogue the completeness period obtained from both the approaches are almost similar. Despite the best efforts, these catalogues are limited to the information that is available, which makes it difficult to estimate the rupture potential of the faults that are dormant or possibly with longer recurrence cycles, such as stable continental regions. In order to overcome this issue, an alternative approach has been used for establishing the seismicity parameters of sources and is briefly discussed in the following section.

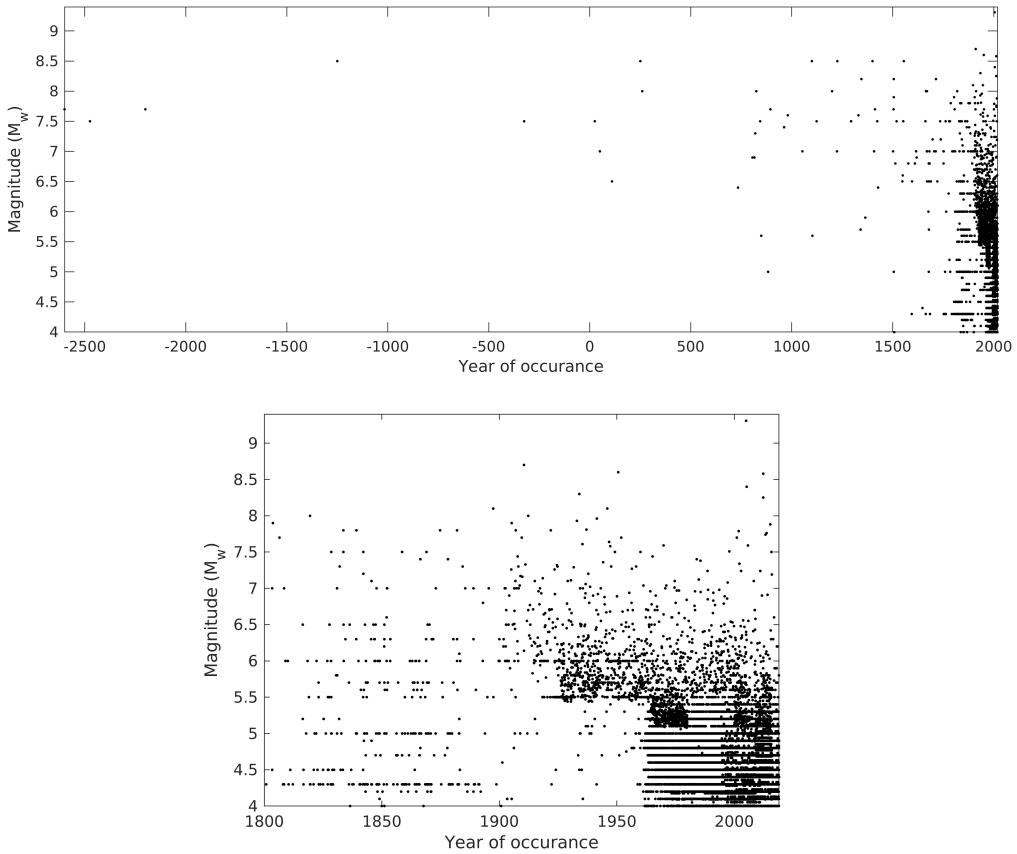

Figure 2.5: [Top] Temporal distribution of seismic events dating from 2600 BCE up to 2019 CE observed within the study region [Bottom] Magnified view of the records since 1800 CE.

2.4 Seismic Characteristics of the Probable Sources

2.4.1 Zonal recurrence relationship

In the probabilistic seismic hazard analysis framework, Gutenberg-Richter recurrence relations are utilized to quantify the seismic activity rate in each of the potential sources. For the present study region, there are 33 seismogenic zones demarcated based on the activity characteristics (Figure 2.1). Using the Gutenberg-Richter relations the potential rate at which the seismogenic zone is triggered by an event of a certain magnitude and the possible maximum magnitude can be estimated for each of the zones. Thus, if $N(M_w)$ represents the number of events $\geq$a magnitude 'M_w' recorded during a time period (T) due to seismic activity in the region of

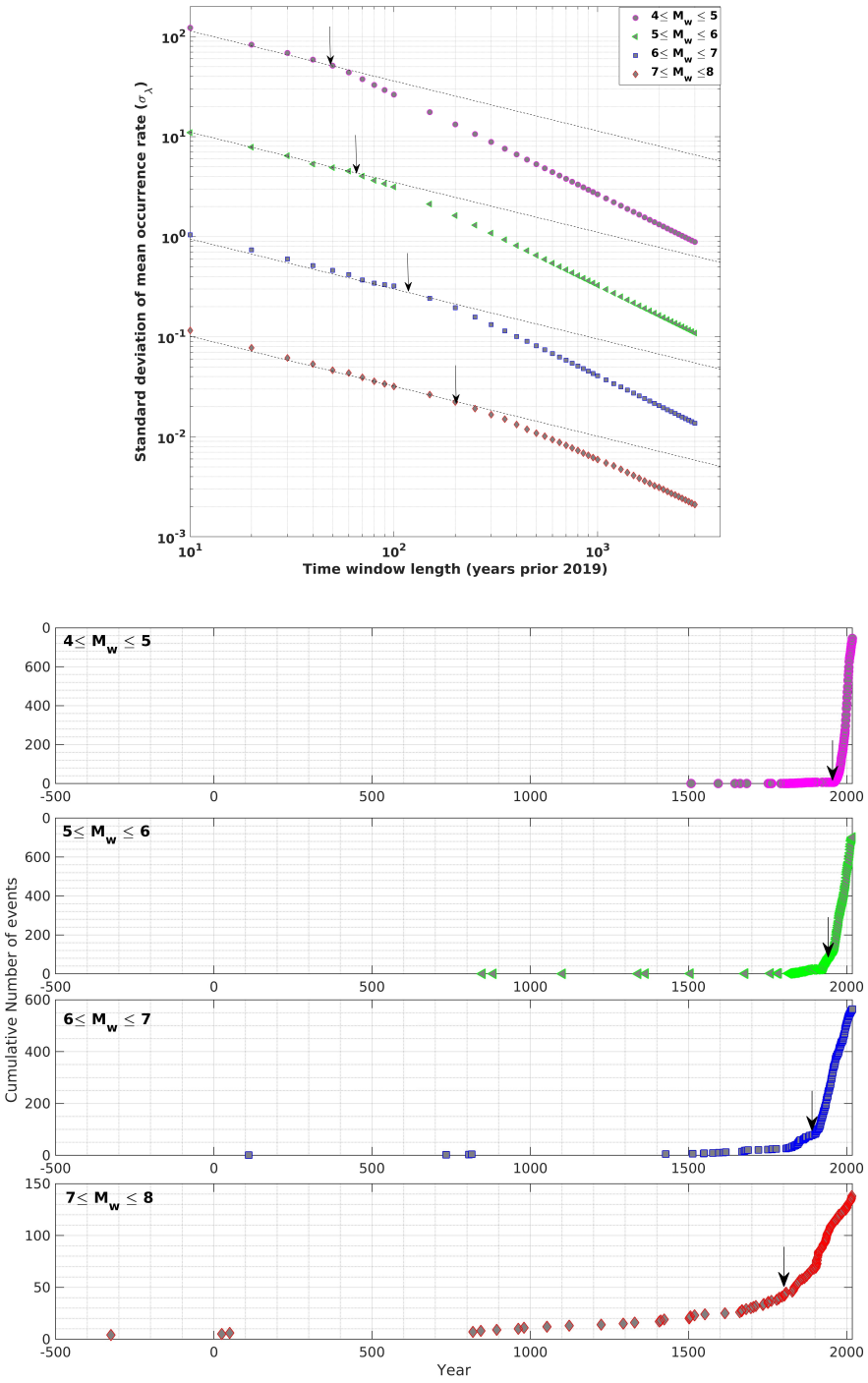

Figure 2.6: Completeness test of earthquake data for the all India catalogue using [top](Stepp, 1972) where Theoretically, $\sigma(\lambda)$will vary at a constant slope of $1/\sqrt{T}$ (indicated by thin grey lines) as long as the data is complete. [bottom] Tinti and Mulargia (1985) where the period with the highest apparent seismicity is visually identified and taken as complete

Table 2.4: Completeness intervals for the seismogenic zones.

Zone	Magnitude							
	$4-4.5$	$4.5-5$	$5-5.5$	$5.5-6$	$6-6.5$	$6.5-7$	$7-7.5$	$7.5-8$
SZ 1	31	51	51	100	150	71	110	630
SZ 2	21	51	56	86	110	-	-	-
SZ 3	21	46	56	81	-	-	-	-
SZ 4	31	56	56	81	-	-	-	-
SZ 5	31	51	51	91	61	-	110	-
SZ 6	26	46	51	91	91	110	-	-
SZ 7	46	36	-	6	-	61	-	-
SZ 8	36	46	51	170	86	-	-	-
SZ 9	26	41	51	170	200	-	150	230
SZ 10	36	46	51	91	100	91	66	-
SZ 11	46	46	56	86	81	61	-	110
SZ 12	21	51	51	86	91	-	-	-
SZ 13	41	41	51	91	91	-	100	-
SZ 14	21	41	46	-	36	-	-	-
SZ 15	41	41	51	91	86	81	-	-
SZ 16	11	26	-	-	-	-	-	-
SZ 17	91	-	-	-	-	-	-	-
SZ 18	21	21	-	-	-	-	-	-
SZ 19	-	-	-	-	-	-	-	-
SZ 20	36	51	66	-	-	-	-	-
SZ 21	26	41	51	86	51	-	-	-
SZ 22	36	56	56	170	76	-	-	-
SZ 23	26	51	51	76	100	-	-	-
SZ 24	21	51	51	91	-	31	130	-
SZ 25	41	46	91	86	-	-	-	-
SZ 26	46	56	55	91	160	-	-	41
SZ 27	16	46	26	-	-	-	-	-
SZ 28	21	50	190	190	190	320	-	-
SZ 29	26	36	-	-	-	-	-	-
SZ 30	41	46	51	86	90	76	110	110
SZ 31	36	51	51	-	-	-	-	-
SZ 32	16	26	40	-	21	-	-	-
SZ 33	30	50	57	90	120	-	-	-

interest, then the mean annual rate of exceedance ($\lambda(M_w)$) can be expressed as

$$log_{10}\left(\lambda(M_w)\right) = a - bM_w \tag{2.1}$$

where a is the intercept which represents the logarithmic value of the mean annual value corresponding to the threshold magnitude (M_0); and the slope b indicates the activity rate of the event of particular magnitude. The value of M_0 is taken to be 4 in the present work. The reason is the inference that the structures are not subjected to significant damage for earthquakes of magnitudes (M_w) < 4. Furthermore, the catalogue is not coherent for smaller magnitudes. Additionally, Knopoff and Kagan (1977) suggested that the above recurrence relation in Eqn. 2.1 should be constrained with an upper bound to reflect the maximum potential realistically. However, the corresponding precise information cannot be determined from the catalogue due to the randomness associated with the occurrence of future events.

In order to estimate fault level the bounded G-R recurrence parameters (a, b and M_{max}, complete information fault level seismic information is essential, however, the corresponding association is quite difficult. Hence, a common practice is to estimate the recurrence parameters at seismogenic zone parameters then deaggregate the same to the individual fault level based on fault characteristics as suggested by Iyengar and Ghosh (2004*b*); NDMA (2010). In this study, the recurrence parameters such as a, b and M_{max} are estimated for all the 33 seismogenic zones for the updated de-clustered catalogue using the Kijko and Graham (1998) and Kijko (2004) methods. Furthermore, Weichert (1980) method based on maximum likelihood principle for the estimation of recurrence parameters is also utilized in this study. This statistical procedure accounts for the uncertainty in the catalogue information and completeness periods. Thus, the updated catalogue is divided into complete and extreme parts according to the completeness interval estimated in section 2.3.2. The uncertainty associated with the reported magnitudes is taken as 0.5 in the extreme part and 0.3 complete part (NDMA, 2010).

The estimated zonal seismicity parameters estimated using Kijko's approach for bounded G-R distribution for all the 33 seismogenic zones of the study region are summarized in Table 2.5. Additionally, the comparison of the λ and $b-$ estimated from Kijko's and Weichert (1980) are compared and summarized in Table 2.6. The values slightly differ from each other owing to the data variability and estimation algorithms. It is noted that the estimates from Kijko's method is sensitive to the initial guess while that estimated from Weichert (1980) methods are observed to be more stable. From the estimated recurrence characteristics, it is noted that most of the seismogenic zones are having maximum potential magnitude > 7. It is also observed that the seismogenic zones SZ-1 (Western Himalaya), SZ-2 (Central Himalaya -I), SZ-3 (Central Hi-

malaya -II), and SZ-5 (Mishmi Block) have the highest maximum magnitude potential. While the SZ-30 (Hindukush-Pamir), SZ-33 (Tibetan), SZ-10 (Indo-Burmese Arc) and SZ-15 (East Andaman II) regions have a relatively higher annual occurrence of earthquakes with magnitude $M_w \geq 4$. All illustration on the zonal recurrence characteristics is also shown in Figure 2.7. The variability in these parameter estimates should stabilise as the catalogue becomes more robust. However, with the available information in the hazard estimations, it is advisable to account the recurrence characteristics from both algorithms with equal weightage. However, seismic activity rate varies within the individual zones. Hence, the next step is to disintegrate the zonal recurrence characteristics to each grid point in the zone. One such practice is to associate the observed recurrence characteristics suitably to the fault identified within each zone. To accomplish this, NDMA (2010) followed a heuristic approach to disaggregate the zonal parameters obtained here. In this approach, the zonal parameter 'N(4)' is disaggregated to individual faults while conserving the regional seismicity. The corresponding procedure is explained in detail in the following section

2.4.2 M_{max}

The maximum magnitude M_{max} is considered as the upper bound physical limit in hazard computations. The usual way of arriving at the M_{max} for each of the seismogenic zone is to obtain the maximum magnitude from the catalog. As the magnitude of many past earthquakes has been fixed based on historic transcripts and other geologic evidence, there is a large variation associated with it. Hence,in this study, the M_{max} suggested by the members of the map committee is utilized to perform hazard analysis. These M_{max} values are shown in Figure 2.8. The zones 27, 28, and 8 are subdivided with a higher M_{max} for Kutch, Aravalli ranges and Shillong Plateau. At Himalayan region, the observed maximum magnitude was M8.8. However, for the past 700 years the higher magnitude observed in Himalaya is M8.2 at Nepal. In general, largest Himalayan earthquakes are not expected to have recurrence period larger than 250 – 500 years. Based on expert elicitation, a value of 8.3 is fixed for Himalaya. As this M_{max} estimation is rationalized w.r.t 500 to the 2500 year return period accelerations and add that the possibility of bigger/ in frequent events would need to be considered if accelerations for higher return period (eg: 10000years) are to be evaluated.

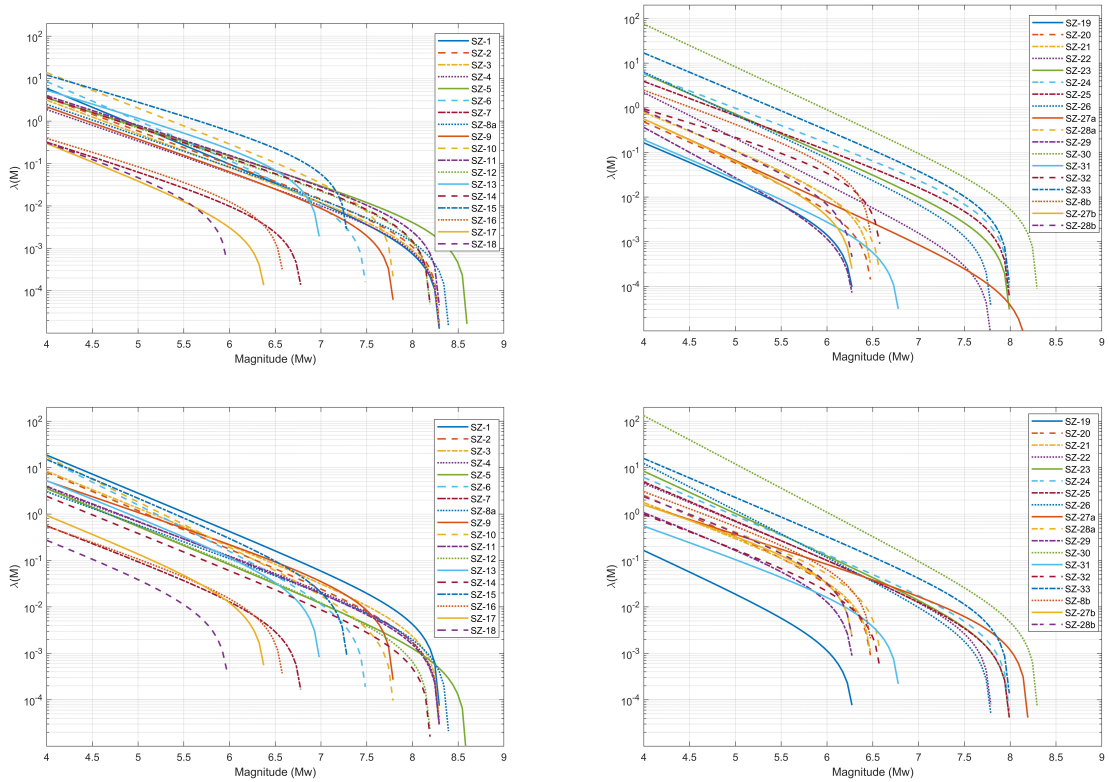

Figure 2.7: Zonal bounded magnitude-frequency relationships. '$\lambda(M)$' indicates the mean annual recurrence rate of events with magnitude exceeding M_w.[Top Panel] Using Kijko's method [Bottom Panel] Using Weichert (1980) method

2.4.3 Fault level recurrence relationship

Since the faults within the same zone exhibit varying levels of seismicity, it may be even more appropriate to consider the fault level recurrences. However, the gaps in the existing catalogue and lack of information on the slip characteristics of the faults make it difficult to achieve a clear consensus on the rupture potential of all the identified faults. In order to circumvent this issue, NDMA (2010) followed a heuristic approach to disaggregate the zonal parameters obtained earlier. In this approach, the zonal parameter 'N(4)' is disaggregated to individual faults while conserving the regional seismicity. Thus, the fault specific $N(4)$ values are estimated by taking into consideration the potential of a fault to rupture and known activity. The background seismicity within a source zone is also taken into consideration by associating these events with the nearest faults in the zone. The disaggregation factor for an individual fault is obtained as the average of fault length ratio and fault activity ratio. The fault length ratio is defined as the ratio of individual fault length (L_i) to the sum of the length of all the faults in the zone (L_z).

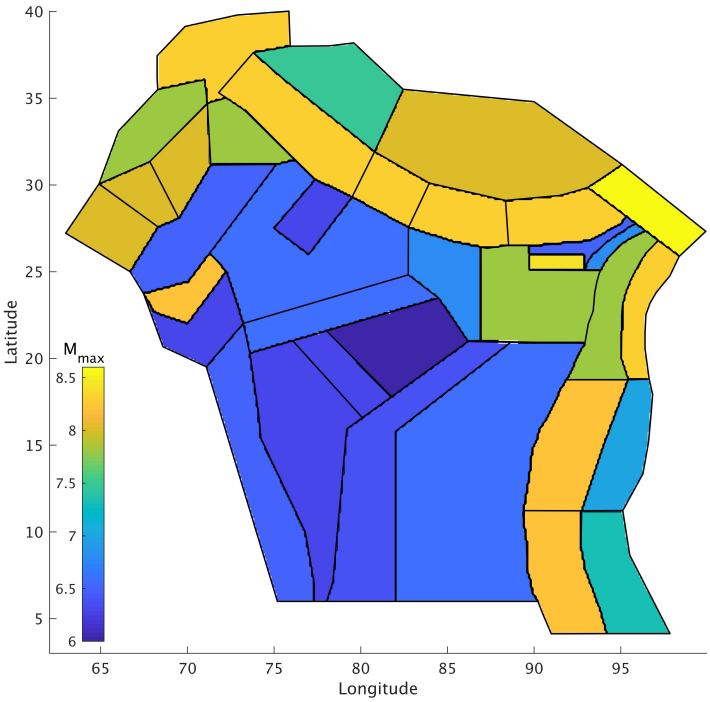

Figure 2.8: Maximum magnitude fixed for each of the zones based on expert elicitation. Refer Figure 2.1 and Figure 2.2 for the seismotectonic details

Similarly, the fault activity ratio is defined as the ratio of the number of fault-level events (s_i) to total zonal events (S_z). Thus, '$N(4)$' of ith fault is determined as,

$$N_i(4) = 0.5\left(\frac{s_i}{S_Z} + \frac{l_i}{L_Z}\right) N_z(4) \tag{2.2}$$

where $N_z(4)$ is the zonal value of $N(4)$. Using this approach, the recurrence parameters of the source zones have been disaggregated to fault level recurrence parameters. The fault level seismicity 's_i' is estimated by associating the earthquakes with the closest fault. Since it is difficult to ascertain the magnitude versus rupture potential of individual faults due to the uncertainties in the fault activity, the b-value of all the faults within a zone is assumed to be the same as the zonal b-value. The M_{max} value for all the faults in each zone is taken as the maximum magnitude of past events associated with the fault and an additional 0.5 units to account for uncertainty in the data. For faults lacking past event records, Wells and Coppersmith (1994a) relation has been used to evaluate M_{max} based on rupture length. Furthermore, the M_{max} values for individual faults are constrained by the zonal M_{max} values. These fault level recurrence

parameters are estimated for all the faults identified in the 33 seismogenic zones considered in this study. The fault level recurrence relations were obtained from the above procedure. The curves of high seismic activity is observed to be that of the major faults situated in the active regions of Himalayas, Andaman, and Assam region. These values define the seismicity of all these causative faults while performing the PSHA. However, a major limitation is that many times epicentres are not closely associated with the delineated fault lines and also all the faults need not be known for a region. Hence a more appropriate approach would be to perform seismicity estimates from the spatial distribution of epicentres and fault orientations as discussed further

2.4.4 Spatial smoothening recurrence relationship

Another approach followed in this study is based on the seismic activity rate estimated from earthquake catalog. Here, seismic hazard analysis is performed by considering the earthquake epicentres which are not assigned to specific fault, known as distributed seismicity. As per Frankel (1995),Lapajne *et al.* (2003), the study area is divided into grids of suitable dimension and the count of earthquakes which are having magnitude greater than the threshold magnitude is taken. In this study, a grid size of 0.1^0 x 0.1^0 is adopted with a threshold magnitude per grid as M_w 4 for the same reason stated in previous section. The number of earthquakes per grid is then smoothed using circular smoothing procedure proposed by Frankel (1995).

$$n_i = \frac{\sum_j n_j e^{-\frac{\Delta_{ij}^2}{c^2}}}{\sum_j e^{-\frac{\Delta_{ij}^2}{c^2}}} \tag{2.3}$$

where, n_j is the number of earthquakes in j^{th} grid, Δ_{ij} is the distance between $i^{th}$and j^{th} grid points, c represents the correlation distance that accounts for the reported epicentre location uncertainties and the radius of smoothing is taken as $3c$. In this study, a smoothing radius of 150km is used in the estimations. The corresponding seismic activity rate is illustrated in Figure 2.9. As expected, the active regions along the Indian plate subduction region having a relatively greater occurrence of events are observed to have higher rate compared to the stable continental region.

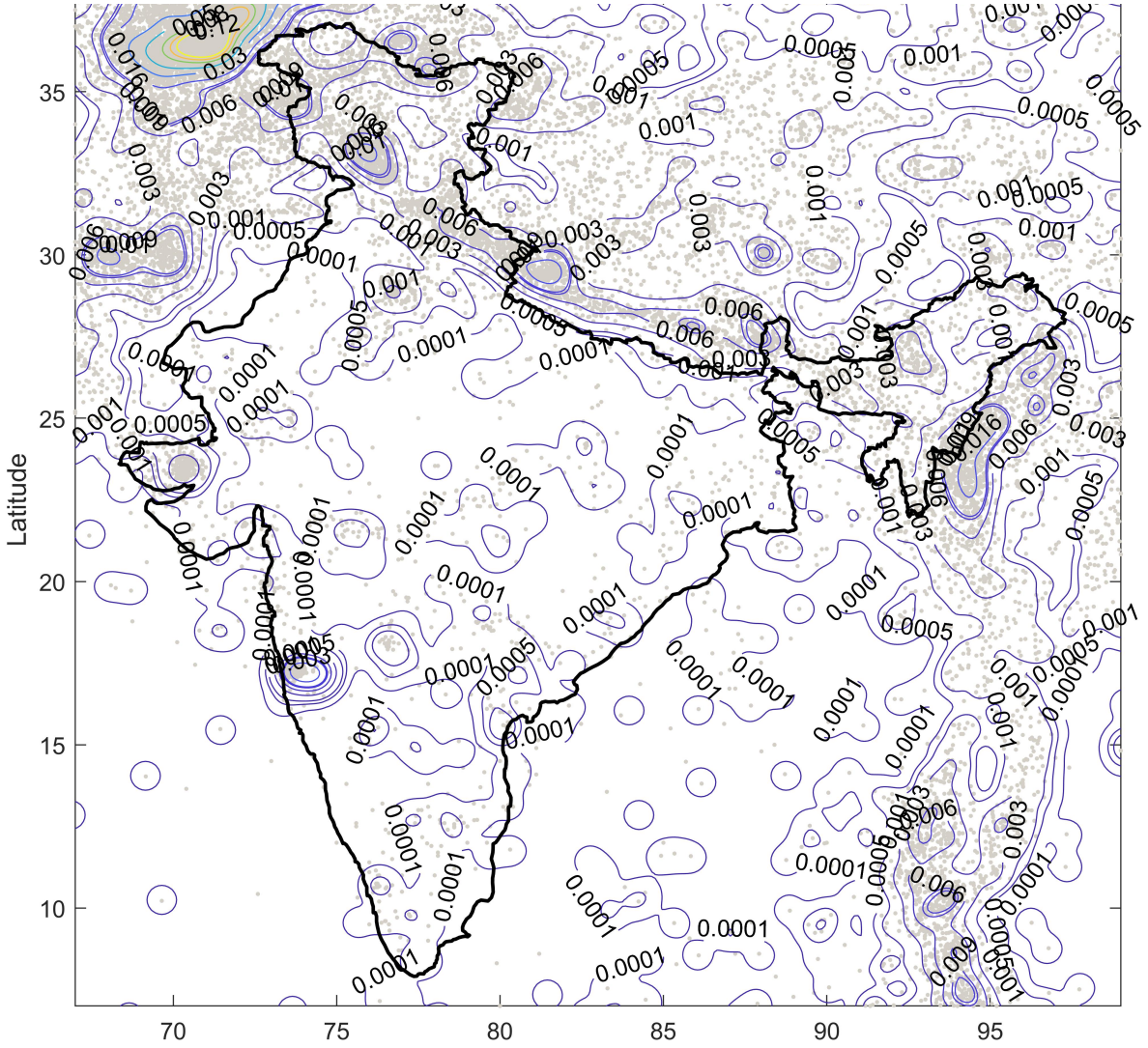

Figure 2.9: Circularly smoothed seismic activity rate for the study region

Furthermore,Lapajne *et al.* (2003) suggested the smoothing process should take into account for the predominate rupture direction in each sesimogenic zone. Hence, obtained circular smoothened sesmicity is further elliptical smoothened. The assumption taken here is that the earthquakes occur on faults or in fault zones of past earthquakes. The fault orientation can be suitably identified for each zone based on the information given in Figure 2.1. Then, the seismic activity rate is further smoothed according directions and the corresponding weighttages identified for the seismogenic zones. For this purpose, fault-rupture-oriented elliptical Gaussian smoothing is used as proposed in Lapajne *et al.* (2003) such that

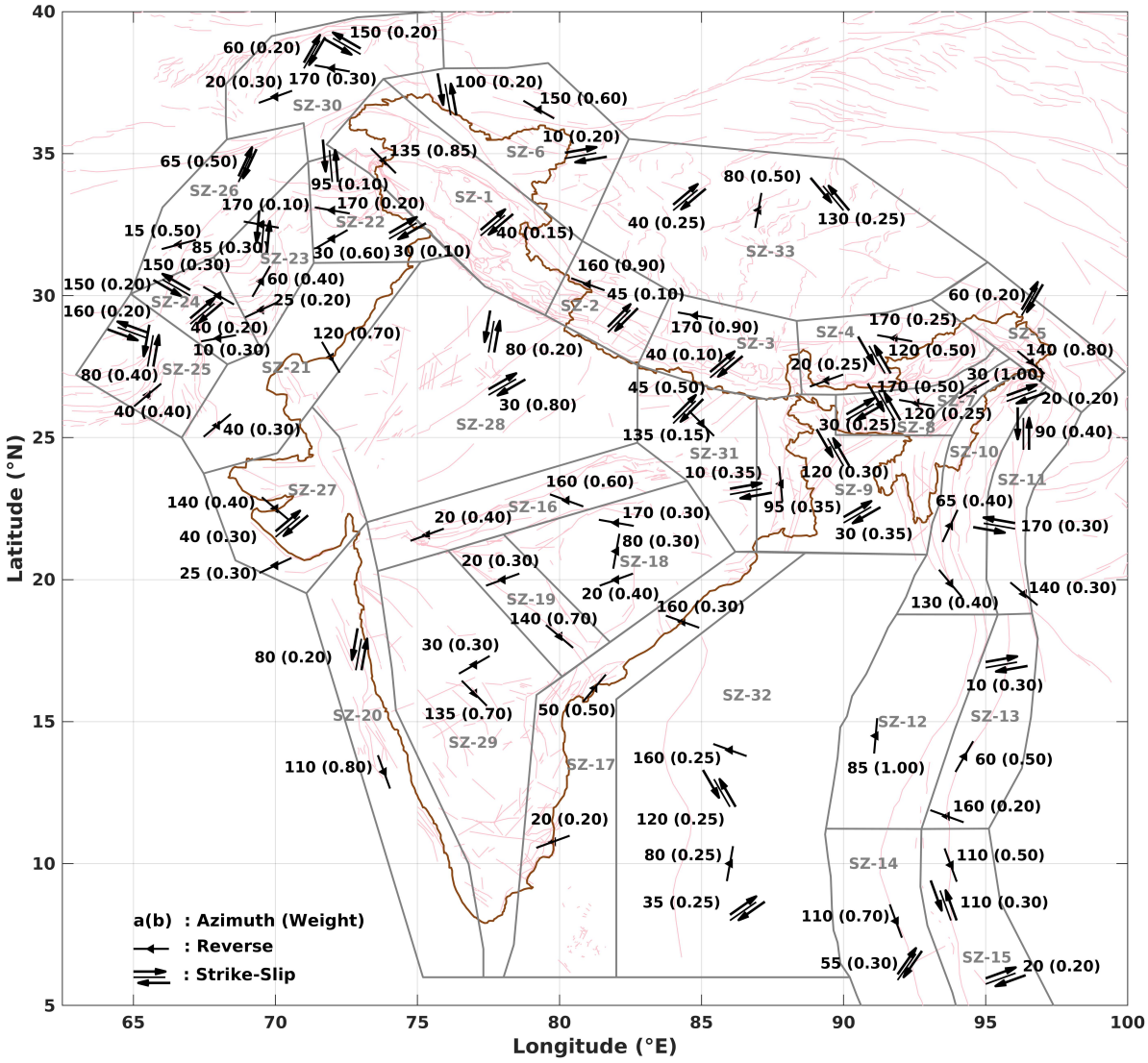

Figure 2.10: The major azimuth (angle with respect to horizontal measured anticlockwise) direction and corresponding focal mechanism along with respective weights in each of the seismogenic zones considered for the study region

$$n_{e(i)} = \frac{\sum_j n_j e^{-1/2\vec{\delta_{ij}}^T \mathbf{V}^T \mathbf{R} \mathbf{V} \vec{\delta_{ij}}}}{\sum_l e^{-1/2\vec{\delta_{il}}^T \mathbf{V}^T \mathbf{R} \mathbf{V} \vec{\delta_{il}}}} \tag{2.4}$$

where $n_{e(i)}$ is the number of earthquakes in grid points i estimated from elliptical smoothing. n_j is the circular smoothened seismicity value in grid point j, indices j and l denote all grid points with in the elliptical smoothing area around i^{th} grid identified based on the fault orientation. T means the transposition and the vector $\vec{\delta_{ij}}$defines the distance from cell i to cell j. The correlation matrix $\mathbf{R}$ is given by

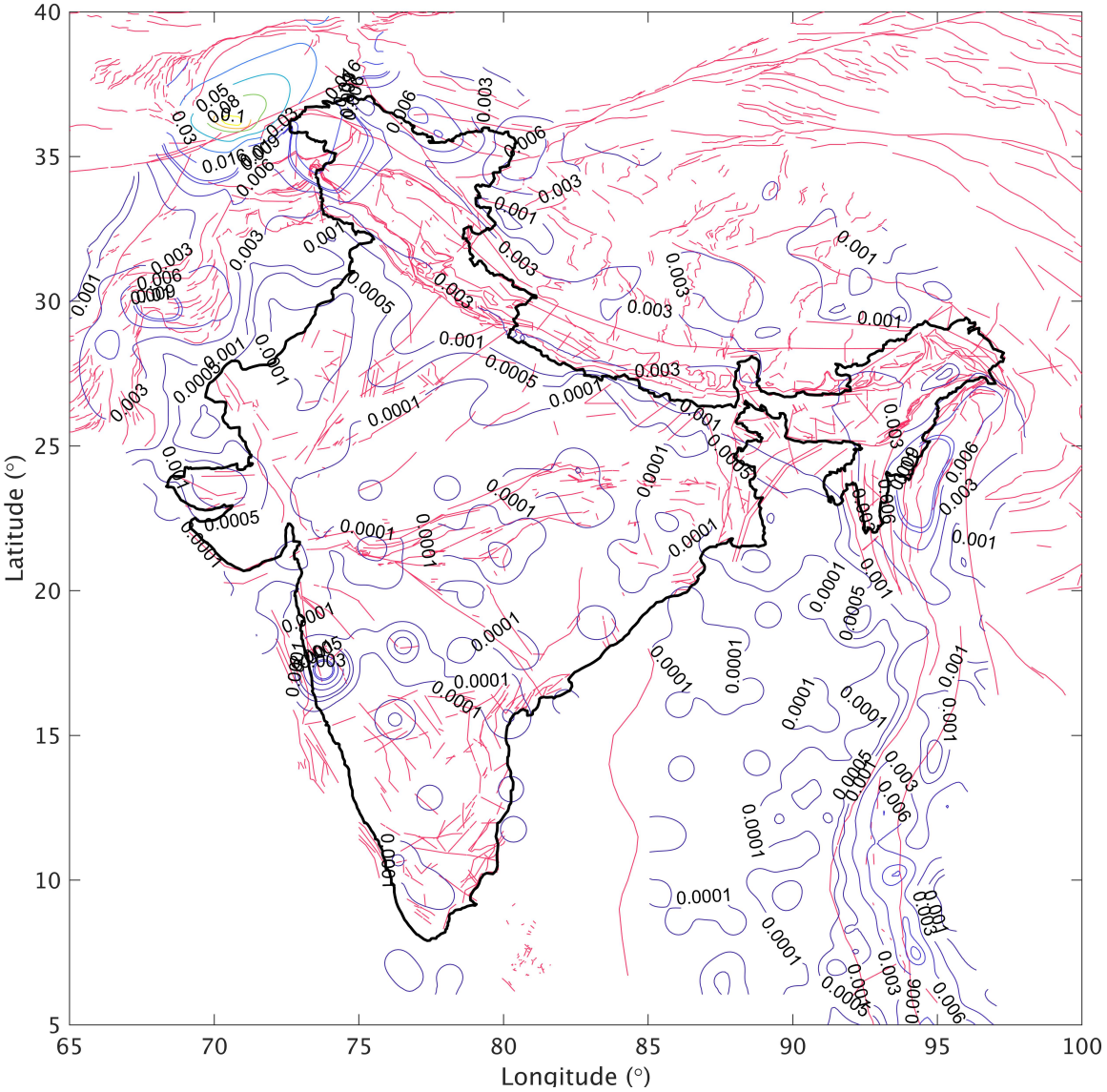

Figure 2.11: Elliptically smoothed seismic activity rate for the study region

$$\mathbf{R} = \begin{bmatrix} \frac{1}{\sigma^2} & 0 \\ 0 & \frac{1}{\tau^2} \end{bmatrix} \tag{2.5}$$

where, σ half the length of major principal axis of the ellipse is considered for smoothening and τ the corresponding value for the minor principal axis. Furthermore, these lengths are taken corresponding to the fault rupture possible per zone. The corresponding value can be estimated based on the maximum possible magnitude in each zone using suitable scaling relations like

$$log\ L = c_1 + c_2 M_{max} \tag{2.6}$$

where c_1 and c_2 are regression coefficients. The most widely used scaling relation to estimating rupture length is that proposed by Wells and Coppersmith (1994*b*). Here, for the reverse faulting mechanism the coefficients c_1 and c_2 take the values -2.86 and 0.63 respectively, and for strike-slip faulting mechanism the corresponding values are -3.55 and 0.74. The axis τ represents the width of rupture in each of seismogenic zones and is assumed to be proportional to length (L) such that $\tau = kL$ where $k < 1$. In the present study k is taken as 0.5 for reverse faulting mechanism and 0.25 for strike slip faulting mechanism considering the observation that the rupture influences area differences in fault normal direction for both the mechanisms. Furthermore, 'α' is the predominant fault orientation in each seismogenic zone. For the study region the corresponding estimates are arrived at based on the predominant angles determined based on the statistics by dividing the study region into $0.05^\circ \times 0.05^\circ$ grids and considering the available focal plane solutions (from ISC-GEM catalogue and Global CMT databases). The corresponding information is extracted for each of the 33 seismogenic zones considered in the study (Figure 2.1) The final azimuth directions along with the corresponding weights and mechanism for each of the 33 seismogenic zones in the region is summarized in Figure 2.10. Then matrix $\mathbf{V}$ is provided to transform the data according to the identified orientation (α) such that.

$$\mathbf{V} = \begin{bmatrix} cos\alpha & -sin\alpha \\ sin\alpha & cos\alpha \end{bmatrix} \tag{2.7}$$

The corresponding orientation ensures that the first principal axis of the ellipse is in line with the particular fault orientation identified for the zone. The corresponding elliptically smoothened seismic activity rate after performing smoothening in each of the grid points with in the zone with the consideration of zonal fault orientation, maximum earthquake magnitude, mechanism, and corresponding weights is shown in Figure 2.11. The overall pattern of seismic activity is observed to be similar to that obtained for circular smoothening. Whereby, relatively higher seismicity rate values are observed along the active parts of the study region. However, the results from the elliptically smoothed seismiciy is observed to orient along the prominent

fault directions. Thus it is seen that by utilizing this data in the hazard estimations the activity based on zonal characteristics, earthquake occurrence and fault orientations are included in the recurrence characterization. Thus, these can be suitably utilized to obtain reliable seismic hazard at any site with in the region.

Once the recurrence characteristics are obtained the next important aspect is the selection of suitable GMPEs for the region. A discussion on the development of suitable GMPEs for the region with a limited database and the global GMPE models which can be applied to the region are discussed in the next chapter.

Table 2.5: Seismicity parameters for thirty-two seismogenic zones of the study region using the updated catalogue (up to 2019 CE) using Kijko's approach.

Source No.	Zones	b value	Lambda(4)	Max. potential	No of earthquakes
SZ-1	Western Himalaya	0.89 ± 0.04	5.61	8.3	1153
SZ-2	Central Himalaya-I	0.77 ± 0.06	3.16	8.3	455
SZ-3	Central Himalaya-II	0.79 ± 0.06	2.89	8.3	477
SZ-4	Eastern Himalaya	0.72 ± 0.07	1.93	8.3	222
SZ-5	Mishmi Block	0.68 ± 0.06	3.49	8.6	221
SZ-6	Altya Tegh & Karakoram	0.92 ± 0.05	8.51	7.5	908
SZ-7	Naga Thrust	0.68 ± 0.16	0.35	6.8	37
SZ-8a	Shillong Plateau & Assam valley	0.75 ± 0.08	0.89	8	74
SZ-8b	valley	0.73 ± 0.08	0.91	6.5	124
SZ-9	Bengal Basin	0.76 ± 0.07	2.06	7.8	331
SZ-10	Indo-Burmese Arc	0.84 ± 0.04	13.90	7.8	1030
SZ-11	Shan-Sagaing Fault	0.70 ± 0.07	4.01	8.3	253
SZ-12	West Andaman-I	0.71 ± 0.06	3.57	8.2	225
SZ-13	East Andaman-I	0.64 ± 0.06	5.30	7	323
SZ-14	West Andaman-II	0.71 ± 0.04	3.32	8.2	145
SZ-15	East Andaman-II	0.63 ± 0.02	12.15	7.3	930
SZ-16	SONATA	0.64 ± 0.16	0.40	6.6	36
SZ-17	Eastern Passive Margin	0.86 ± 0.15	0.30	6.4	58
SZ-18	Mahanandi Graben & Eastern Craton	0.75 ± 0.19	0.29	6	16
SZ-19	Godavari Graben	0.86 ± 0.20	0.16	6.3	10
SZ-20	Western Passive Margin	0.91 ± 0.12	0.48	6.5	155
SZ-21	Sindh-Punjab	0.84 ± 0.11	0.81	6.5	115
SZ-22	Upper Punjab	1.03 ± 0.08	2.23	7.8	292
SZ-23	Koh-e-Sulaiman	0.90 ± 0.06	5.82	8	510
SZ-24	Quetta-Sibi	0.80 ± 0.07	4.00	8	378
SZ-25	Southern Baluchistan	0.77 ± 0.08	3.76	8	306
SZ-26		0.96 ± 0.06	6.90	7.8	744
SZ-27a	Gujarat Region	0.88 ± 0.11	0.68	8.2	71
SZ-27b		0.88 ± 0.13	0.24	6.3	34
SZ-28a	Aravali-Bundelkhand	0.88 ± 0.12	0.55	6.6	72
SZ-28b		0.84 ± 0.12	0.38	6.3	79
SZ-29	Southern Craton	1.11 ± 0.16	0.36	6.3	67
SZ-30	Hindukush and Pamirs	0.96 ± 0.02	80.39	8.3	7835
SZ-31	Gangetic region	0.87 ± 0.17	0.19	6.8	35
SZ-32	Bay of Bengal	0.60 ± 0.14	0.94	6.6	62
SZ-33	Tibet region	0.87 ± 0.05	18.28	8	1065

Table 2.6: Comparison on recurrence parameter values estimated from Kijko's method and Weichert (1980) methods

Source No.	Kijko's method			Weichert (1980) method		
	b value	std(b value)	Lambda(4)	b value	std(b value)	Lambda(4)
SZ-1	0.82	0.02	6.33	0.89	0.04	5.61
SZ-2	0.81	0.03	5.89	0.77	0.06	3.16
SZ-3	0.78	0.03	5.80	0.79	0.06	2.89
SZ-4	0.71	0.04	5.17	0.72	0.07	1.93
SZ-5	0.82	0.05	5.62	0.68	0.06	3.49
SZ-6	0.98	0.03	6.89	0.92	0.05	8.51
SZ-7	0.72	0.11	4.45	0.68	0.16	0.35
SZ-8a	0.76	0.08	4.89	0.75	0.08	0.89
SZ-8b	0.67	0.05	4.79	0.73	0.08	0.91
SZ-9	0.69	0.03	5.27	0.76	0.07	2.06
SZ-10	0.97	0.03	6.90	0.84	0.04	13.90
SZ-11	0.76	0.04	5.43	0.70	0.07	4.01
SZ-12	0.81	0.05	5.59	0.71	0.06	3.57
SZ-13	0.79	0.04	5.66	0.64	0.06	5.30
SZ-14	0.82	0.06	5.45	0.71	0.04	3.32
SZ-15	0.84	0.03	6.31	0.63	0.02	12.15
SZ-16	0.69	0.10	4.30	0.64	0.16	0.40
SZ-17	0.80	0.10	4.98	0.86	0.15	0.30
SZ-18	0.76	0.17	4.25	0.75	0.19	0.29
SZ-19	0.92	0.28	4.66	0.86	0.20	0.16
SZ-20	0.86	0.07	5.64	0.91	0.12	0.48
SZ-21	0.76	0.06	5.10	0.84	0.11	0.81
SZ-22	0.83	0.04	5.78	1.03	0.08	2.23
SZ-23	0.91	0.04	6.36	0.90	0.06	5.82
SZ-24	0.81	0.04	5.81	0.80	0.07	4.00
SZ-25	0.85	0.05	5.90	0.77	0.08	3.76
SZ-26	0.98	0.04	6.81	0.96	0.06	6.90
SZ-27a	0.63	0.07	4.36	0.88	0.11	0.68
SZ-27b	0.64	0.10	4.11	0.88	0.13	0.24
SZ-28a	0.78	0.08	4.99	0.88	0.12	0.55
SZ-28b	0.71	0.07	4.72	0.84	0.12	0.38
SZ-29	0.78	0.09	4.93	1.11	0.16	0.36
SZ-30	1.04	0.01	8.06	0.96	0.02	80.39
SZ-31	0.70	0.11	4.35	0.87	0.17	0.19
SZ-32	0.73	0.08	4.72	0.60	0.14	0.94
SZ-33	0.86	0.02	6.45	0.87	0.05	18.28

CHAPTER 3

Ground Motion Prediction Equation

3.1 Introduction

Ground motion prediction equations (GMPE) are essential in understanding the regional characteristic of seismic waves and resultant hazards. However, it is challenging to estimate reliable GMPE, especially in regions with sparse recorded data. Many researchers utilize the recorded data to develop GMPEs (Douglas, 2018). But reliability and applicability of these GMPEs are limited to the data used in the modelling. Additionally, the most commonly adopted method for such regions with sparse recorded data is by resorting to a synthetic database (Iyengar and Raghukanth, 2004). In that case, also the results will be biased towards the input parameters used in the simulations as well as on the other computational limitations of the methodology used in generating database. Furthermore, it is well known that accounting for all the inhomogeneities exhibited in the process of generation and propagation of seismic waves is computationally very expensive. Thus the best representatives of the region's ground motion characteristics are the recorded ground motion databases. Taking this into consideration, Campbell (2003) proposed a hybrid empirical technique, where modification factors for Western North American records are estimated, to scale the records to Eastern North America which is having relatively fewer records. These factors are estimated using the regional seismological model parameters reported in the literature. Similar studies have been reported in Tavakoli and Pezeshk (2005); Pezeshk *et al.* (2011). One can observe that the modification factors are obtained using stochastic seismological model approach and hence the estimates are affected by the uncertainty regarding the parameters chosen in estimating the ground motion transfer function. Recently, there are numerous researches pointing to the efficiency of artificial neural network in handling the complex ground motion characteristics (Derras *et al.*, 2014; Dhanya and Raghukanth, 2018). It is observed that the neural network based ground motion prediction can adapt all the features of ground motion with minimum number of unknowns and lesser

standard deviation. However, effectiveness of neural network based approaches in handling regions with sparse records is not discussed in literature.

In India, Himalayan mountain ranges which are formed from the Indo-Eurasian subduction are seismically very active due to the continuous tectonic movements. The vulnerability in the region is also high due to the proximity of several mega-cities including the capital city Delhi to these seismically active faults. However, the seismic instrumentation got commissioned for the region only in the recent decades and hence there is only limited recorded information. Owing to the sparsity in recorded data, Sharma *et al.* (2009) combined the available ground motion record for the Himalayas with the Zagros region of Iran having a similar geological regime and utilized the data for the prediction of spectral acceleration. The results are only based on 6 Indian and 10 Iranian events. Moreover, as all the ground motion records are considered together, one cannot avoid the possibility of results getting biased to the data from Zagros used in developing the model. In another direction, Natural Disaster Management Agency (NDMA, 2010), Raghukanth and Kavitha (2014) used simulation based approaches to predict GMPE for spectral accelerations for India. It should be noted that these GMPEs are valid for only at rock type soil condition. Hence, the application of the model to Himalayas and adjoined regions constituting a wide range of geological characteristics is limited. To address local site conditions typically modification factor and scaling are proposed in literature (IBC, 2015). However, the methodology adopted is based on equivalent linear site responses and hence the 3D scattering of wave is not accounted for in models.

3.2 Ground motion database

The database for Western Himalayas and North-Eastern India is obtained from records available in COSMOS (Consortium of Organizations for Strong-Motion Observation Systems, `https://strongmotioncenter.org/`) and PESMOS(Program for Excellence in Strong-Motion Studies) networks. Additionally, ground motions records provided by CESMD (Center for Engineering Strong Motion Data) for the 2015 Mw 7.8 Nepal earthquake and its aftershocks and records from 14 stations in IG-Basin during the main-event recorded by the CIGN (Central Indo-Gangetic Plains network) (Chadha *et al.*, 2015) are included in the database. The recorded

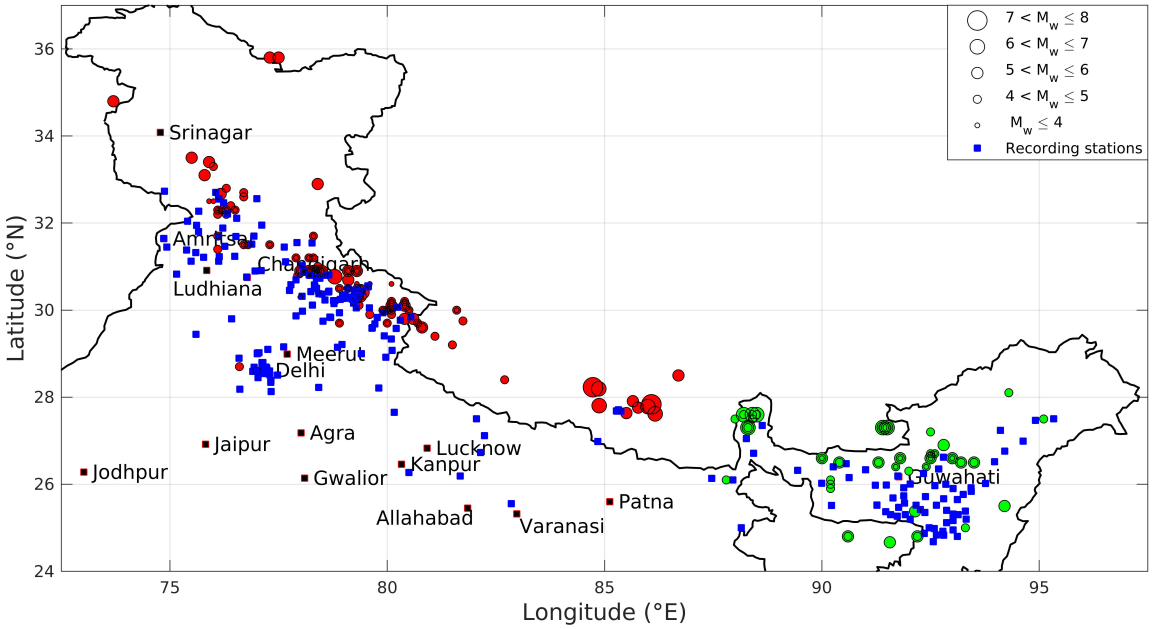

Figure 3.1: Spatial Distribution of the events along with recording stations (blue squares) for Western Himalayas and North Eastern India in the period 1986-2017 considered for the analysis performed in this work along with the location of some major cities in the region [Note: Circles filled with red color indicate the Western Himalayan events and those filled with green color indicate North Eastern Indian events]

data is segregated into Western Himalayas and North-Eastern India owing to the variabilities associated with the geological and tectonic conditions in both regimes. The distribution of events along with the recording stations is illustrated in Figure 3.1. The distribution consists of 108 events in the magnitude range Mw 3-7.8 in the Western Himalayan region and 38 events with Mw 4-6.8 in North-Eastern India during the period 1986-2017. It is clear from the figure that the recording stations are spread over a larger domain, which constitutes the Indo-Gangetic basin. It should be noted that the hypocentral depths of Western- Himalayan events range from 2-80 km whereas that of North-Eastern Indian events vary between 5-56 km. It should also be noted here that the events from the Indo-Burmese region are not considered in the present study owing to the variability associated with the tectonic characteristic attributed from deep subduction events. Thus, there are a total of 374 records for Western Himalayas and 124 records for North-Eastern India. Among the events in Western Himalayas, 8 (45 records) are strike-slip event , 98 (322 records) are with reverse mechanism and 1 (1 record) with normal faulting mechanism. For North Eastern India the corresponding tally is 21 (67 records), 16 (56 records) and 1(1 record) respectively. Note that the events are sorted into different faulting mechanisms

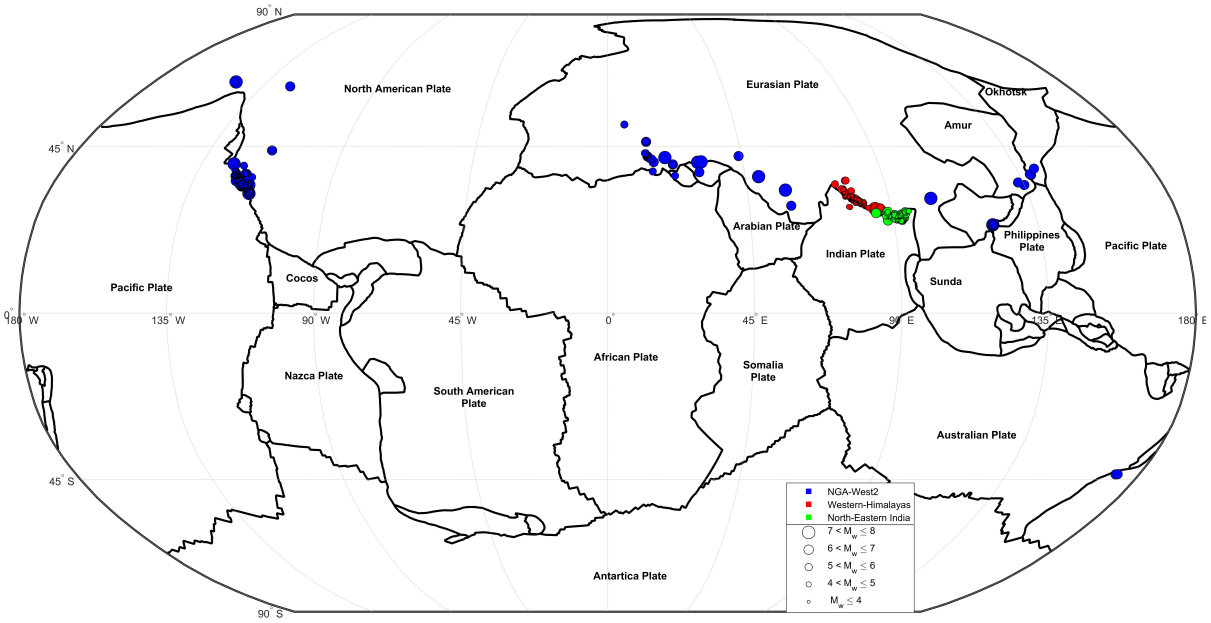

Figure 3.2: Spatial Distribution of the events considered for developing Artificial Neural Network based Ground motion Prediction Equations [Note: Color is given to differentiate the events in different regions]

based on the rake angle. The available records for Western Himalayas from the sites with V_{s30} between 167 to 828 m/s and for North-Eastern India between 150 to 840 m/s It should be noted that the processing of the recorded data is performed as per the study of Gupta (2018). Furthermore, 5% damped rotd50 horizontal spectra, which corresponds to the median values for response spectra of a ground motion when rotated over all horizontal orientations between 0° and 180°, is taken for analysis in this work. The distribution of the database with respect to magnitude and distance is illustrated in Figure 3.3. It is clear from the figure that the available data for the region is not comprehensive having a considerable gap between the records. A suitable way to address this issue is to combine the available data with a more comprehensive database. In this study, we chose to combine the available data for the region with well tested NGA West2 database. The choice is judicial as NGA-West2 also comprises of data from active regions similar to the region under consideration. We sorted out 13294 records from the reported 21540 records in the database based on data quality analysis as reported in Dhanya and Raghukanth (2018). Thus the database considered in the model is from 286 events, the

distribution of these events along with that for Western Himalayas and North-Eastern India is shown in Figure 3.2. Among the events considered 179 (7851 records) from strike-slip, 69 (3100 records) from reverse and 38 (318 records) from normal faulting mechanisms. From the distribution shown in Figure 3.3, it is evident that the NGA West2 database covers a broader and more comprehensive range of records in comparison with that available for regions under study. Thus it can be seen that NGA-West 2 is a suitable candidate, especially in models based on data-driven methods for ascertaining the ground motion features. This information can be suitably combined with regions with sparse records to arrive a more efficient GMPE as discussed further.

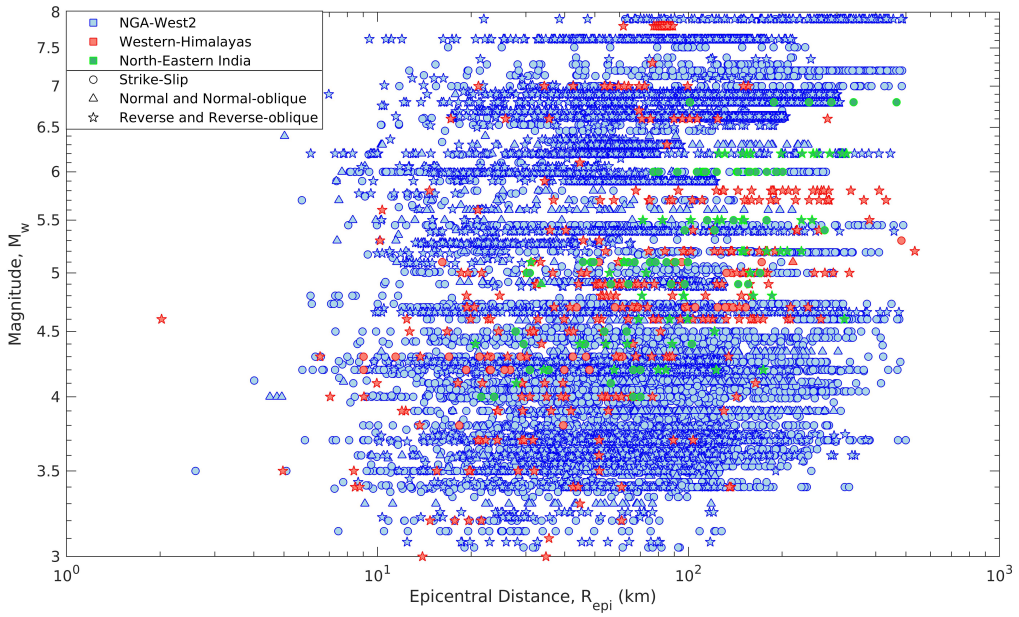

Figure 3.3: Distribution of ground motion records with respect to Magnitude (M_w) and Epicentre distance (R_{epi}) corresponding data available form NGA West2 database and that form PESMOS and COSMOS for Western Himalayas and North-Eastern India

3.3 Hybrid Ground motion Prediction Equation for Western Himalayas and North Eastern India

The hybrid ground motion prediction equation idea postulated from this study is to combine the records from regions with sparse data along with that from the more comprehensive database

Table 3.1: Weights and bias between the input and the hidden layer

Weights	**Input parameter** (i)	**Number of hidden neurons (k)**					
		1	2	3	4	5	6
$W_{ik,1}$	M_w	-0.859	-0.933	-0.892	-0.817	0.682	-0.902
	$\log_{10}(V_{s30})$	0.239	0.078	0.126	0.240	-0.338	0.306
	R_{epi}	10.082	-2.429	-2.487	0.006	1.024	0.027
	$\log_{10}(R_{epi})$	-1.504	7.880	8.514	0.350	0.348	0.309
	F_{mech}	-0.111	0.138	0.156	0.027	-0.052	0.034
	F_{loc}	-0.342	1.771	1.939	0.227	-0.144	0.320
$bias_{k,1}$		9.451	-4.097	-4.234	-0.977	0.871	-1.329

and segregate with regional flags. The formulation chosen for the ground motion prediction can be represented as follows:

$$\begin{bmatrix} log_{10}(PA) \\ log_{10}(Sa_{0.01s}) \\ log_{10}(Sa_{0.02s}) \\ \vdots \\ log_{10}(Sa_{4.00s}) \end{bmatrix} = f(M_w,\, log_{10}(V_{s30}),\, R_{epi},\, log_{10}(R_{epi}),\, F_{mech}, F_{loc}) \tag{3.1}$$

where, PA represents peak acceleration, Sa denotes spectral acceleration, M_w the moment magnitude,V_{s30} the shear wave velocity from top 30m of the soil, R_{epi} the epicentral distance, F_{mech} represents the flag for faulting mechanism (1 for strike-slip, 2- normal and 3- reverse mechanisms) and F_{loc} represents the regional flag. It should be noted that F_{loc} = 1 is given for records from the NGA-West2 database, 2 for those from Western Himalayas and 3 for those from North-Eastern India. The network architecture considered for the modelling is shown in Figure 3.4. The number of hidden nodes is taken after proper trial and error between the size of the input and output layers and less than twice the size of input nodes as suggested by Berry and Linoff (1997). A minimum of six hidden nodes is found ideal for the data under consideration. Here, tanh function is used between the input and hidden nodes and linear function between the hidden and output nodes. The resultant functional form for ground motion prediction can be represented as

Table 3.2: Weights and bias values between the hidden and output layer

Weights	**Output parameter** (j), $\log_{10}(.)$	**Number of hidden neurons (k)** 1	2	3	4	5	6	**bias**$_{j,2}$
$W_{jk,2}$	PA	-0.065	1.444	-1.289	-5.149	-0.296	5.490	1.581
	$Sa_{0.01s}$	-0.065	1.442	-1.288	-5.145	-0.297	5.491	1.585
	$Sa_{0.02s}$	-0.065	1.440	-1.285	-5.167	-0.299	5.526	1.600
	$Sa_{0.03s}$	-0.063	1.411	-1.260	-5.194	-0.301	5.624	1.652
	$Sa_{0.04s}$	-0.059	1.392	-1.246	-5.265	-0.308	5.782	1.731
	$Sa_{0.05s}$	-0.055	1.404	-1.257	-5.332	-0.315	5.907	1.796
	$Sa_{0.06s}$	-0.050	1.409	-1.266	-5.332	-0.318	5.934	1.819
	$Sa_{0.075s}$	-0.045	1.443	-1.300	-5.310	-0.323	5.901	1.816
	$Sa_{0.09s}$	-0.044	1.476	-1.330	-5.210	-0.320	5.745	1.759
	$Sa_{0.10s}$	-0.044	1.480	-1.333	-5.043	-0.312	5.507	1.652
	$Sa_{0.15s}$	-0.058	1.598	-1.435	-4.837	-0.301	5.070	1.476
	$Sa_{0.20s}$	-0.076	1.664	-1.490	-4.647	-0.282	4.652	1.239
	$Sa_{0.30s}$	-0.104	1.658	-1.482	-4.356	-0.238	4.089	0.939
	$Sa_{0.40s}$	-0.133	1.626	-1.456	-4.298	-0.201	3.895	0.820
	$Sa_{0.50s}$	-0.148	1.527	-1.370	-4.152	-0.165	3.684	0.718
	$Sa_{0.60s}$	-0.163	1.462	-1.313	-4.152	-0.138	3.657	0.657
	$Sa_{0.70s}$	-0.169	1.372	-1.235	-4.072	-0.112	3.576	0.590
	$Sa_{0.75s}$	-0.177	1.374	-1.238	-4.168	-0.106	3.654	0.599
	$Sa_{0.80s}$	-0.180	1.380	-1.244	-4.223	-0.099	3.711	0.624
	$Sa_{0.90s}$	-0.187	1.349	-1.220	-4.236	-0.082	3.725	0.602
	$Sa_{1.00s}$	-0.192	1.314	-1.190	-4.263	-0.069	3.757	0.610
	$Sa_{1.20s}$	-0.197	1.186	-1.080	-4.255	-0.039	3.824	0.638
	$Sa_{1.50s}$	-0.208	1.070	-0.979	-4.437	-0.008	4.099	0.747
	$Sa_{2.00s}$	-0.205	0.869	-0.805	-4.521	0.027	4.372	0.860
	$Sa_{2.50s}$	-0.206	0.792	-0.746	-4.614	0.049	4.625	0.959
	$Sa_{3.00s}$	-0.198	0.714	-0.682	-4.668	0.065	4.818	1.066
	$Sa_{4.00s}$	-0.191	0.609	-0.598	-5.037	0.091	5.449	1.335

$$Y_j = bias_{j,2} + \sum_{k=1}^{m} W_{jk,2} \left(\frac{1 - exp\left(-2\left(bias_{k,1} + \sum_{i=1}^{n} W_{ik,1} X_i\right)\right)}{1 + exp\left(-2\left(bias_{k,1} + \sum_{i=1}^{n} W_{ik,1} X_i\right)\right)} \right) \tag{3.2}$$

where, Y_j represents the values for output parameter, X_i represents the input parameters, $W_{ik,1}$ and $bias_{k,1}$ represents the weights and biases between the input and hidden nodes and $W_{jk,2}$ and $bias_{j,2}$ are the connection weight and biases between hidden and output nodes, n is the number of input nodes and m is the number of hidden nodes respectively. In the network architecture chosen for the study n=m=6. It should be noted that the choice of tanh function for the model

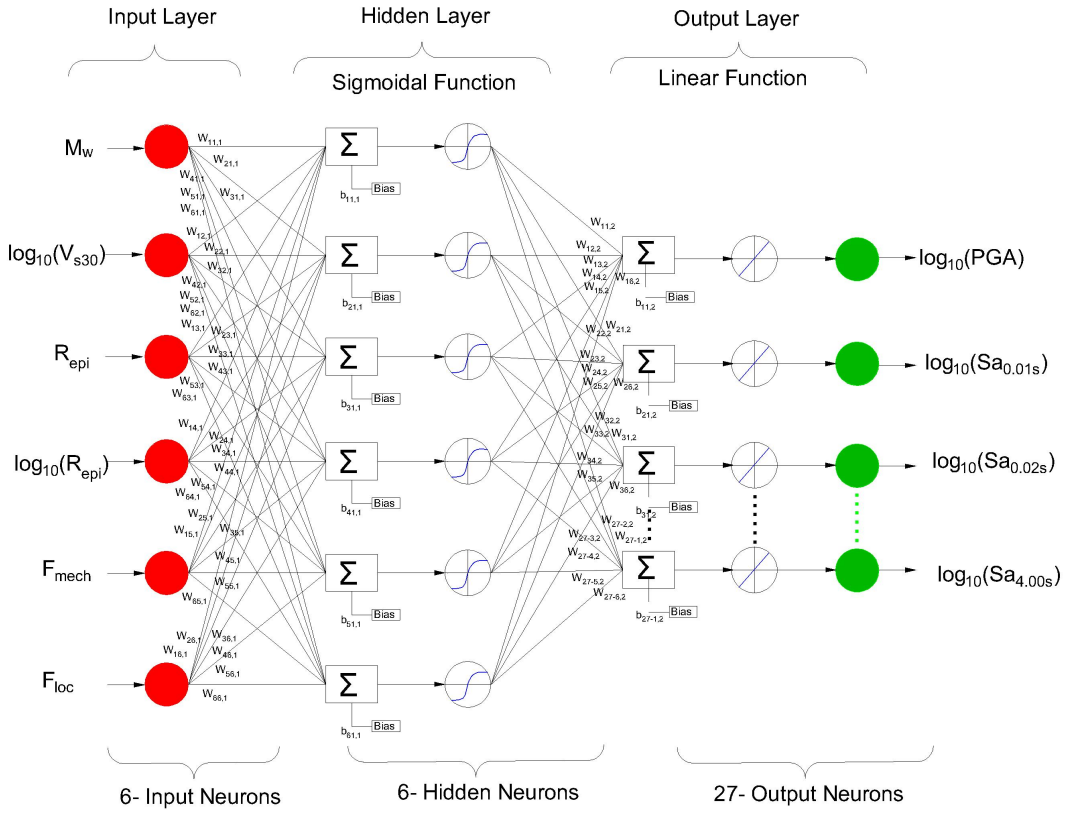

Figure 3.4: Artificial Neural Network (ANN) architecture considered for developing the Ground Motion Prediction Equations (GMPE) for the region

is because the problem belongs to regression analysis. Further, the input and output parameters are scaled between -1 and $+1$ such that

$$Y = a\,(Y - y_{min}) + x_{min} \quad \text{where} \quad a = \frac{x_{max} - x_{min}}{y_{max} - y_{min}} \tag{3.3}$$

where, $x_{min} = -1$ and $x_{max} = +1$, and y_{min} and y_{max} corresponds to the minimum and maximum value of the parameter that need to be mapped. In total there are 231 unknowns to predict spectral accelerations at 27 periods for 3 regions taken for the study. The network is trained using Ga-ANN methodology as proposed by Dhanya and Raghukanth (2018). Thus Ga algorithm is used for initializing the weights and further training is performed based on Levenberg-Marquardt(LM) technique. To ensure the predictive capacity of the model the data

is divided as 70% for training 15% for validation 15% for testing. The corresponding random distribution is done such as representative sample of each region are equally distributed in all sets without overlap. Further, the residual analysis is performed following the mixed effect regression procedure as proposed by Abrahamson and Youngs (1992). The resultant weights and biased obtained after the training process for the database under consideration is summarized in Table 3.1 for that between input and hidden nodes and that between hidden and output nodes are summarised in Table 3.2. The next step in modelling is to ascertain how good are the prediction. The details of performance analysis are summarized in the following section

Furthermore, it is important to estimate the standard deviation of the residues. The corresponding values are important in quantifying the uncertainties in hazard estimations. It is known that the earthquake records show variability between events and within events. Hence it is more acceptable to split the obtained residues into inter (η_i) and intra (ε_{ij}) event residuals. The corresponding functional form can be expressed as:

$$log_{10}\hat{\mathbf{Y}} = f(M_w,\, V_{s30},\, R_{epi},\, F_{mech},\, F_{loc},\, W,\, b) + \eta_i + \varepsilon_{ij} \tag{3.4}$$

where i indicate the event and j represent the recording at j^{th} station for the i^{th} event and f(.) is the mean prediction. As the proposed GMPE has interconnected nodes the best way to estimate residuals is through a mixed effect algorithm proposed by Abrahamson and Youngs (1992). The algorithm is applied similar to that explained in Dhanya and Raghukanth (2018). The corresponding procedure is briefed for better clarity. Here, first estimate the initial weights and biases using the fixed effect regression technique for the data and functional form under consideration. Then, estimate τ^2 and ϕ^2 using the weights and biases employing maximizing the likelihood using equation (7) of Abrahamson and Youngs (1992). Further, estimate the random inter-event term η_i using equation (10) in Abrahamson and Youngs (1992). Estimate new weights and biases for $\left(log_{10}\left(\hat{\mathbf{Y}} - \eta_i\right)\right)$. Repeat the procedure till the likelihood in the second step is maximized. Following this procedure inter and intra event residuals are extracted for the developed model and the corresponding values are summarized in Table 3.3 for Western Himalayas and North-Eastern India separately. It can be observed that the regional level standard deviations is in the range of 0.302 to 0.498, which are less or almost of the same order in comparison with that available in literature (Sharma *et al.*, 2009; Raghukanth and Kavitha, 2014).

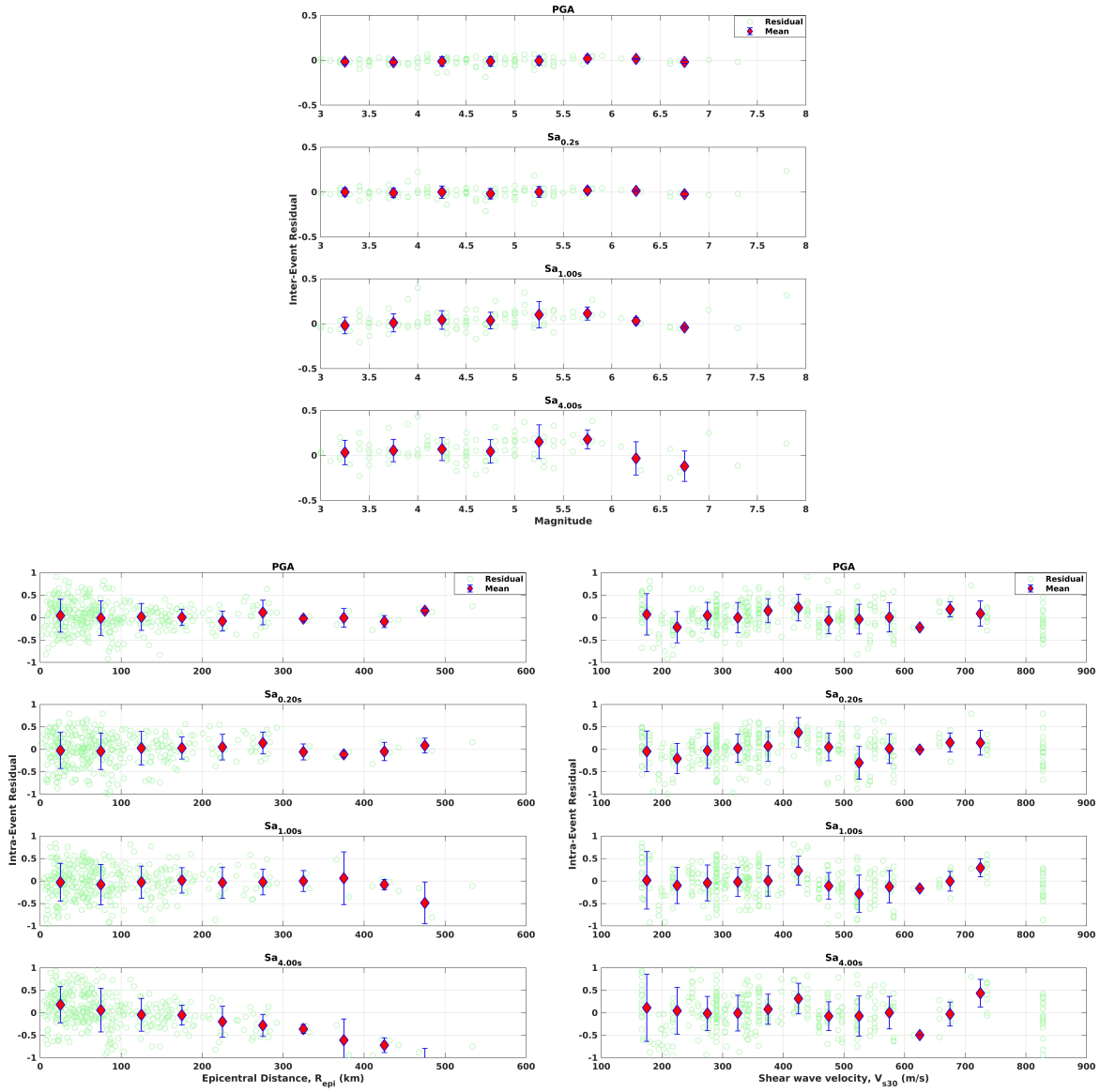

Figure 3.5: Inter-Event Residual with respect to moment magnitude (M_w) and Intra-Event Residual with respect to epicentral distance (R_{epi}) and Shear wave velocity (V_{s30})corresponding to PA (T = 0s), Sa at T = 0.20s, 1.00s and 4.00s considering events at Western Himalayas.

Furthermore, to check for any bias with the input variables, the variation of inter event residue with magnitude and intra event residue with epicentral distance and shear wave velocity. The corresponding plots for the Western Himalayan region is shown Figures 3.5 and that corresponding to records from North-Eastern India is Illustrated in Figures 3.6. It is evident from the all these illustrations that the residual distribution pattern that the developed ANN model is unbiased for the regional records. Furthermore, it would be interesting to check whether the

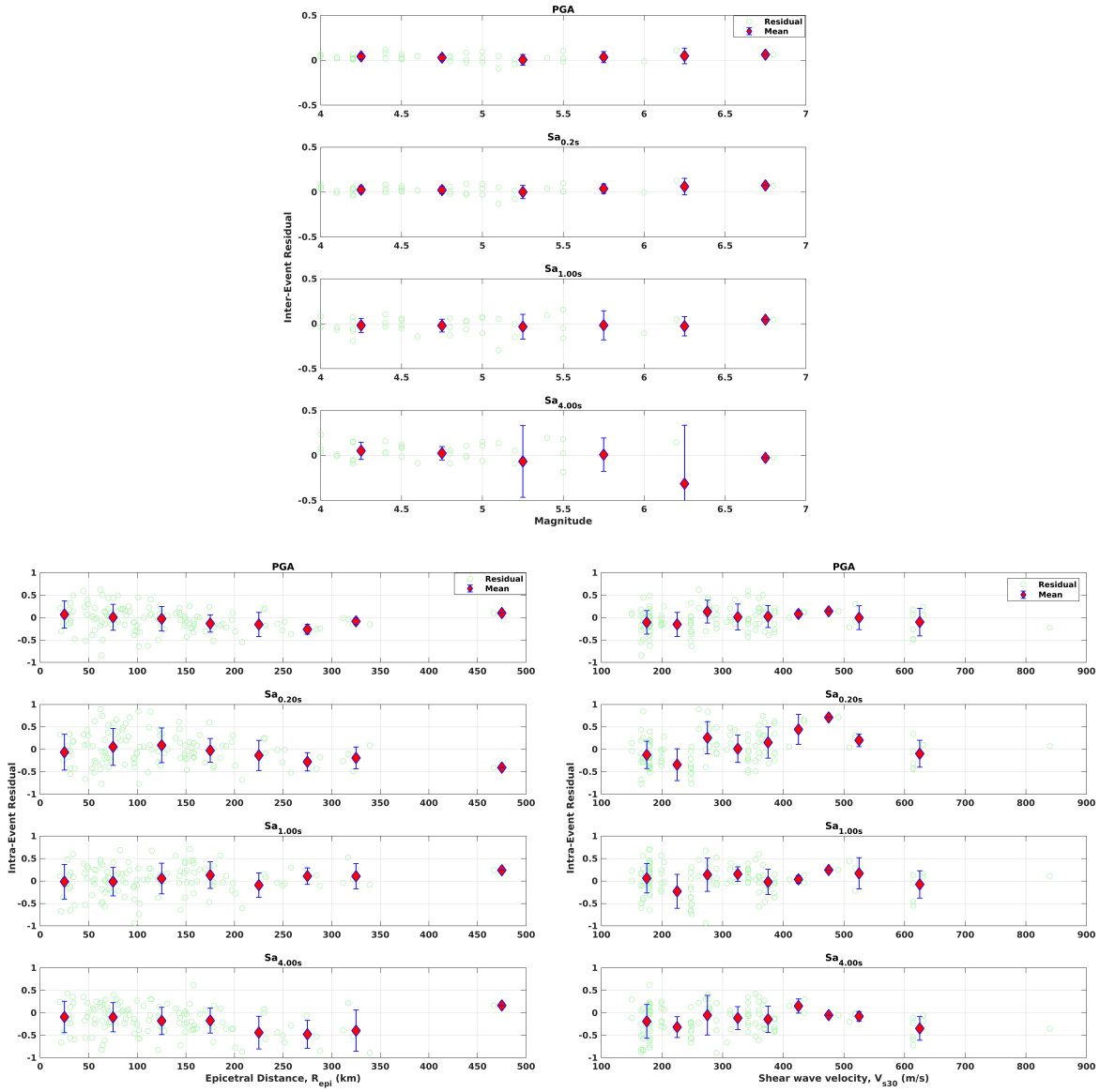

Figure 3.6: Inter-Event Residual with respect to moment magnitude (M_w) and Intra-Event Residual with respect to epicentral distance (R_{epi}) and Shear wave velocity (V_{s30})corresponding to PA (T = 0s), Sa at T = 0.20s, 1.00s and 4.00s considering events at North-Eastern India.

regional level ground motion prediction equation can capture all known attenuation features of seismic waves. Hence, spectral acceleration is estimated for varying magnitude, distance, shear wave velocity, and fault mechanisms as shown in Figure 3.7 for Western-Himalayas and North-Eastern India. It can be noted by comparing the figures that the amplitudes are different for both the regions. However, both regions can exhibit general ground motion patterns. Whereby, with distance, the amplitudes are reduced and the peak period is shifting towards

Table 3.3: Standard deviations of the residuals (aleatory uncertainty) in the developed ANN model considering separately the records at Western Himalayas and North-Eastern India

	Western Himalaya			North-Eastern India		
Parameter	Inter-Event τ ($\log_{10}$ units)	Intra-Event ϕ ($\log_{10}$ units)	Total σ($\log_{10}$ units)	Inter-Event τ ($\log_{10}$ units)	Intra-Event ϕ ($\log_{10}$ units)	Total σ($\log_{10}$ units)
PA	0.053	0.340	0.344	0.044	0.270	0.274
$Sa_{0.01s}$	0.055	0.343	0.347	0.044	0.270	0.274
$Sa_{0.02s}$	0.112	0.334	0.353	0.095	0.264	0.281
$Sa_{0.03s}$	0.060	0.350	0.355	0.046	0.273	0.277
$Sa_{0.04s}$	0.067	0.354	0.360	0.048	0.276	0.280
$Sa_{0.05s}$	0.071	0.350	0.357	0.051	0.283	0.288
$Sa_{0.06s}$	0.071	0.348	0.355	0.056	0.283	0.288
$Sa_{0.075s}$	0.068	0.341	0.348	0.054	0.291	0.296
$Sa_{0.09s}$	0.066	0.340	0.346	0.055	0.295	0.301
$Sa_{0.10s}$	0.066	0.340	0.347	0.054	0.287	0.292
$Sa_{0.15s}$	0.062	0.361	0.366	0.048	0.298	0.302
$Sa_{0.20s}$	0.060	0.373	0.378	0.051	0.373	0.376
$Sa_{0.30s}$	0.062	0.402	0.407	0.049	0.353	0.356
$Sa_{0.40s}$	0.068	0.396	0.402	0.047	0.327	0.330
$Sa_{0.50s}$	0.075	0.399	0.406	0.058	0.320	0.325
$Sa_{0.60s}$	0.085	0.403	0.412	0.063	0.321	0.327
$Sa_{0.70s}$	0.097	0.416	0.427	0.072	0.322	0.330
$Sa_{0.75s}$	0.101	0.399	0.412	0.076	0.312	0.321
$Sa_{0.80s}$	0.105	0.410	0.423	0.078	0.320	0.330
$Sa_{0.90s}$	0.110	0.393	0.408	0.087	0.307	0.319
$Sa_{1.00s}$	0.115	0.401	0.418	0.094	0.322	0.335
$Sa_{1.20s}$	0.126	0.386	0.406	0.111	0.317	0.336
$Sa_{1.50s}$	0.135	0.394	0.417	0.128	0.323	0.348
$Sa_{2.00s}$	0.144	0.383	0.409	0.160	0.332	0.369
$Sa_{2.50s}$	0.146	0.408	0.434	0.179	0.307	0.356
$Sa_{3.00s}$	0.147	0.399	0.425	0.199	0.348	0.401
$Sa_{4.00s}$	0.153	0.440	0.466	0.235	0.334	0.409

longer periods. Thus from the illustrations, it is can be seen that the developed ANN model is unbiased and capable of capturing the known ground motion patterns.

3.4 Ground motion Prediction Equations for India

The list of GMPEs developed for India which are used in the present work along with their characteristics are discussed further

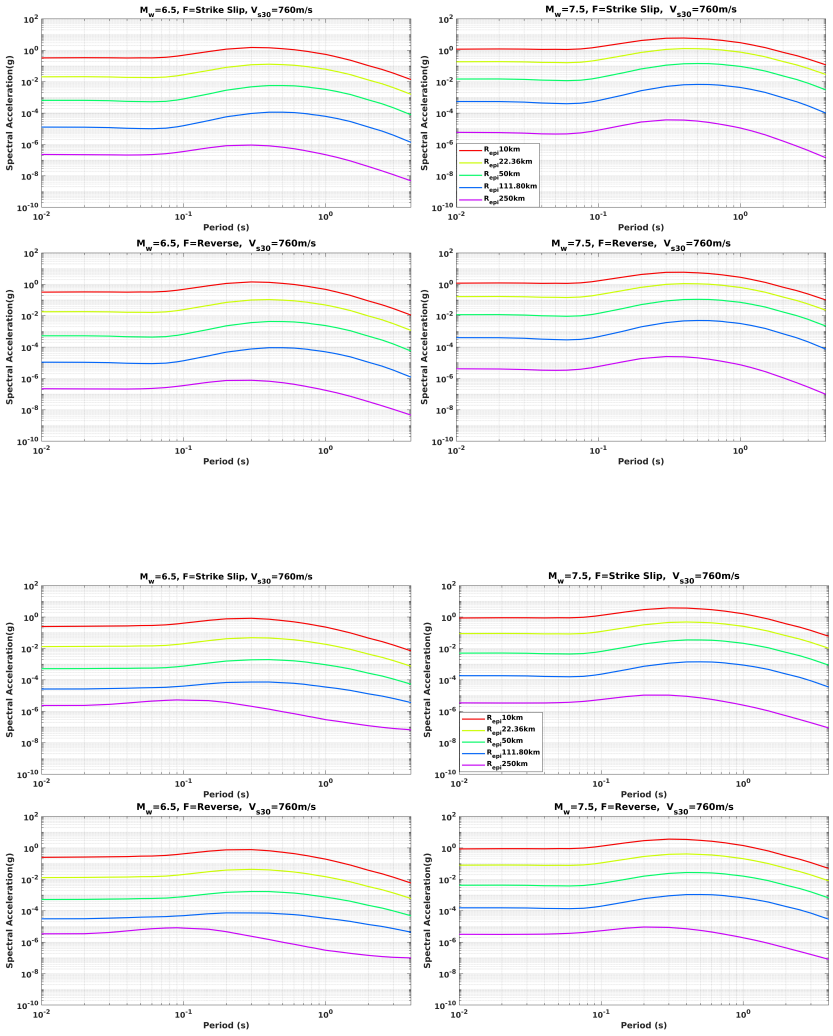

Figure 3.7: Attenuation characteristics of spectral acceleration with respect to epicentral distance (R_{epi}) corresponding to GMPE developed for [top] Western Himalayas [bottom] North-Eastern India

1. NDMA (2010) reported GMPEs for seven regions in India namely Himalaya, North-East India, Indo-gangetic, Gujarat, Central India, Peninsular India and Andaman-Nicobar for A type Soil Class based on synthetic database generated using seismological model. The functional form of corresponding equation to predict Spectral Acceleration (S_a) is as follows

$$ln\left(\frac{S_a}{g}\right) = C_1 + C_2M + C_3M^2 + C_4R + C_5ln\left(R + C_6e^{C_7M}\right) + C_8log_{10}(r)f_0 + ln(\epsilon)$$
$$f_0 = max(ln(r/100), 0) \tag{3.5}$$

Where M is magnitude, R is hypo-central distance andC_* are the corresponding coefficients. The attenuation of GMPE with distance for the regions is illustrated in Figure

2. Singh *et al.* (2017)developed GMPE for Indo-Gangetic Basin based on the 2015 Nepal earthquake and its after shocks. The corresponding functional form is as follows

$$ln(y) = C_1 + C_2 M + C_3 ln\left[\frac{E_1(C_4 R) - E_1(C_4\sqrt{R^2 + r_0^2})}{r_0^2}\right] \tag{3.6}$$
$$r_0^2 = 1.4447^{-5} e^{2.303M}$$

where, y is the geometric mean of the two horizontal components, $E_1(x)$ is the well-known exponential integral function, M is moment magnitude and R is closest distance to rupture.

3. Gupta and Trifunac (2018a) proposed GMPE corresponding to pseudo spectral velocity (PSV) for Hindukush Subduction and Western Himalayas based on uniformly processed strong motion database for the region available in PESMOS. The corresponding functional form is as follows

$$\begin{aligned} log_{10}(PSV) =& M + A_0 ln(\Delta) + C_1 + C_2 M + C_3 M^2 + C_4 \nu \\ &+ C_5 s + C_6^0 S_L^0 + C_6^1 S_L^1 + C_6^2 S_L^2 \end{aligned} \tag{3.7}$$

Here, M denotes the earthquake magnitude,ν denotes the component of motion (ν = 0 for horizontal and 1 for vertical component), s denotes the site geology parameter (s = 0 for alluvium, 1 for intermediate sites, and 2 for basement rock sites), and S_L^0, S_L^1, and S_L^2 are variables taking on the value of 1 for the site soil parameters s_L = 0, 1, and 2 representing rock soil, stiff soil, deep soil, respectively, and zero otherwise. Δ corresponds to representative distance and A_0 is the period dependent attenuation function derived separately for Hindu-Kush Subduction and Western Himalayas.

4. Gupta and Trifunac (2018b) proposed GMPE corresponding to pseudo spectral velocity (PSV) for Burmese Subduction zone and North-Eastern India based on uniformly processed strong motion database for the region available in PESMOS.. The corresponding functional form is similar to Eqn. 3.7. Where, A_0 is the period dependent attenuation function derived separately for Burmese Subduction zone and North-Eastern India and the corresponding coefficients are also estimated based on the regional database.

3.5 Ground motion Prediction in Global database

As there are limited data or GMPE available for the region, It is would be idealistic to consider GMPEs in Global Database from similar tectonic regime. The active regions in India like Himalayas, NorthEastern India, etc. are having predominantly having shallow crustal earthquake similar to NGA West2 database. Furthermore, stable continental regions like Peninsular India are similar to that of NGA East 2. The description on the GMPEs developed from these

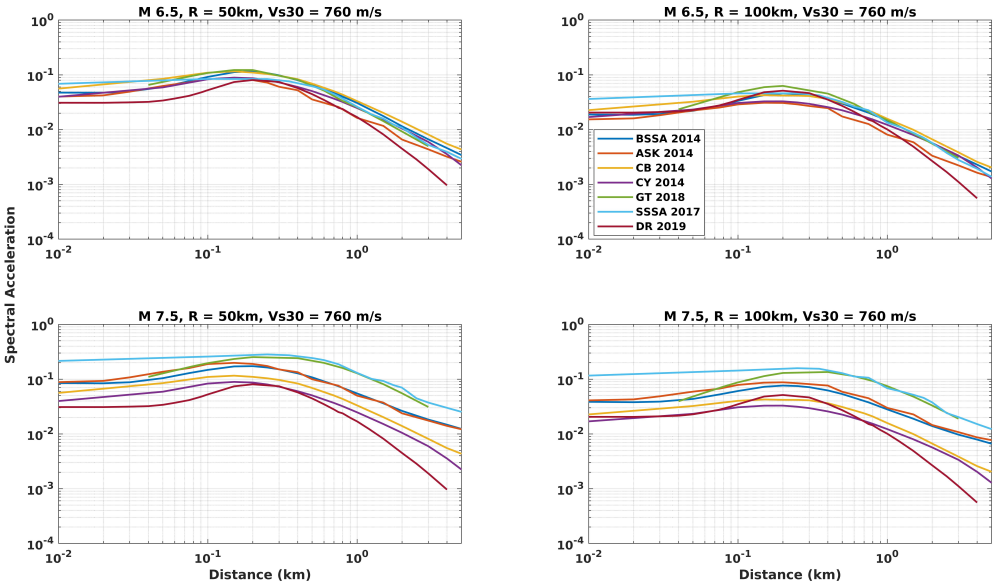

Figure 3.8: Attenuation Characteristics of GMPEs applicable to Active Crustal regions [Note:"BSSA 2014"-Boore *et al.* (2014); "CB 2014"-Campbell and Bozorgnia (2014); "CY 2014"-Chiou and Youngs (2014); "SSSA 2017"-Singh *et al.* (2017); "GT 2018"-Gupta and Trifunac (2018a); DR 2019- Hybrid GMPE explained in section 3.3; ASK 2014-Abrahamson *et al.* (2014)]

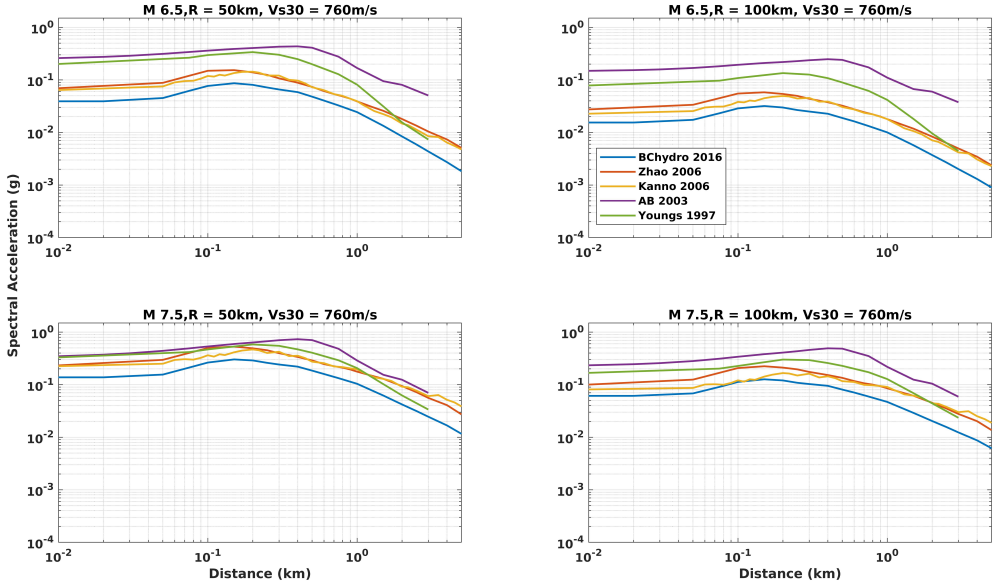

Figure 3.9: Attenuation Characteristics of GMPEs applicable to Subduction regions[Note:"AB 2003"-Atkinson and Boore (2003); "Youngs 1997"-Youngs *et al.* (1997);"Zhao 2006"-Zhao *et al.* (2006); "Kanno 2006" Kanno *et al.* (2006); "BCHydro 2016"-Abrahamson *et al.* (2016)]

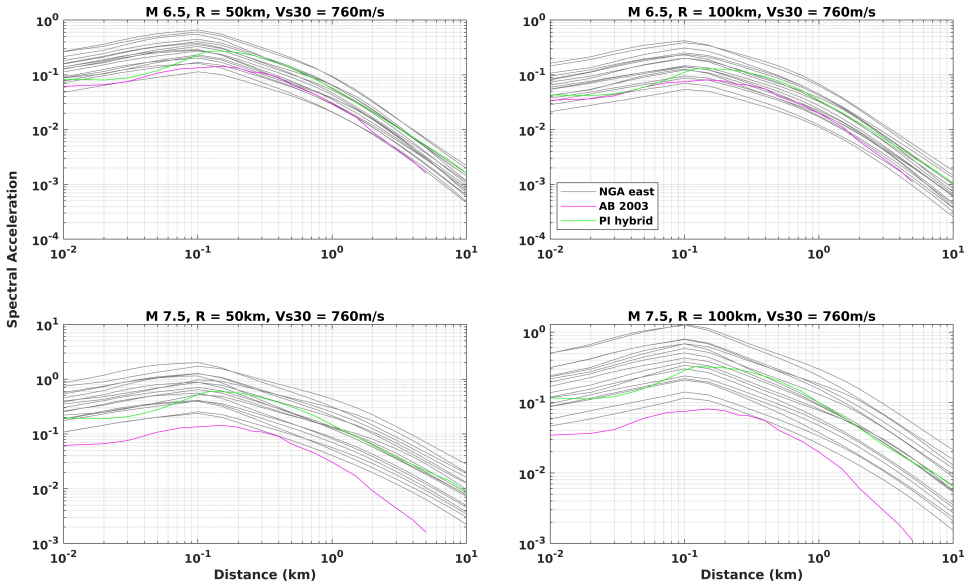

Figure 3.10: Attenuation Characteristics of GMPEs applicable to Stable Continental regions [Note:"NGA East 1-17" Goulet *et al.* (2018); "AB 2006"-Atkinson and Boore (2006)]

database is discussed further.

3.5.1 GMPEs for Active Crustal Region

The GMPEs developed from NGA West2 updated database or European database or Mediterranean database are

1. Abrahamson *et al.* (2014)
2. Boore *et al.* (2014)
3. Chiou and Youngs (2014)
4. Campbell and Bozorgnia (2014)
5. Dhanya and Raghukanth (2018)

The attenuation characteristics of selected GMPEs are illustrated in Figure 3.8. Further, a comparison of these GMPEs for the recorded event in the region is illustrated in Figure 3.11.

3.5.2 GMPEs for Subduction Region

The GMPEs developed for active subduction regions

1. Youngs *et al.* (1997)
2. Atkinson and Boore (2003)
3. Kanno *et al.* (2006)
4. Zhao *et al.* (2006)
5. Abrahamson *et al.* (2016)

The attenuation characteristics of selected GMPEs are illustrated in Figure 3.9. Further, a comparison of these GMPEs for the recorded event in the region is illustrated in Figure 3.11.

3.5.3 GMPEs for Stable Continental Region

Stable Continental regions are most challenging in terms of developing a suitable GMPE. These regions lack a dense set of database due to the relative less seismic activity. One of the preliminary GMPEs developed for the region is that reported in Atkinson and Boore (2006). Recently,there have been efforts to generate synthetic database of such region. Some of the recent efforts to generate suitable GMPEs for NGA-East (belonging to stable continental region) are compiled in Goulet *et al.* (2018). The report proposed 17 ground motion models for the region corresponding to 24 spectral intensities. The GMPEs are valid for moment magnitude range of 4.0 to 8.2 and distances up to 1500 km. The results are valid for A type soil class. The amplification of reported GMPEs at A type soil class to B type with V_{s30} = 760m/s can be taken from that reported by Stewart *et al.* (2019). The attenuation characteristics of these GMPEs are illustrated in Figure 3.10. Further, a comparison of these GMPEs for the recorded event in the region is illustrated in Figure 3.12.

3.5.4 GMPEs for PGD and PGV

Long period characteristics such as PGD and PGV have significance in the design of important life-line structure. However, very few GMPEs are available for the corresponding parameters

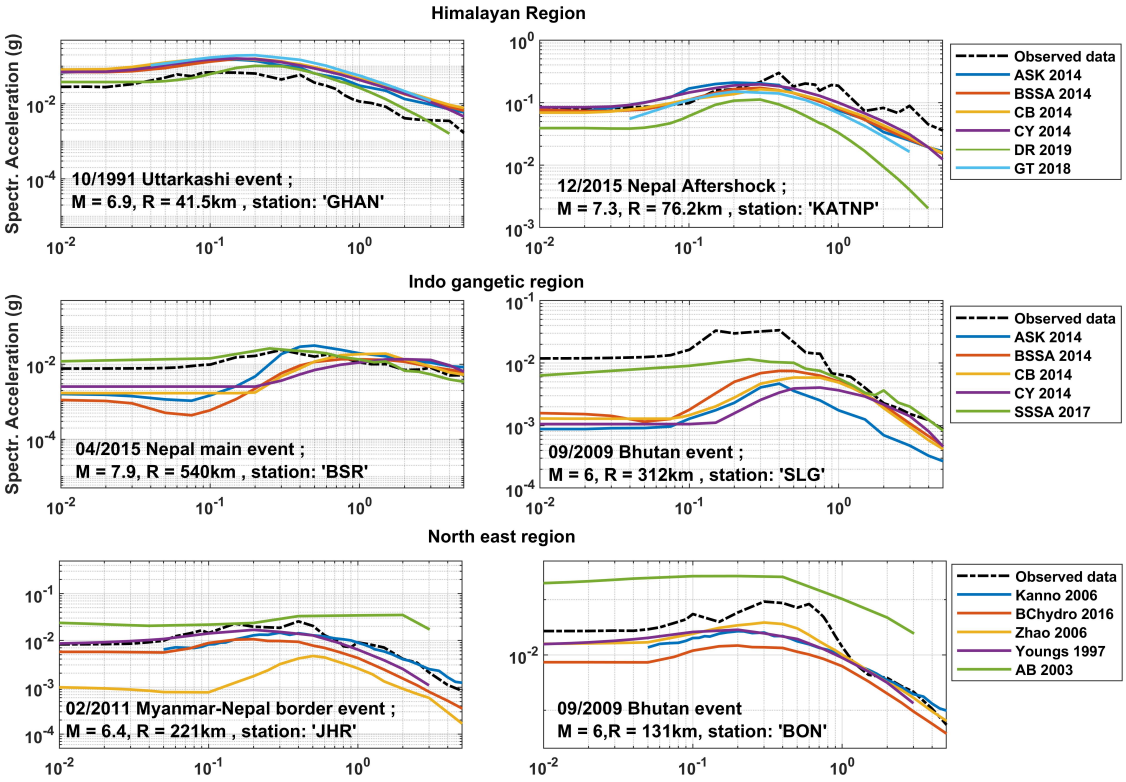

Figure 3.11: Comparison of the selected GMPEs with the recorded data

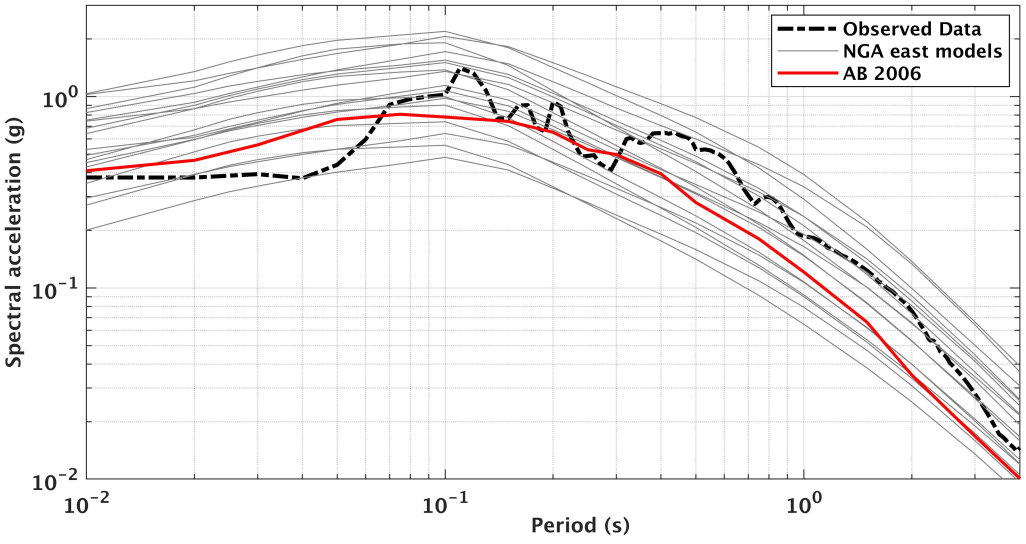

Figure 3.12: Comparison of selected GMPEs with the recorded data of Koyna region

mainly due to the lack of information attributed from the processing of recorded data. However, a preliminary attempt is made in the present study to ascertain hazard corresponding to PGV

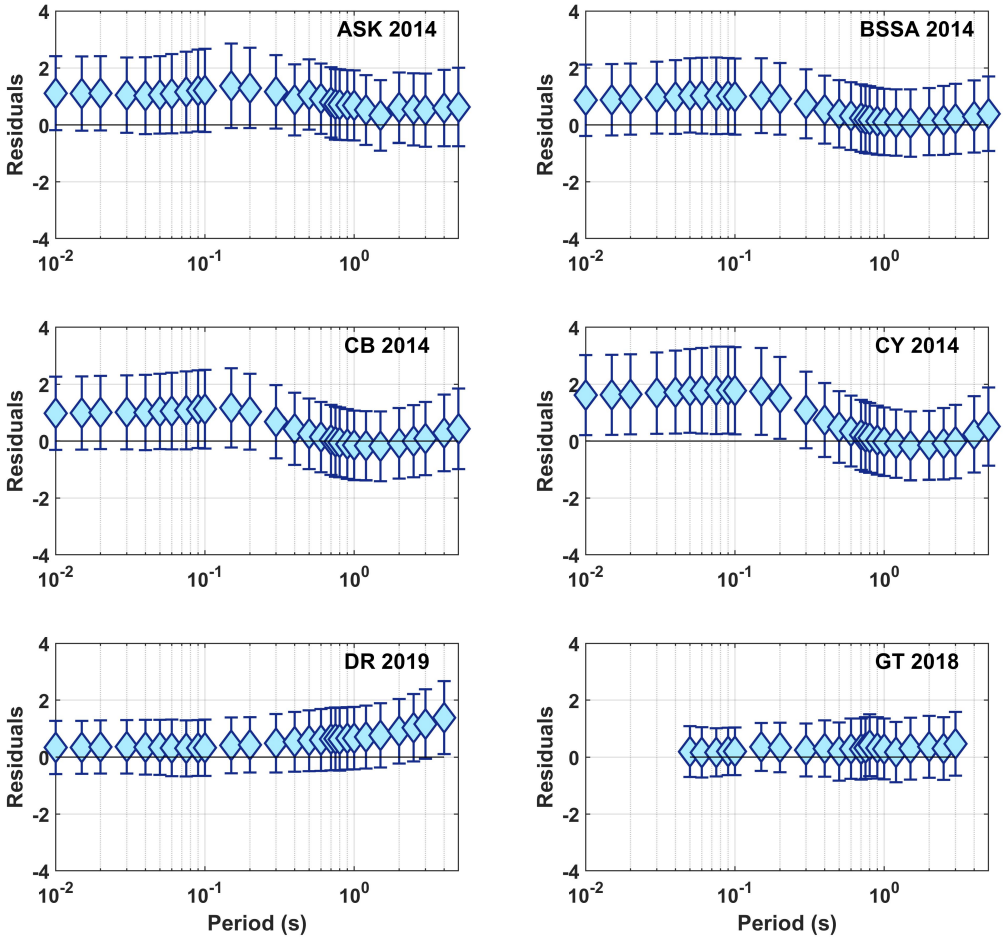

Figure 3.13: Residual of the GMPE prediction with respect to recorded data for the events in Himalayan region

and PGD. Here, for the estimation of hazard corresponding to PGV, Boore *et al.* (2014) model is used for active regions and Atkinson and Boore (2006) for stable continental region. In case of PGD, the GMPE proposed by Cauzzi *et al.* (2015) is used for the study region

3.6 Ranking of GMPEs

Since the models developed are for regions other than India, there is a need to rank the GMPEs for selecting the best fitting GMPE with the recorded data. The deviation between the observed ground motion measure and corresponding predicted measure can be evaluated in many ways.

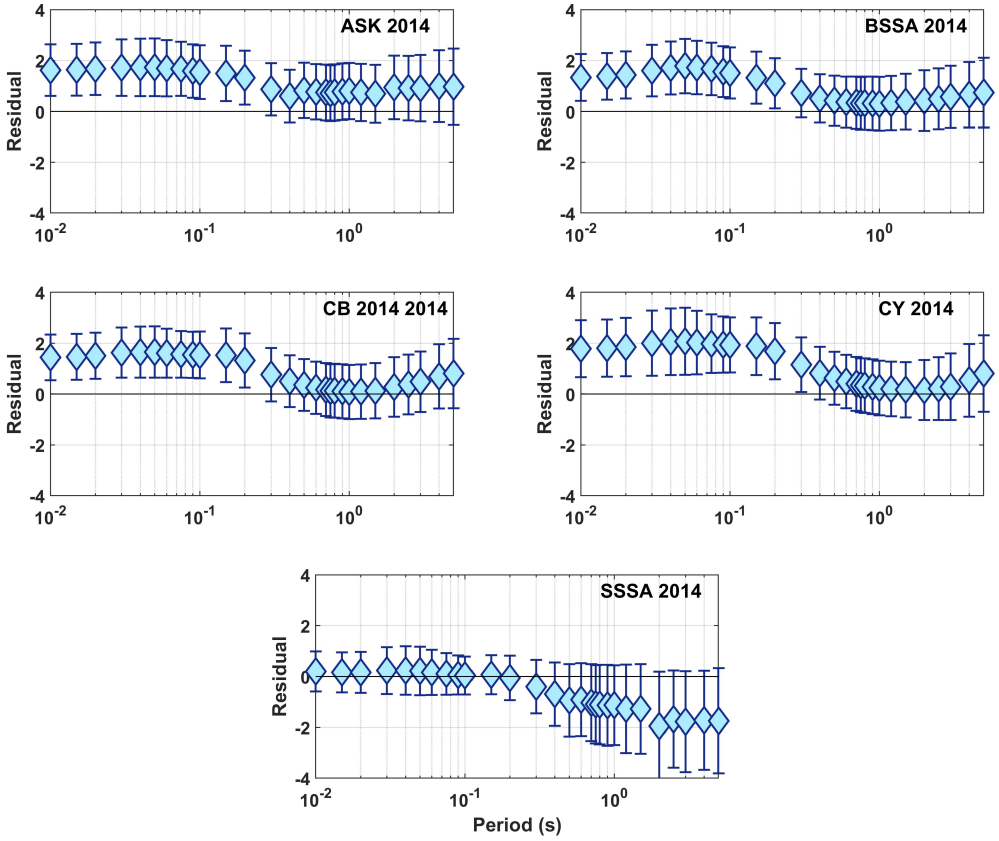

Figure 3.14: Residual of the GMPE prediction with respect to recorded data for the events in Indo-Gangetic region

One of the comprehensive approach is the residual analysis. Here, the residuals are calculated as log(observed data) - log(Median predicted value). The observed data are taken from the database generated from PESMOS and COSMOS network (Section 3.2).

Also, the appropriateness of a model to the recorded dataset can be tested from likelihood studies such as Likelihood (LH) method and Log likelihood (LLH) methods. The likelihood method proposed by Scherbaum *et al.* (2004), determines the exceedance probabilities corresponding to normalized residuals. Here, each ground motion model is assumed as lognormal distribution with mean $\mu(M, R, f)$ and standard deviation $\sigma(M, R, f)$, where M,R and f are the given magnitude, distance and frequency for an observed value of $\ln(Y)$. The normalized residuals can be obtained as $z = \frac{x-\mu}{\sigma}$. Then, an LH distribution derived from residual distribution and

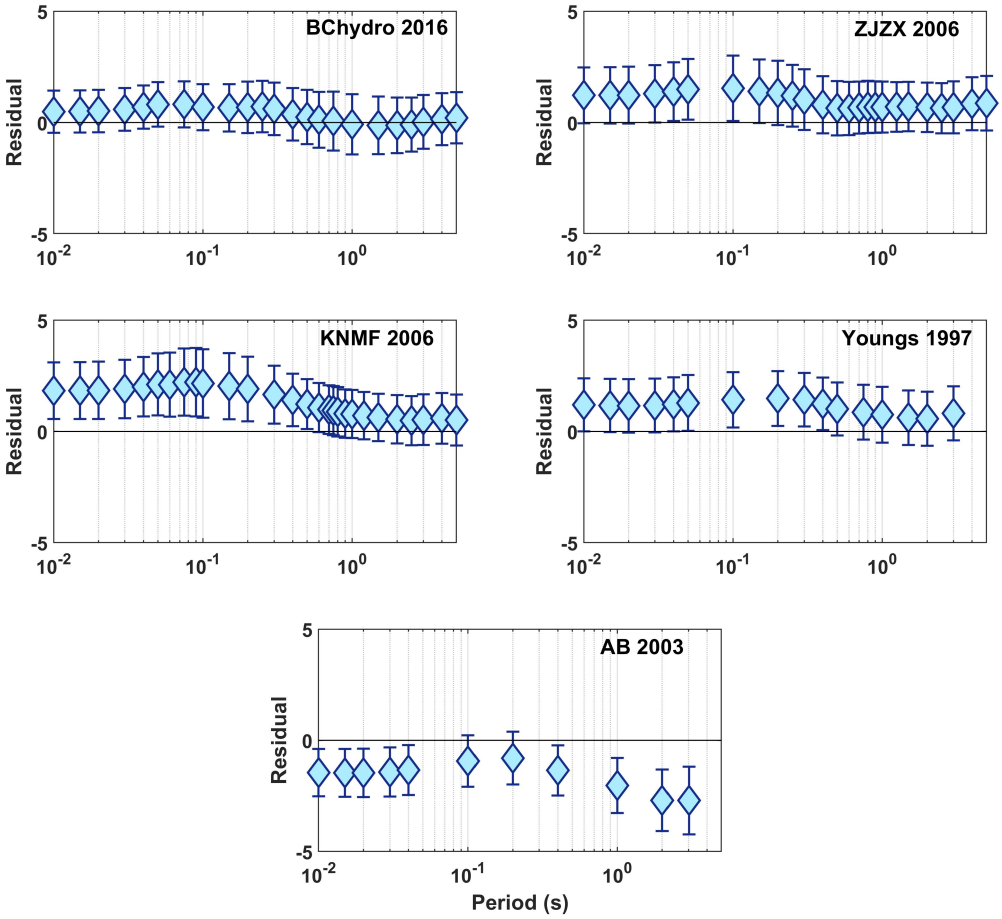

Figure 3.15: Residual of the GMPE prediction with respect to recorded data for the events in North East India region

the likelihood parameter can be expressed, following Scherbaum *et al.* (2004), as:

$$LH(|z_0|) = \frac{2}{\sqrt{2\pi}} \int_{|z_0|}^{\infty} exp(\frac{-z^2}{2})dz \tag{3.8}$$

where, z_0 is the normalized residuals with respect to the standard deviation of the GMPEs. The LH distribution is characterized by its median value. The median value of 0.5 represents the residual distribution as standard normal distribution. As the deviation of median LH value from 0.5 increases, the matching of the model with the observed dataset also decreases.

Table 3.4: Ranking of GMPEs

Himalaya											
GMPE	**LH**	**LHn**	**Rank**	**LLH**	**LLHn**	**Rank**	**EDR**	**EDRn**	**Rank**	**RIn**	**Weight**
ASK 2014	0.509	1	1	2.687	1.112	3	2.419	2.195	5	1.625	0.149
BSSA 2014	0.593	1.186	4	2.416	1	1	2.246	2.038	4	1.566	0.155
CB 2014	0.557	1.114	3	2.473	1.022	2	1.996	1.811	3	1.439	0.168
CY 2014	0.471	1.058	2	2.857	1.183	4	2.606	2.365	6	1.743	0.139
DR 2019	0.354	1.292	6	3.276	1.356	6	1.642	1.49	2	1.478	0.174
GT 2018	0.388	1.224	5	3.118	1.291	5	1.102	1	1	1.128	0.215
IGP											
GMPE	**LH**	**LHn**	**Rank**	**LLH**	**LLHn**	**Rank**	**EDR**	**EDRn**	**Rank**	**Rin**	**Weight**
ASK 2014	0.411	1.178	4	3.176	1.263	4	3.109	2.606	3	1.913	0.161
BSSA 2014	0.501	1	1	2.908	1.156	3	3.122	2.617	4	1.847	0.166
CB 2014	0.465	1.07	2	2.896	1.151	2	1.193	1	1	1.055	0.291
CY 2014	0.376	1.125	3	3.372	1.341	5	3.242	2.718	5	1.975	0.155
SSSA 2017	0.612	1.224	5	2.515	1	1	1.902	1.594	2	1.353	0.227
NEI											
GMPE	**LH**	**LHn**	**Rank**	**LLH**	**LLHn**	**Rank**	**EDR**	**EDRn**	**Rank**	**RIn**	**Weight**
Bchydro 2016	0.645	1.29	3	2.022	1	1	1.496	1	1	1.072	0.271
Zhao 2006	0.48	1	1	2.535	1.254	3	2.062	1.378	2	1.253	0.231
Kanno 2006	0.101	1.798	4	4.535	2.243	4	2.694	1.801	4	1.911	0.152
Youngs 1997	0.536	1.07	2	2.316	1.145	2	2.248	1.503	3	1.305	0.222
AB 2003	0.0184	1.963	5	5.757	2.847	5	3.414	2.282	5	2.343	0.124

However, the estimation of best fit parameters to the model can be done based on the maximum likelihood method. According to this, Scherbaum *et al.* (2009) proposed log likelihood method to rank GMPEs. The backbone of this method is information theory based model selection, consisting of two continuous functions $f(x)$ and $g(x)$. It is assumed that the distribution of observed data points follow the function $f(x)$ and the distribution of the corresponding ground motion estimate is lognormally distributed with the meadian value μ_{GMPE} and standard deviation σ_{GMPE}. The likelihood of a model g, given the sample set x is

$$\mathcal{L}(g|x) = \prod_{i=1}^{N} g(x_i) \tag{3.9}$$

The corresponding loglikelihood value, which is independent of sample size can be obtained as follows:

$$LLH(g, x) = -\frac{1}{N} \sum_{n=1}^{N} \log_2(g(x_i)) \tag{3.10}$$

where, N is the number of observed data points in the record. When a model represents the dataset more or less matchingly, the log likelihood value will be small.

Another method of ranking that make use of the residual analysis concept is Euclidean distance-based ranking (EDR) proposed by Kale and Akkar (2013). The main difference from other methods is that this method considers the bias between the observed and predicted datasets. Also, the aleatory variability in ground motion is addressed by the standard deviation of the GMPE. The Euclidean distance can be defined as the absolute difference between observed and estimated data. i.e., if p_i are the observed data points and q_i are the corresponding predicted data points, then $DE = \sqrt{\sum_{i=1}^{N}(p_i - q_i)^2}$ is the Euclidean distance. The residuals (D) is considered as Normal distribution with mean μ_D and standard deviation σ_D. where $\sigma_D = \sigma_{GMPE}$ and μ_D is obtained from the difference of observed data and the median value predicted from the model. If d_j is the discrete values of D and $Pr(|d_j|)$ is the corresponding probability values, then the Modified Euclidean Distance (MDE) is calculated as:

$$MDE = \sum_{j=1}^{n} |d_j| Pr(|d_j|) \tag{3.11}$$

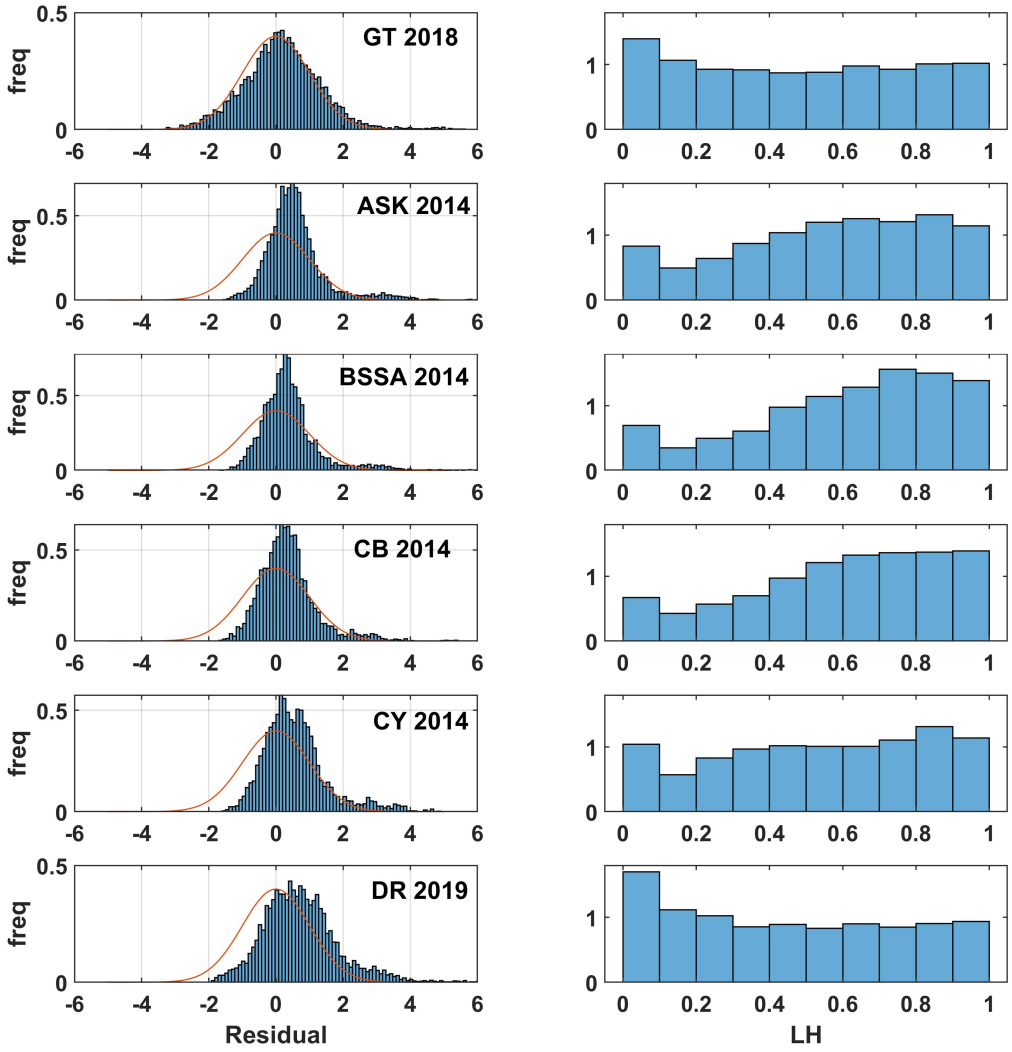

Figure 3.16: Distribution of normalized residuals and likelihood values(LH) for Himalayan region

The EDR value, which is independent of the size of the data, is calculated by incorporating the correction factor for the bias of the model as follows:

$$EDR = \sqrt{k \cdot \frac{1}{N} \cdot \sum_{i=1}^{N} MDE_i^2} \tag{3.12}$$

where, N is the data size and k is the correction factor for model bias, obtained as the ratio of original DE as well as the corrected DE. The corrected DE is obtained from the observed data and the median corrected GMPE by fitting a straight line for observed as well as the predicted data points.

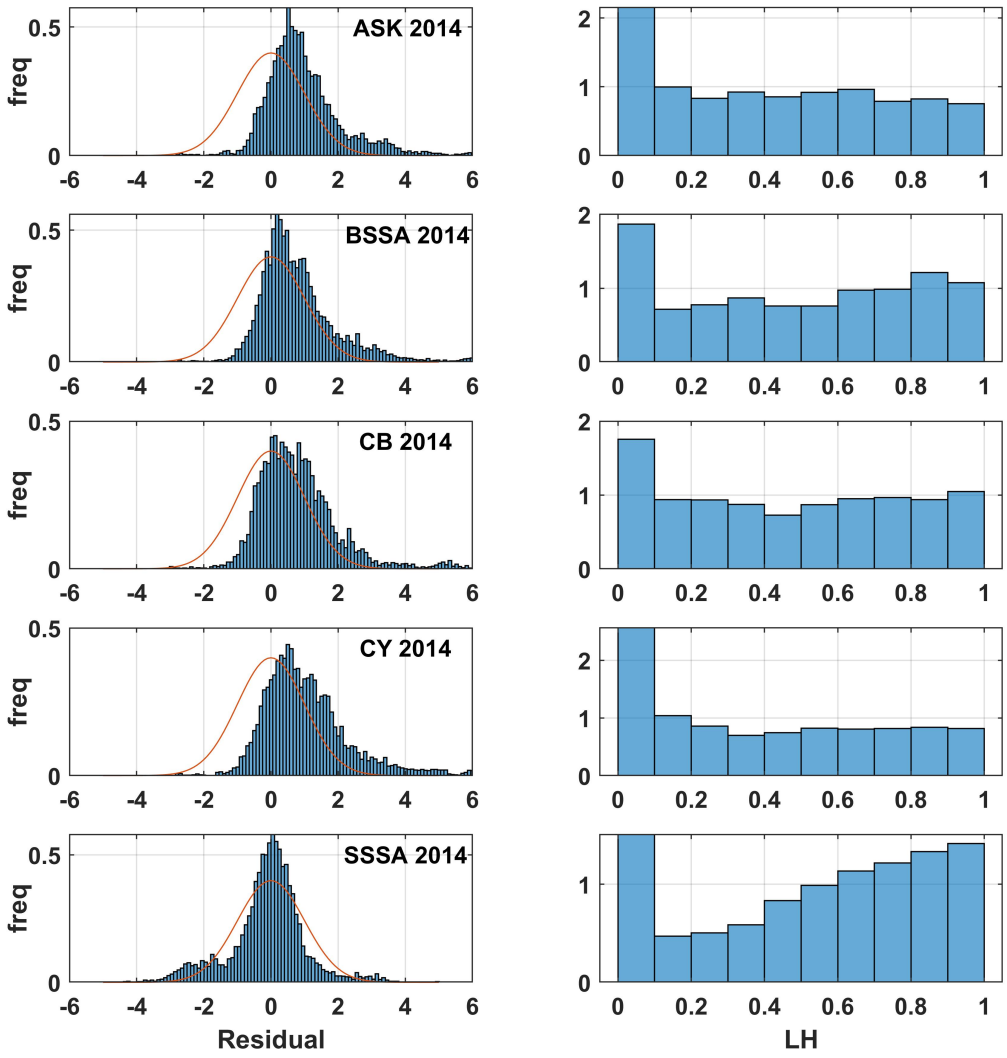

Figure 3.17: Distribution of normalized residuals and likelihood values(LH) for Indo-Gagetic region

Often, different ranking schemes give different ranks to each GMPEs. However, it is suitable to use a single value which can be obtained from combining and normalizing all the ranking schemes. The corresponding normalized ranking index can be arrived as,

$$RI_{N,i} = \frac{index_i}{index_{best}} \tag{3.13}$$

where, $index_i$ is the ranking index for the i^{th} GMPE. $index_{best}$ is the ranking index for the top ranked GMPE. For LH method, $index_{best}$ is taken as 0.5. Hence, LH_N, LLH_N , EDR_N are the normalized ranking indices for LH method, LLH method and EDR method respectively.

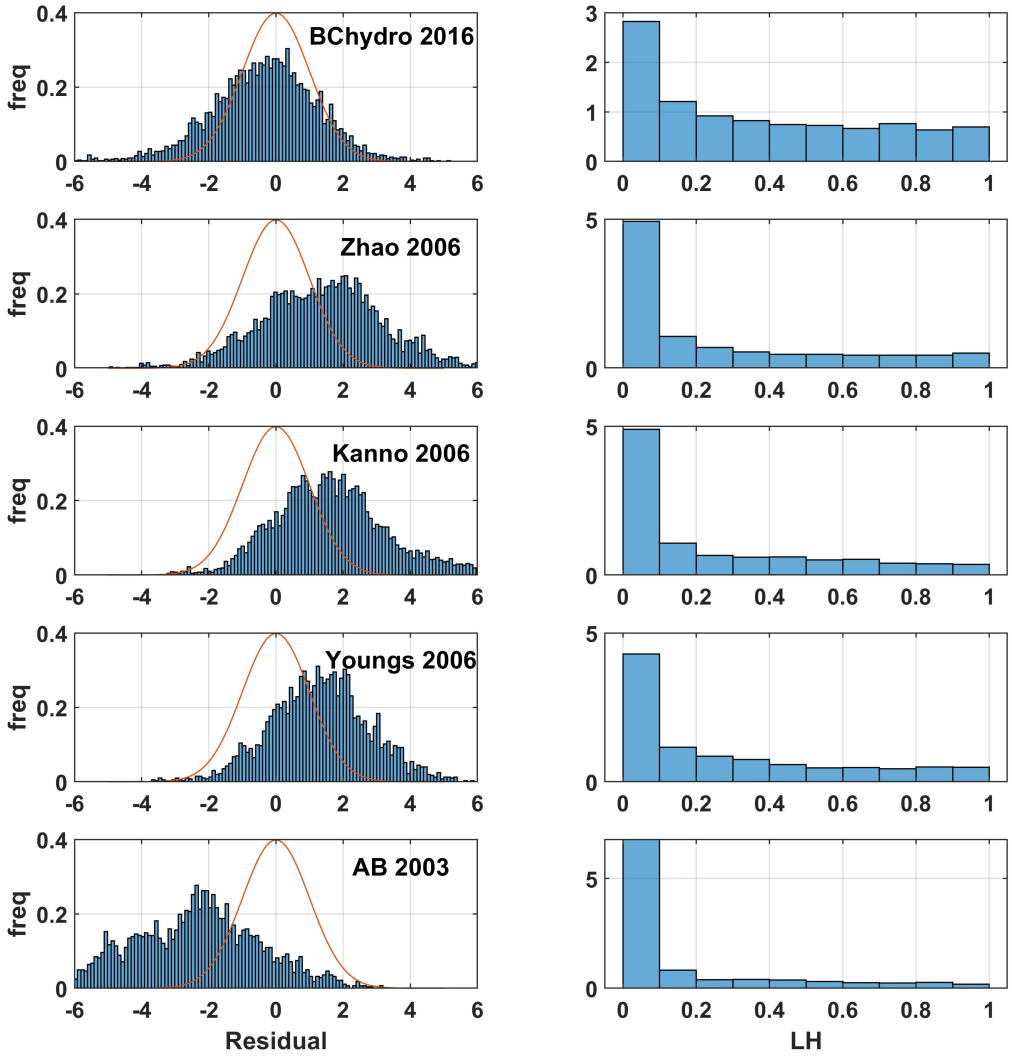

Figure 3.18: Distribution of normalized residuals and likelihood values(LH) for North East India region

The final R_N value is arrived from the normalised ranking indices by giving weights of 0.25 each for Likelihood (LH_N) as well as Log likelihood (LLH_M) method and 0.5 for EDR_M values (Kale (2019)). The final weightages are obtained from the final ranking index R_N using the expression,

$$w_j = \frac{2^{-\log_2(R_N)}}{\sum_{j=1}^{k} 2^{-\log_2(R_{Nj})}} \tag{3.14}$$

where R_N is the normalized ranking index. Following this scheme, the GMPEs used in the active region having instrumental data is suitably given weightage. The residual between the recorded and the GMPE prediction for the regions are illustrated in Figure 3.13 for Himalayan

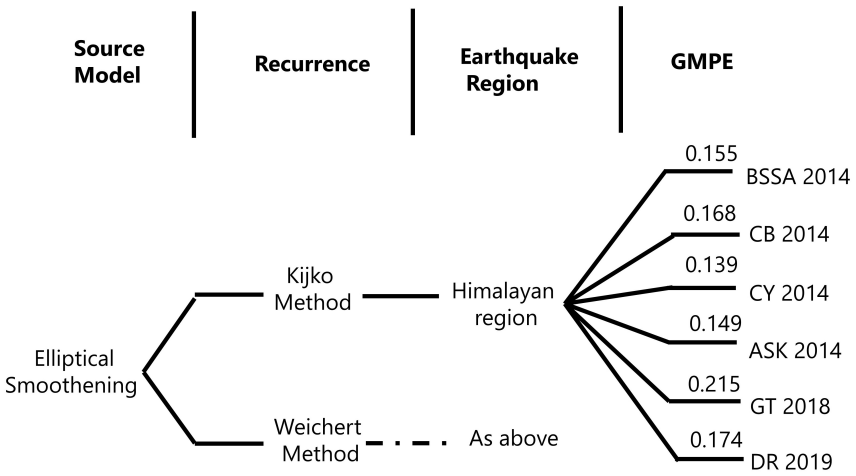

Figure 3.19: Logic Tree to estimate seismic hazard values in Himalayan Region [Note:"BSSA 2014"-Boore *et al.* (2014); "CB 2014"-Campbell and Bozorgnia (2014); "CY 2014"-Chiou and Youngs (2014); "ASK 2014"-Abrahamson *et al.* (2014); "GT2018"-Gupta and Trifunac (2018a); DR 2019- Hybrid GMPE explained in section 3.3]

region, Figure 3.14 for Indo-Gangetic region and Figure 3.15 for North-East India. Additionally the normaized residuals and the log-likelihood values is shown in Figure 3.16 for Himalayan region, Figure 3.17 for Indo-Gangetic region and Figure 3.18 for North-East India. Furthermore, the ranking parameters values obtained for each of the GMPEs considered in this study are summarized in Table 3.6. For the region with no recorded information, equal weigtages are assigned to the utilized GMPEs. The corresponding logic tree along with the estimated weightages are illustrated in Figure 3.19 for Himalayan Region, Figure 3.20 for Indo-Gangetic Plain region, Figure 3.21 for stable continental regions like Central India, Peninsular India, Gujarat and Figure 3.22 for the subduction regions like North-Eastern India subduction and Andaman regions.

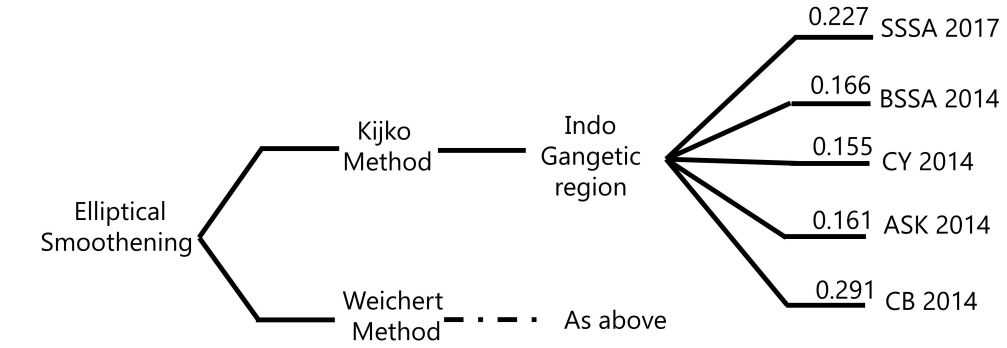

Figure 3.20: Logic Tree to estimate seismic hazard values in Indo-Gangetic Plain Region[Note:"BSSA 2014"-Boore *et al.* (2014); "CB 2014"-Campbell and Bozorgnia (2014); "CY 2014"-Chiou and Youngs (2014); "SSSA 2017"-Singh *et al.* (2017); ASK 2014-Abrahamson *et al.* (2014)]

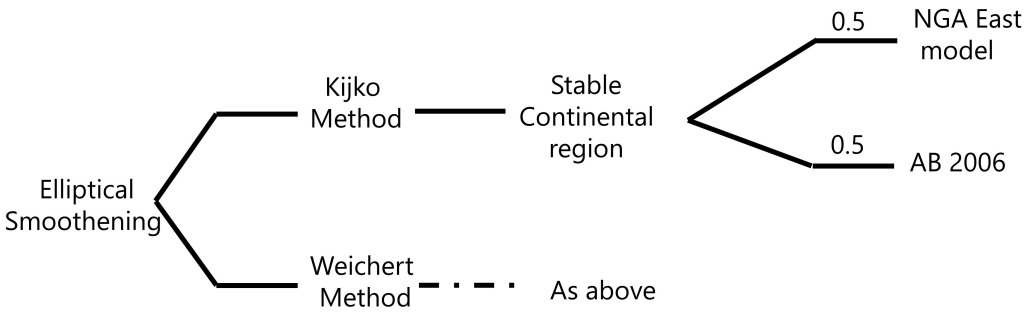

Figure 3.21: Logic Tree to estimate seismic hazard values in Stable Continental region Region [Note:"NGA East 1-17" Goulet *et al.* (2018); "AB 2006"-Atkinson and Boore (2006)]

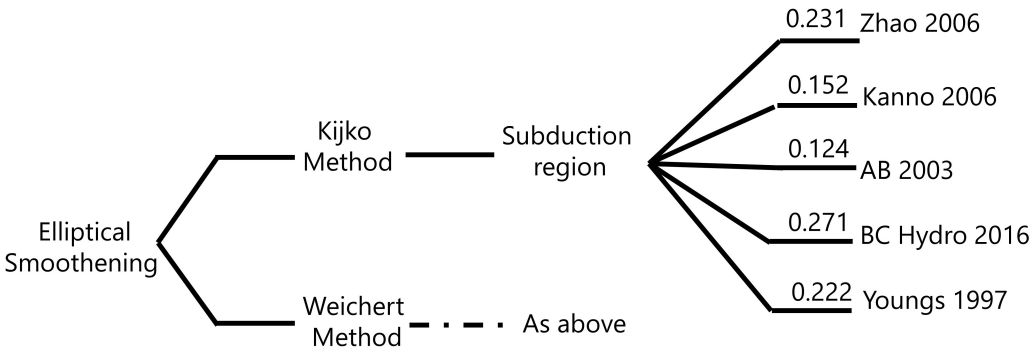

Figure 3.22: Logic Tree to estimate seismic hazard values in Subduction Region [Note:"AB 2003"-Atkinson and Boore (2003); "Youngs 1997"-Youngs *et al.* (1997);"Zhao 2006"-Zhao *et al.* (2006); "Kanno 2006" Kanno *et al.* (2006); "BCHydro 2016"-Abrahamson *et al.* (2016)]

CHAPTER 4

Seismic Hazard Maps

4.1 Introduction

Characterization of seismic source zones and estimation of recurrence parameters are discussed in Chapter 2. Suitable GMPEs are selected based on the ranking schemes of Kale (2019) and the weights to each of the logic tree branches are obtained as discussed in Chapter 3. Now, it remains to link the assembled results together to arrive at the ground motion probabilities at every grid point at the spacing of 0.1 ° x 0.1 °, which covers the whole Indian land mass. Around each of the grid points, a radius of 500km is considered such that any site gets affected by the events occurring within this radius of influence. Within this circle of influence, normally there will be several sources that can give rise to earthquakes of differing strengths. Now, this information of sources and attenuation relation are combined in a deterministic and probabilistic approach to obtain the final hazard for the region.

4.2 Deterministic Seismic Hazard Analysis (DSHA)

The DSHA involves the development of a particular seismic scenario, upon which a ground motion hazard evaluation is carried out. The DSHA approach uses the known seismic sources near the site and available historical seismic and geological data to generate discrete, single-valued events or models of ground motion at the site. The site ground motions are estimated deterministically, given the magnitude, source-to-site distance, and site condition. The steps involved in DSHA (Kramer 1996) are described in brief as follows

1. Identification of all sources capable of producing significant ground motion at the site. Source characterization includes a definition of source details and earthquake potential.
2. Selection of Controlling Earthquakes is based on ground motion parameter(s). Consider all sources, assume M_{max} occurs at Rmin for each source. Compute ground motion

parameter(s) based on M_{max} and R_{min} . Then, determine the critical value(s) of the ground motion parameter(s).

3. Definition of hazard using controlling earthquake involves the use of M and R to determine parameters such as Peak acceleration, spectral acceleration and Duration

The deterministic analysis performed for the region using source characteristics, and the different attenuation relations discussed in Chapter 3. Here, DSHA is performed by considering the earthquake corresponding to a 2% probability of exceedance in 50 years (2475 yrs return period). For the lower bound of deterministic estimates, the PSHA map committee has recommended using the magnitudes and focal depths as listed in Table 4.1. It is assumed that the event occurs at smaller of the closest distance to the nearest known fault in the respective source zone or 25km. Figure 4.1 shows the magnitude corresponding to the 2475-year RP suggested by the PSHA map committee. The same figure shows the minimum source distance to each grid point. The minimum distance is calculated as the distance to each grid point from the nearest active fault located in the region. Further, the hazard is computed at all the grid points using all the GMPEs discussed in Chapter 3. The weighted averaged hazard is computed following the logic tree discussed in section 3.6. The hazard map thus obtained for 50% confidence levels is shown in Figure 4.2. As the maps are prepared with an upper bound distance of 25km, higher hazard values are observed near the major faults located in the region.

Table 4.1: Magnitude and focal depth suggested by PSHA map committee for use in DSHA of the study region

Source Zones	Magnitude	Focal Depth (km)
Z-1 to 4, 5, 6, 22 to 26, and 33	6.5	20
Z-30	7	200
Z-21 & Z-28 excluding Delhi Fold Belt part	5	20
Z-28 Delhi Fold Belt Part	5.5	15
Z-31 North of 25° N	6.5	50
Z-7 and Z-8 excluding Shillong Plateau	6	25
Z-8 Shillong Plateau Part and Z-9	6.5	30
Z-10	6.5	30
Z-11	7	100
Z-12 to 15	6.5	25
Z-17, 18, 29, 20 south of about 16° N, Z-31 South of 25° N,and Z-27 excluding Kutch region	5	15
Z-20 north of 16° N	5.5	10
Z-27 Kutch region part	6	20
Z-32	6	20
Z-16 and 19	5	20

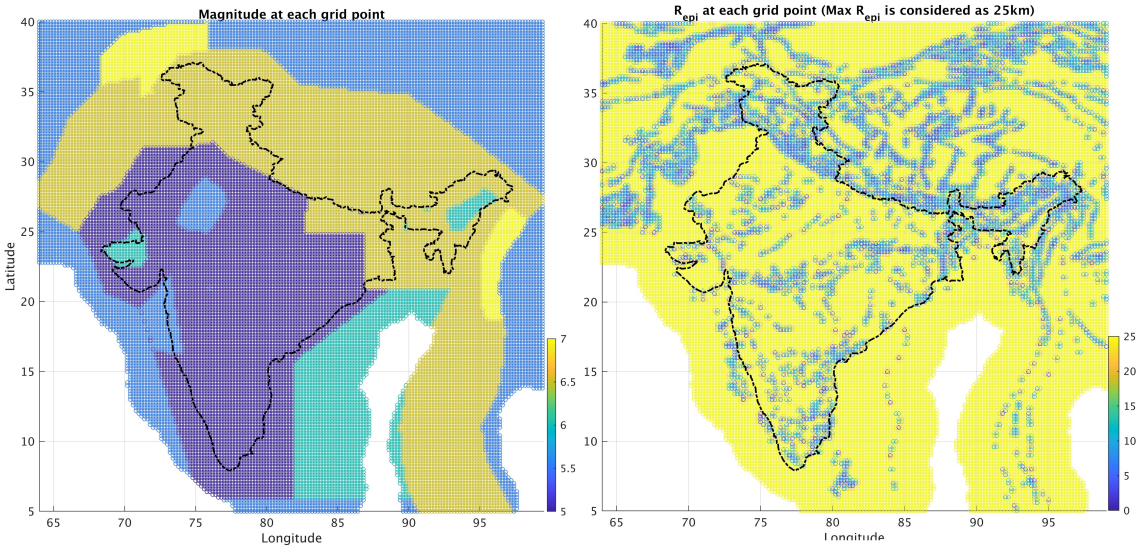

Figure 4.1: Magnitudes for 2475 year RP and the minimum source distance to each grid point as suggested by the PSHA map committee

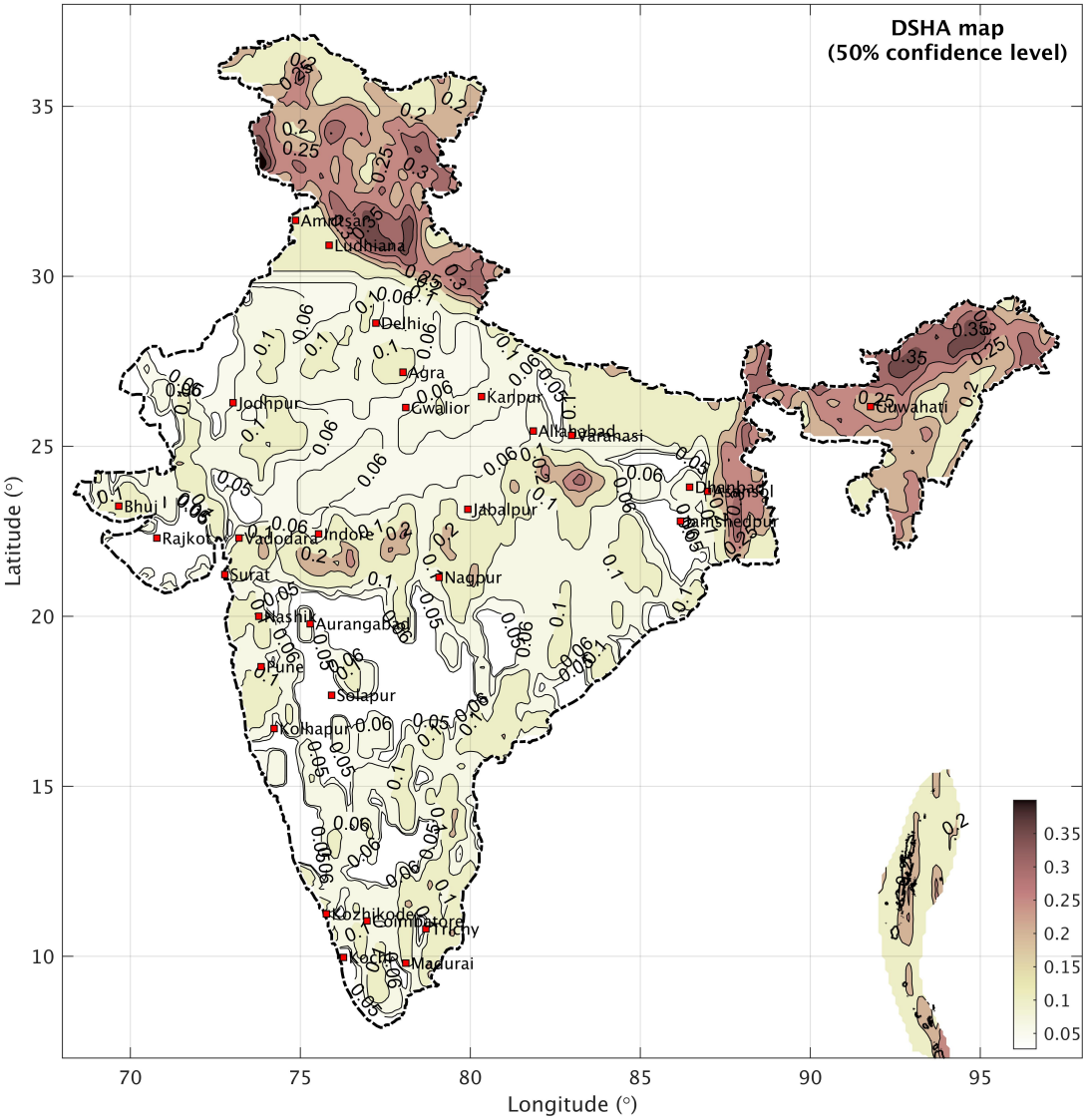

Figure 4.2: DSHA Contour map of peak acceleration PA, for 50% confidence level, corresponding to the 2475 year earthquake magnitudes

4.3 Probabilistic Seismic Hazard Analysis (PSHA)

The PSHA is estimated based on faults and gridded seismicity approaches. The characterization of all the faults in the 33 source zones forms the source database for further work in the fault-based approach. The circular smoothed seismicity and elliptically smoothed seismicity are used to model the seismic activity rates for the gridded seismicity approach (Frankel (1995);Lapajne *et al.* (2003)). In Chapter 3 the details of GMPEs are discussed for the seven regions corresponding to B-type site condition ($V_{s30} = 760m/s$). With the help of the source and the attenuation models, we are now in a position to carry out PSHA for any grid point. The procedure for carrying out PSHA is well known. The three main probability distributions in PSHA are associated with the magnitude, distance, and ground motion intensity. The uncertainty in the magnitude of a future event is represented as an exponential random variable,

$$P_M(m) = \frac{\beta e^{=\beta(m=m_0)}}{1-\beta e^{=\beta(m=m_0)}}; \quad (m_0 \leq m \leq m_u), \quad \beta = 2.303b \tag{4.1}$$

The other unknown factor is the distance R of the site to the future hypocenter. The conditional probability distribution function of R, given that magnitude M = m for a rupture segment uniformly distributed along a fault can be numerically computed following the method of Kiureghian and Ang (1977). The details of fault based approach can be referred from NDMA(2010). In the gridded seismicity approach, this probability $P_R(r)$ is considered as unity as the grid points where the seismic activity rates are defined are considered as the sources. Further, Probabilistic seismic hazard analysis estimates the probability of exceedance of spectral acceleration (S_a) at a site due to all possible future earthquakes as visualized by the previous hazard scenario. Assuming that the number of earthquakes occurring follows a stationary Poisson process, the probability that the control variable Y exceeds level y^*, in a time window of T years is given by

$$P(Y > y^* \; in \; T \; years) = 1 - e^{-\mu_{y^*}T} \tag{4.2}$$

Here, μ_{y^*} indicates the mean annual rate of exceedance of the ground motion measure y^* (reciprocal of μ_{y^*} denotes return period RP) at a site due to all probable earthquakes caused by all probable sources. If there were 'K' number of probable sources in the region whose seismicity

is known, then μ_{y^*} in Equation 4.2can be computed as

$$\mu_{y^*} = \sum_{i=1}^{N_s} N_i(m_0) \int_{m_0}^{m_u} \int_{r_0}^{r_u} P\left[Y > y|m, r\right] P_{R|M}(r|m) P_M(m)\ \partial r\ \partial m \tag{4.3}$$

where, N_s is the total number of faults in the zone, m_0 and m_u indicate the minimum and the maximum threshold magnitude observed at the source; r_0 and r_u are the minimum and maximum site distances from the source. $P_M(m)$ is the probability density function of the exponentially distributed magnitude which can be obtained through the G-R relationship. $p_{R|M}(r|m)$ is the conditional probability density function of hypocentral distance which can be obtained numerically for the identified probable sources. $P[Y > y|m, r]$ denotes the conditional probability that the chosen ground motion intensity level is exceeded for a given magnitude and distance which can be determined using the ground motion relationship. The next two approaches followed in this study is the circular smoothed and elliptical smoothed gridded seismicity approaches. In both these methods, the seismic activity rate is defined at each of the grid points. Hence, the eqn4.3 is rewritten for applying in gridded seismicity-based hazard calculations. The PSHA is carried out by the following expression.

$$\mu_{y^*} = \sum_{i=1}^{N_s} N_i(m_0) \int_{m_0}^{m_u} P\left[Y > y|r_i, m\right] P_M(m)\ \partial m \tag{4.4}$$

Here, $P[Y > y|r_i, m]$ is the conditional probability that the ground motion value would be exceeded if the distance from the source to site (centre of grid, i) is r_i and magnitude is m.

4.4 PSHA map for India

Probabilistic seismic hazard analysis for PA and spectral accelerations at various periods have been carried out for all the grid points spread over the Indian land mass. The estimates are derived for each region using the corresponding applicable GMPEs in a suitable logic tree framework as discussed in Chapter 3. The final hazard contours arrive from three different approaches, viz. fault-based, circular smoothening-based, and elliptical smoothening-based approaches. The final median hazard (50 percentile) results from fault based approach valid for

B-type sites (V_{s30} = 760m/s) are presented as contour maps for 475year and 2475year return periods in Figures 4.3 and 4.4 respectively for peak acceleration. The maps for SA at 0.2s and 1s are shown in Figures 4.5 -4.6 and Figures 4.7-4.8 for 475 year and 2475year return periods. Further, the PA contours from the circular smoothening approach is presented in Figures 4.9 and 4.10 for 475 and 2475-year return period respectively. The corresponding SA at 0.2s and 1s contours are shown in Figures 4.11- 4.12 and Figures 4.13 -4.14.It is noted that the fault based hazard analysis results in a lower hazard estimate whereas, the circular smoothed seismicity-based approach gives higher hazard values.

The PA contours from the third method, based on elliptically smoothed seismicity are shown in 4.15 to 4.19 for 73,475,2475,4975 and 9975-year return periods. The corresponding SA contours at 0.2s and 1s for 475 years and 2475 years return periods are shown in Figures 4.20-4.21 and Figures 4.22 - 4.23. It is noted that the estimates from the elliptical smoothed seismicity approach are more than the values from fault based hazard and lesser than circular based hazard estimates. Hence, the final results for the present study are arrived from the elliptical smoothed approach as the method incorporates both the seismicity and fault orientations. Further, the hazard values from elliptical smoothed seismicity corresponding to PA at the urban agglomerations for various return periods and those corresponding 50 percentile values are also summarized in Table 4.2. Additionally, a comparison of the estimated PA values for 475 years return period with that reported in the literature for various regions in India is summarized in Table 4.3. The current estimates (B Type site class) are slightly higher than that reported for the A-Type site class available from the literature. The estimates of Nath and Thingbaijam (2012) are also observed to be higher for the active regions of India (0.7g) whereas the other studies give a lower hazard estimation (0.3g) for the region. The higher hazard from Nath and Thingbaijam (2012) study can be related to the method of modeling the seismicity distribution. The study of Sitharam et al (2015) has estimated the hazard of India by considering different source models and GMPEs in the logic tree framework. A higher PGA of >0.3g is reported for Himalaya and North East India. Central India is reported to have a PGA<0.05g and Peninsular India has a PGA <0.1g. For Peninsular India, Jaiswal and Sinha (2007) has estimated a PGA value in the range of 0.1-0.2g, with a higher hazard value of 0.36g at the Koyna region. Further, NDMA (2010) have arrived at the hazard of India using a fault-based approach. They have distributed the seismic activity rates along the known faults and lineaments in the region

and the epicenters of past earthquakes are not considered. The hazard values generally gave lower estimates throughout India compared to the present study. Moreover, the significant differences observed in all these hazard estimates can be due to the differences in source zones considered, methodology, GMPEs selected, and the quality of the database available at the time of the study.

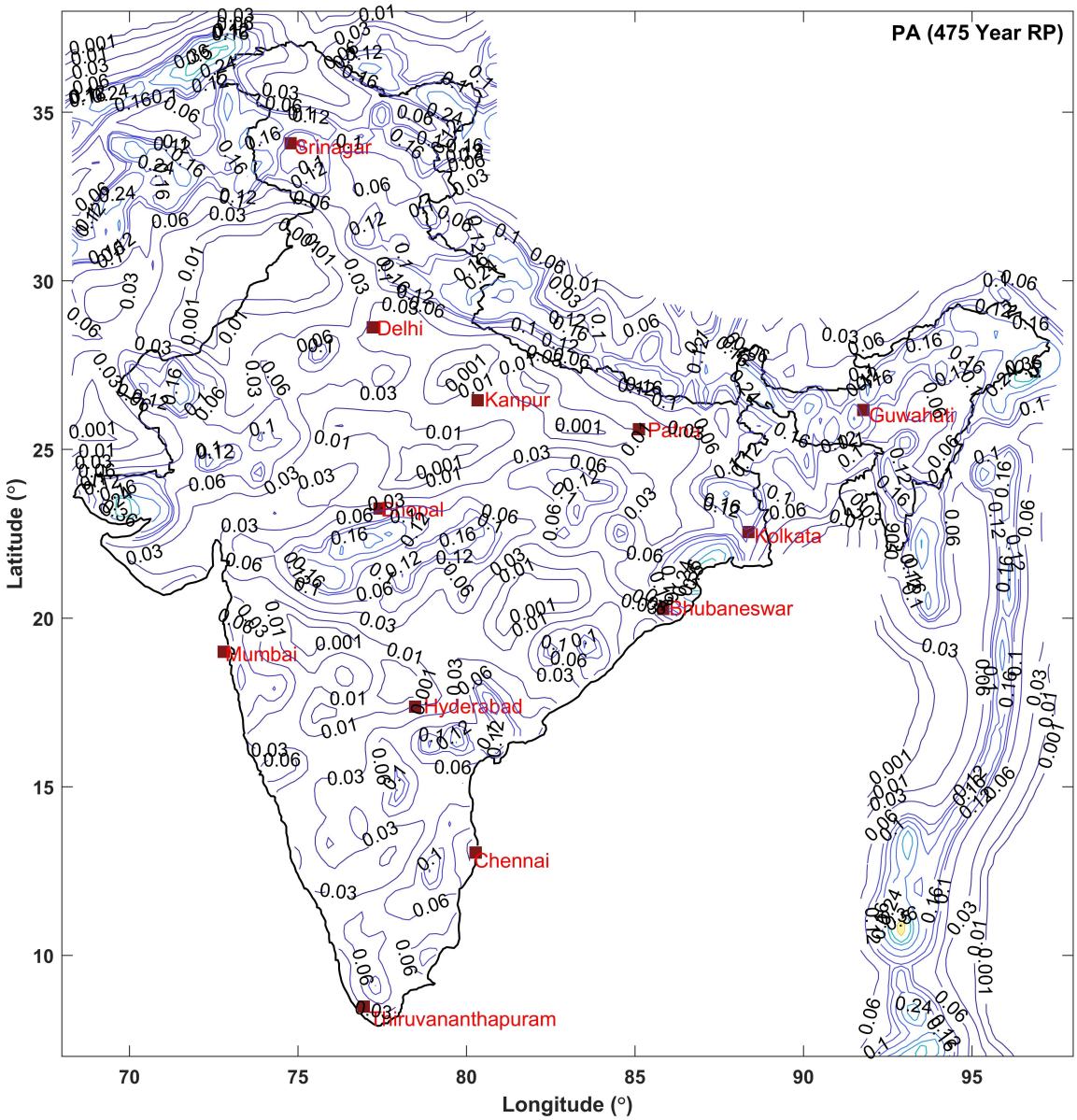

Figure 4.3: PA Contours (Units: g) with 10% probability of exceedence in 50 years (Return Period 475 years) on B-type Sites (V_{s30}=760m/s estimated using Fault based approach.

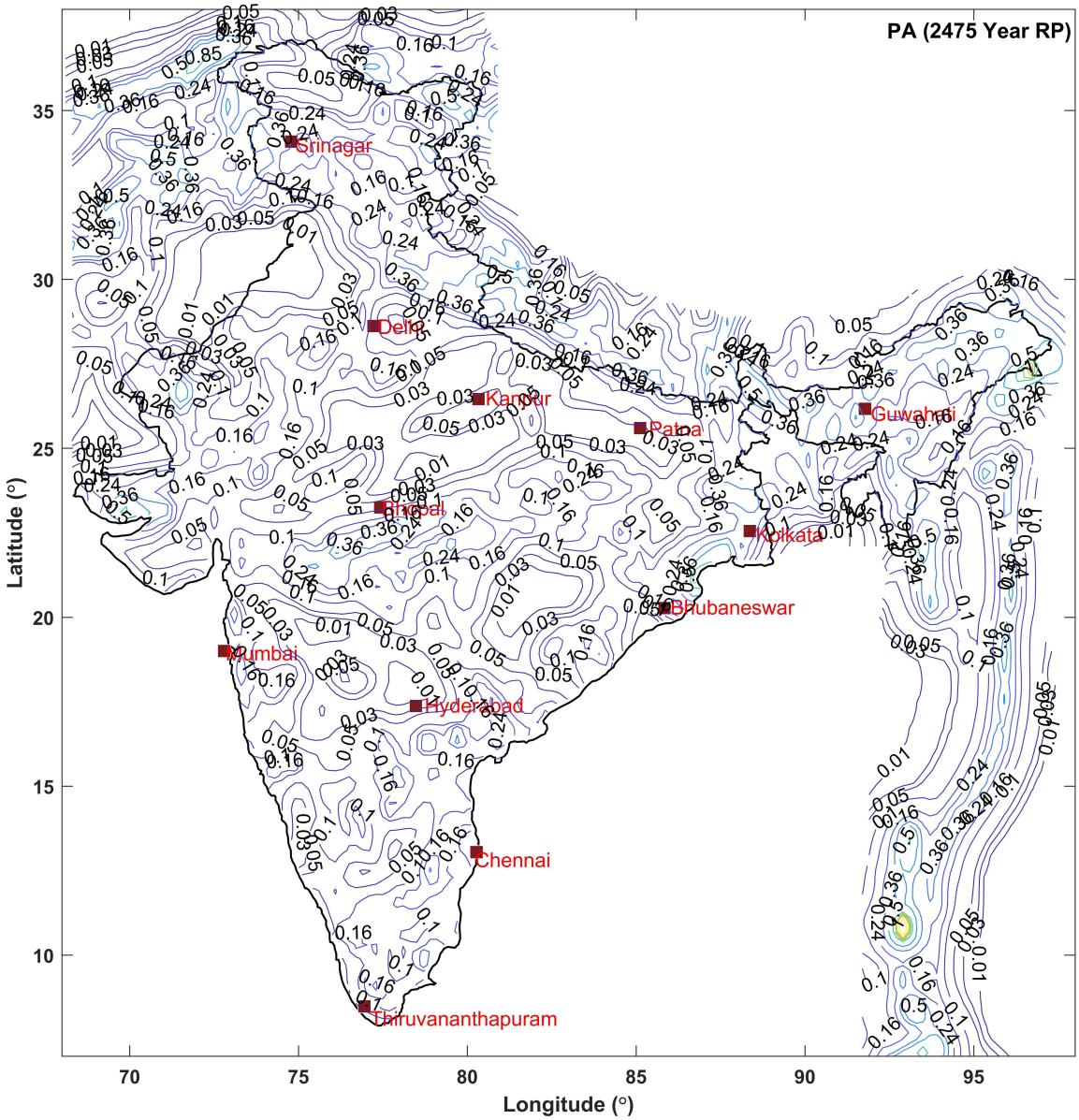

Figure 4.4: PA Contours (Units: g) with 2% probability of exceedence in 50 years (Return Period 2475 years) on B-type Sites (V_{s30}=760m/s estimated using Fault based approach.

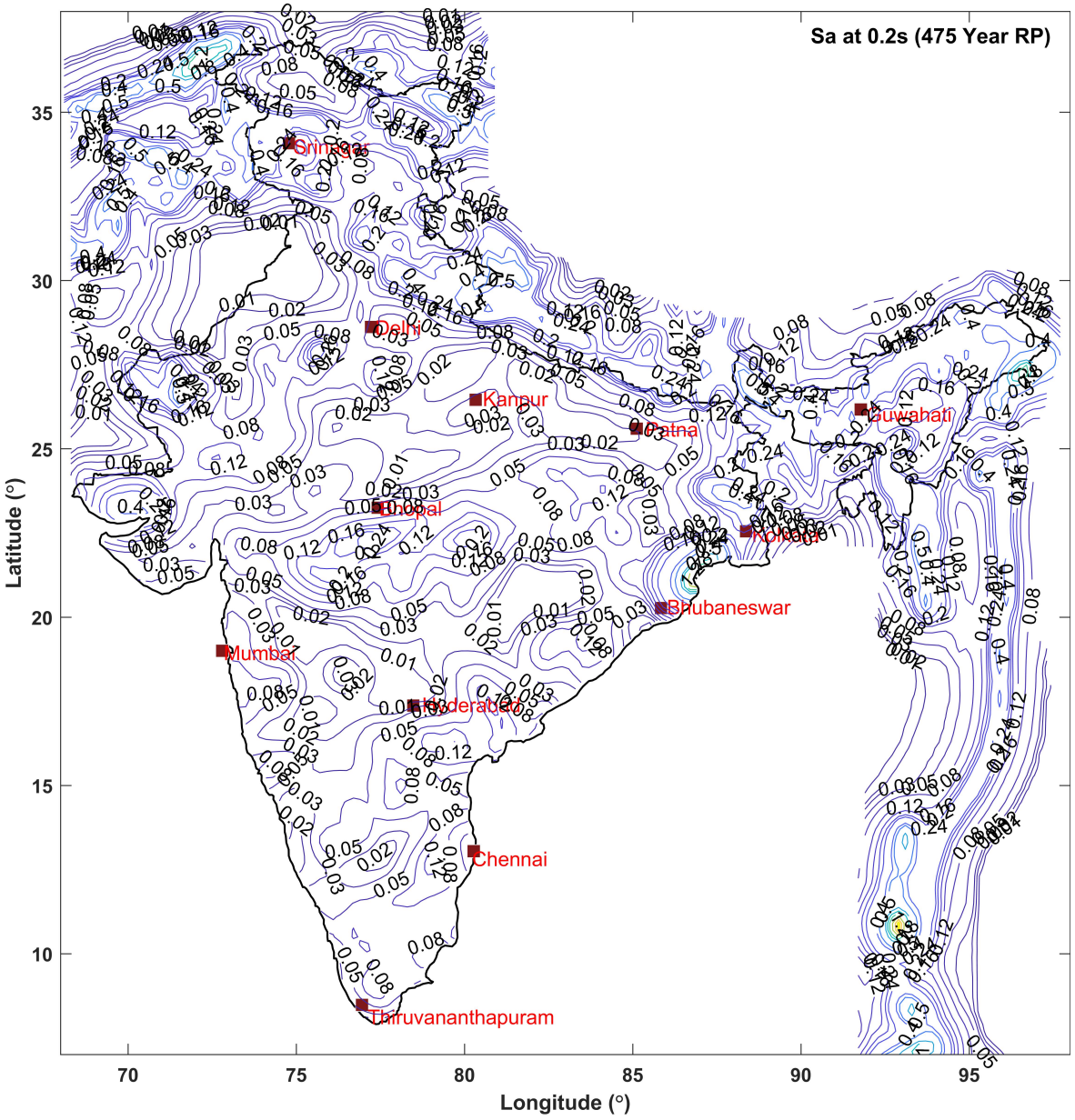

Figure 4.5: Spectral Acceleration at T = 0.2s and 5% damping Contours (Units: g) corresponding to 10% probability of exceedence in 50 years (Return Period 475 years) on B-type Sites (V_{s30}=760m/s estimated using Fault based approach.

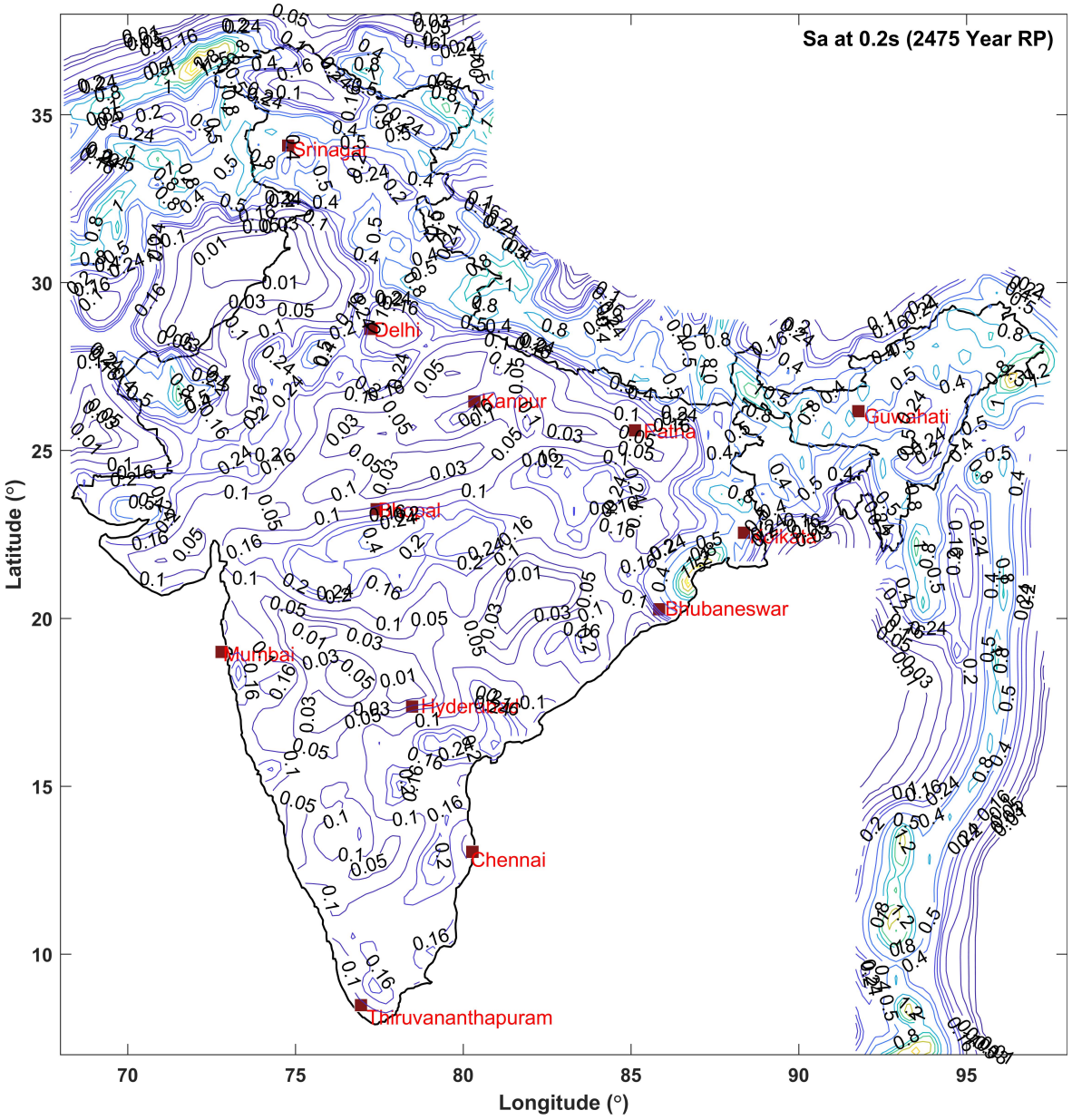

Figure 4.6: Spectral Acceleration at T = 0.2s and 5% damping Contours (Units: g) corresponding to 2% probability of exceedence in 50 years (Return Period 2475 years) on B-type Sites (V_{s30}=760m/s estimated using Fault based approach.

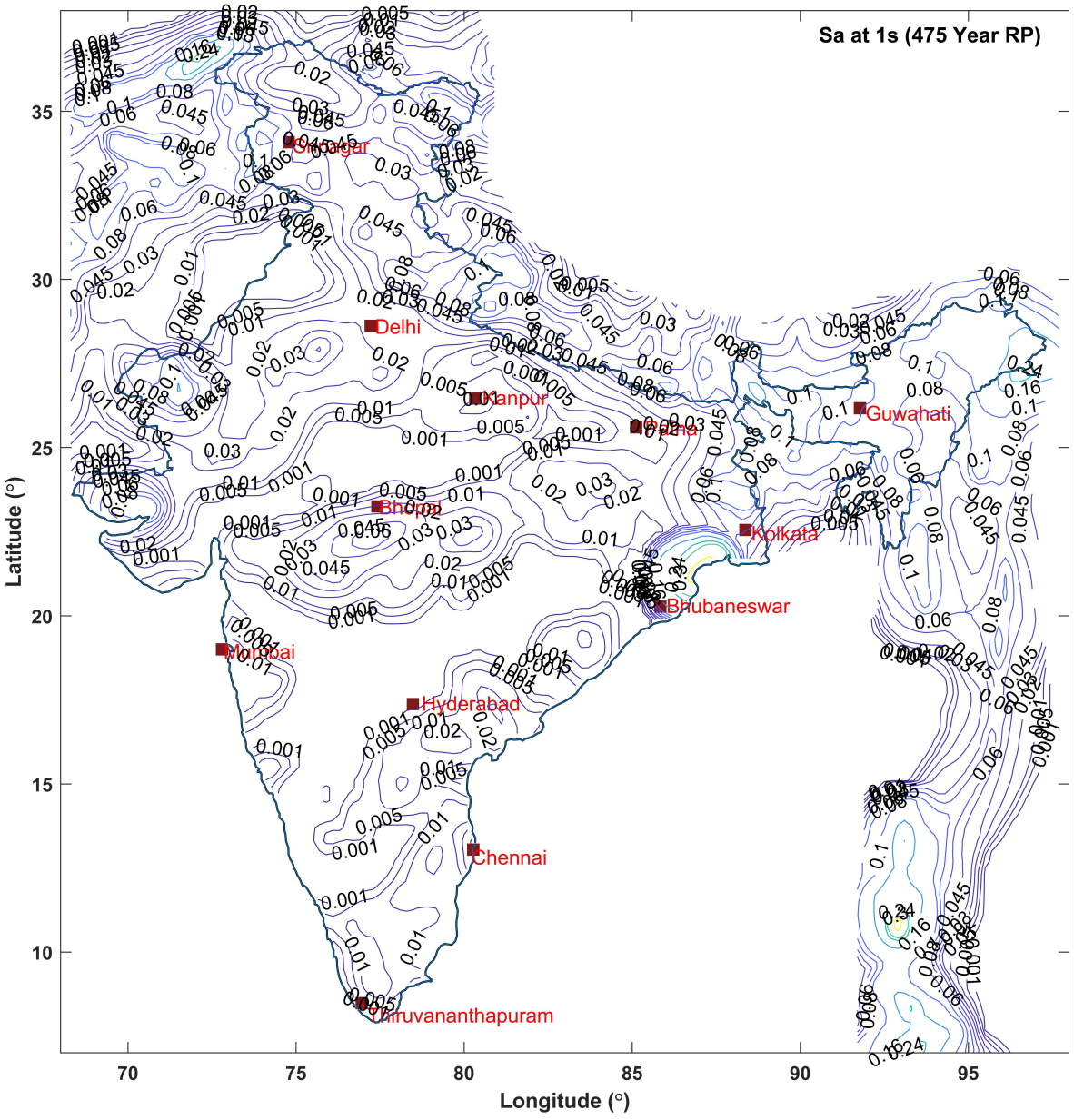

Figure 4.7: Spectral Acceleration at T = 1s and 5% damping Contours (Units: g) corresponding to 10% probability of exceedence in 50 years (Return Period 475 years) on B-type Sites (V_{s30}=760m/s estimated using Fault based approach.

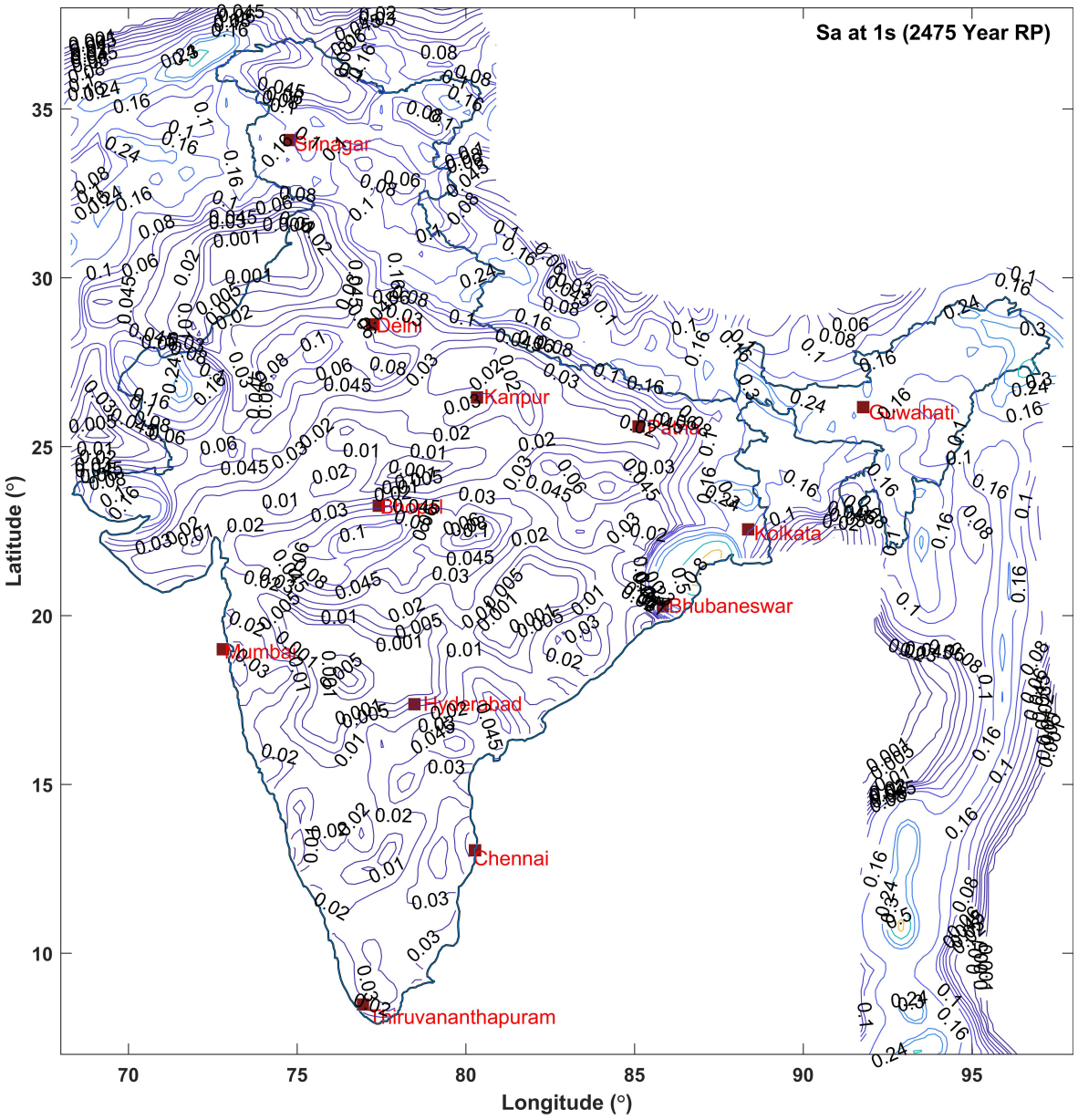

Figure 4.8: Spectral Acceleration at T = 1s and 5% damping Contours (Units: g) corresponding to 2% probability of exceedence in 50 years (Return Period 2475 years) on B-type Sites (V_{s30}=760m/s estimated using Fault based approach.

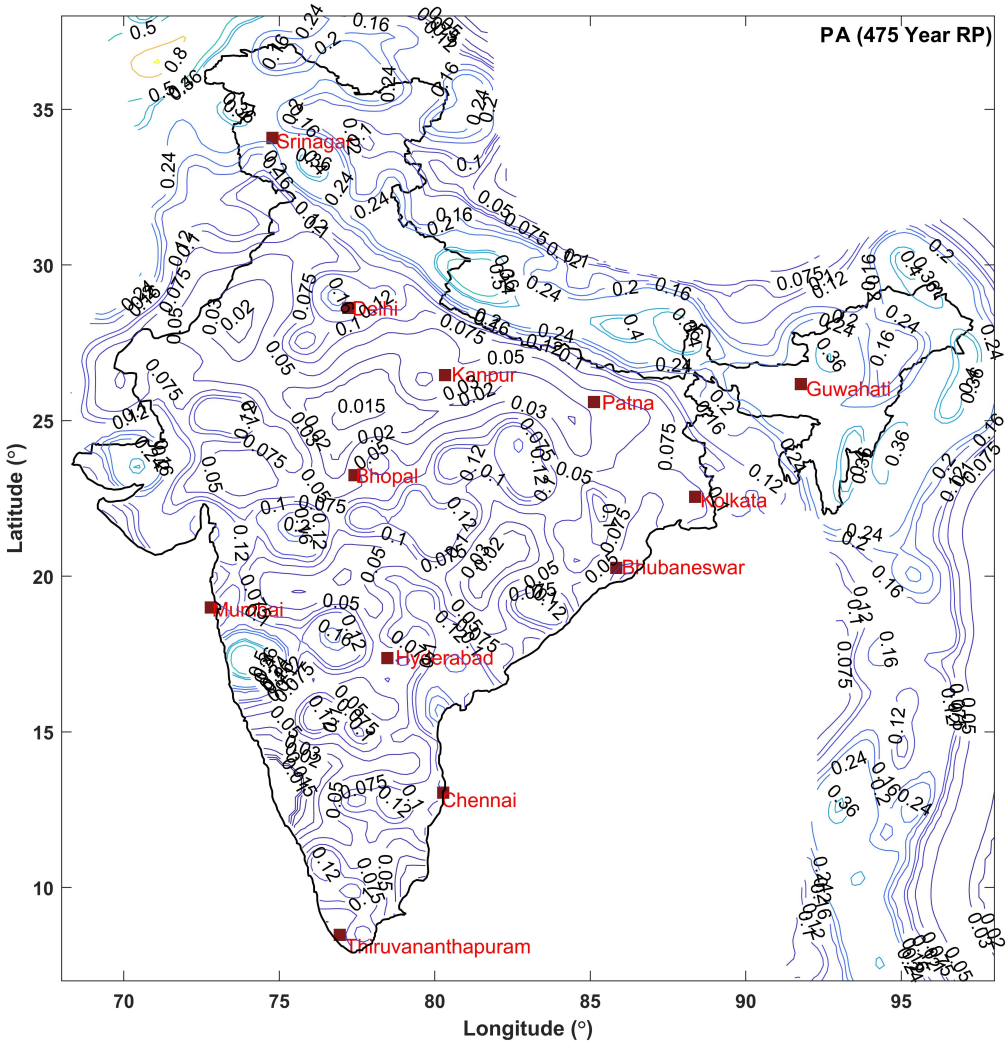

Figure 4.9: PA Contours (Units: g) with 10% probability of exceedence in 50 years (Return Period 475 years) on B-type Sites (V_{s30}=760m/s estimated using Circular Smoothing based approach.

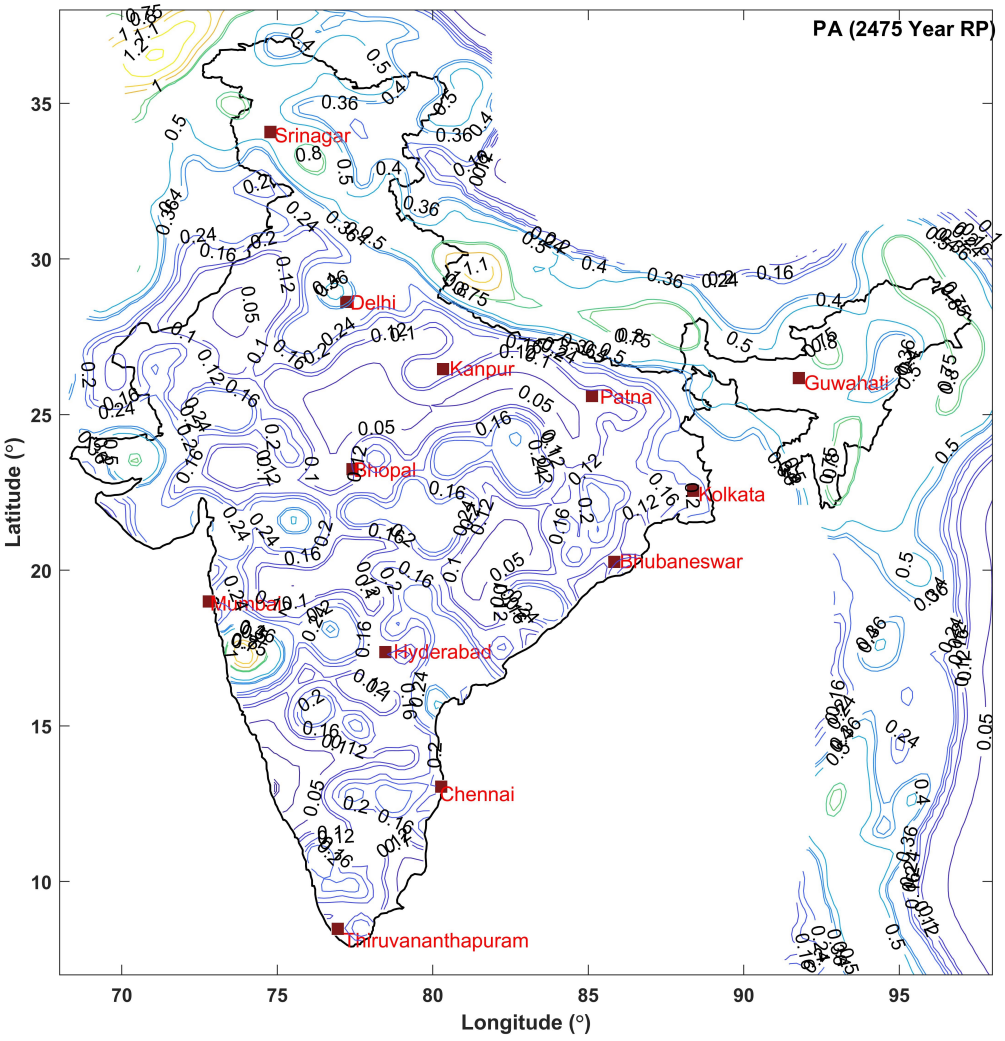

Figure 4.10: PA Contours (Units: g) with 2% probability of exceedence in 50 years (Return Period 2475 years) on B-type Sites (V_{s30}=760m/s estimated using Circular Smoothing based approach.

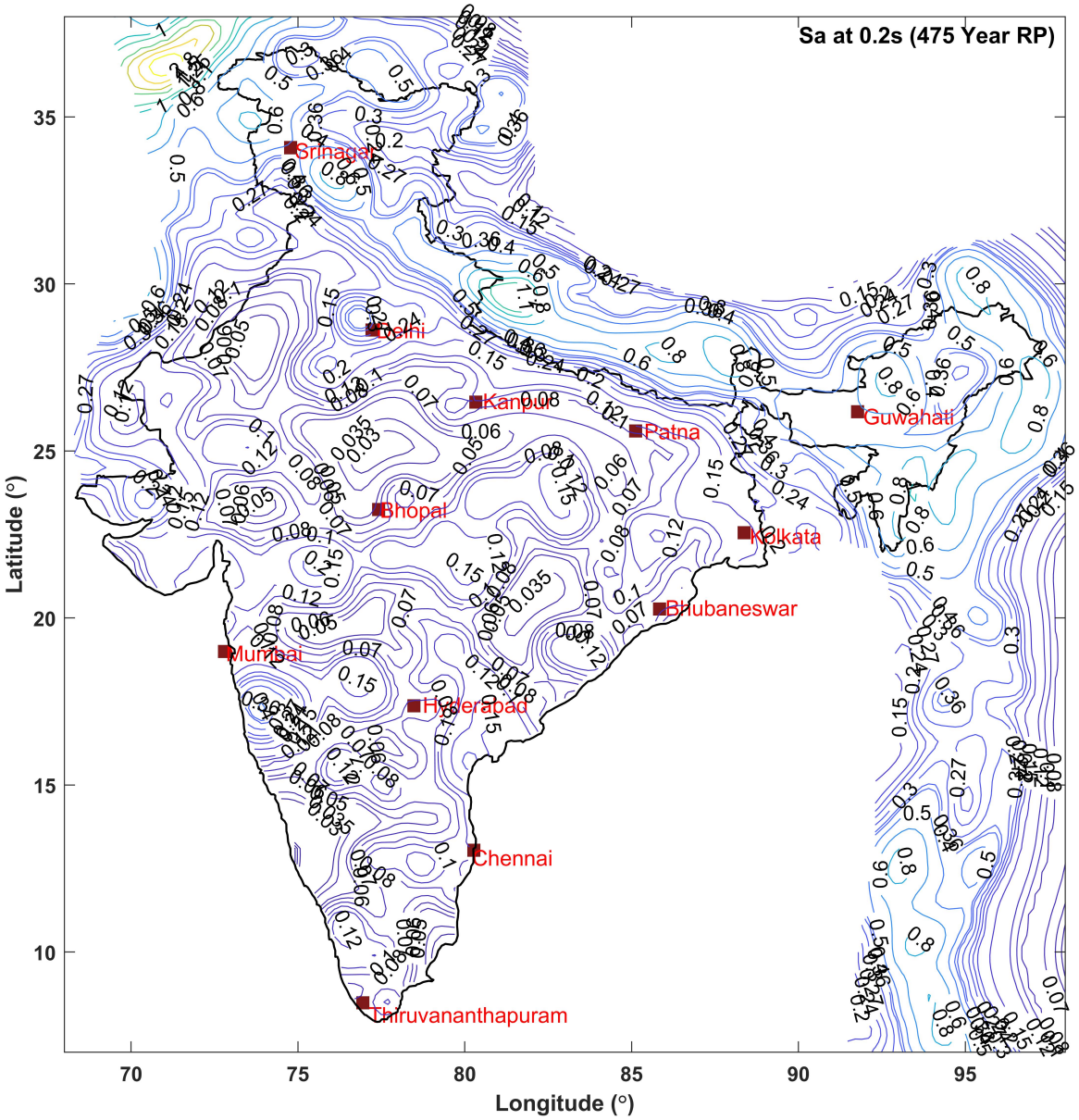

Figure 4.11: Spectral Acceleration at T = 0.2s and 5% damping Contours (Units: g) corresponding to 10% probability of exceedence in 50 years (Return Period 475 years) on B-type Sites (V_{s30}=760m/s estimated using Circular Smoothing based approach.

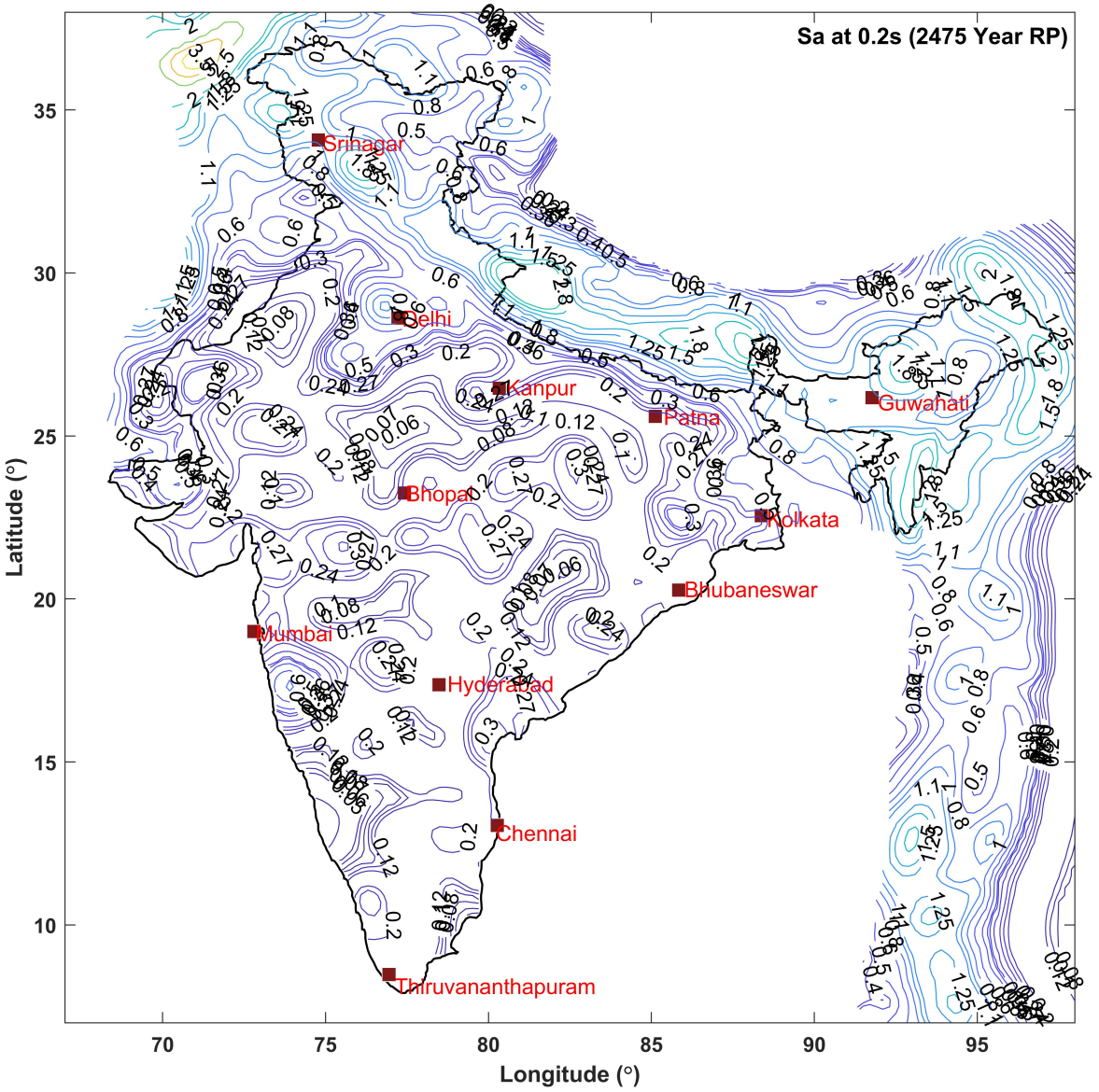

Figure 4.12: Spectral Acceleration at T = 0.2s and 5% damping Contours (Units: g) corresponding to 2% probability of exceedence in 50 years (Return Period 2475 years) on B-type Sites (V_{s30}=760m/s estimated using Circular Smoothing based approach.

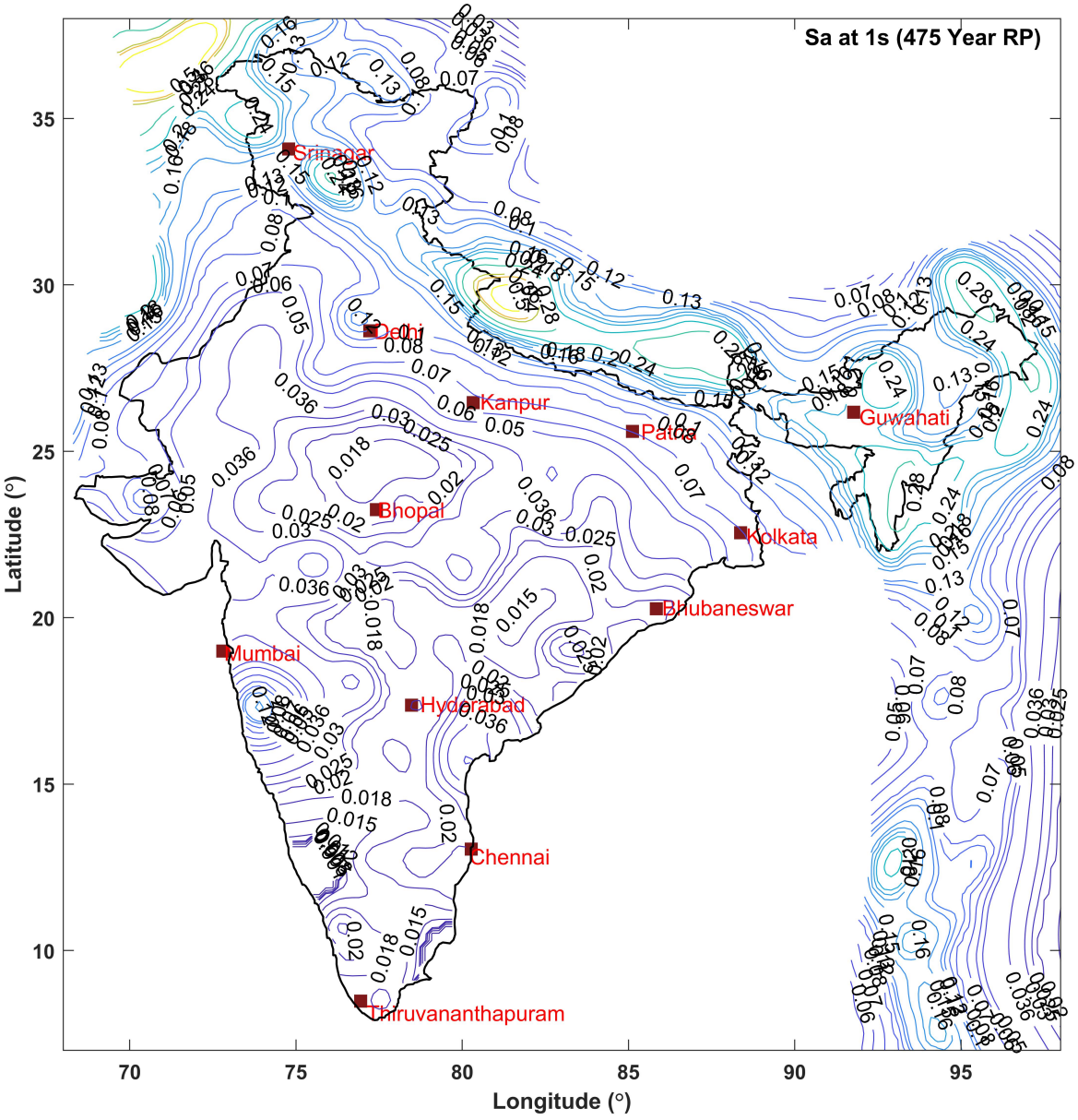

Figure 4.13: Spectral Acceleration at T = 1s and 5% damping Contours (Units: g) corresponding to 10% probability of exceedence in 50 years (Return Period 475 years) on B-type Sites (V_{s30}=760m/s estimated using Circular Smoothing based approach.

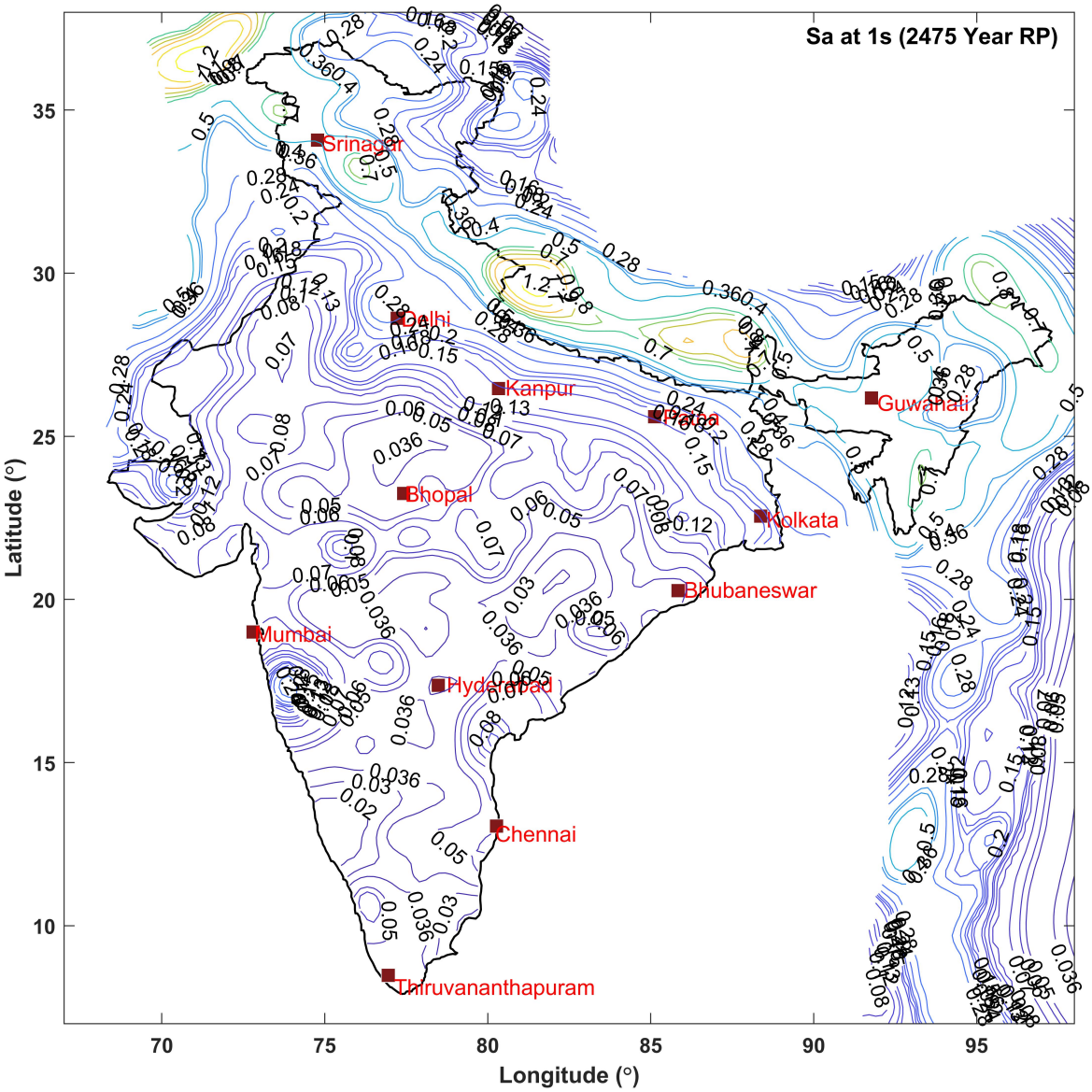

Figure 4.14: Spectral Acceleration at T = 1s and 5% damping Contours (Units: g) corresponding to 2% probability of exceedence in 50 years (Return Period 2475 years) on B-type Sites (V_{s30}=760m/s estimated using Circular Smoothing based approach.

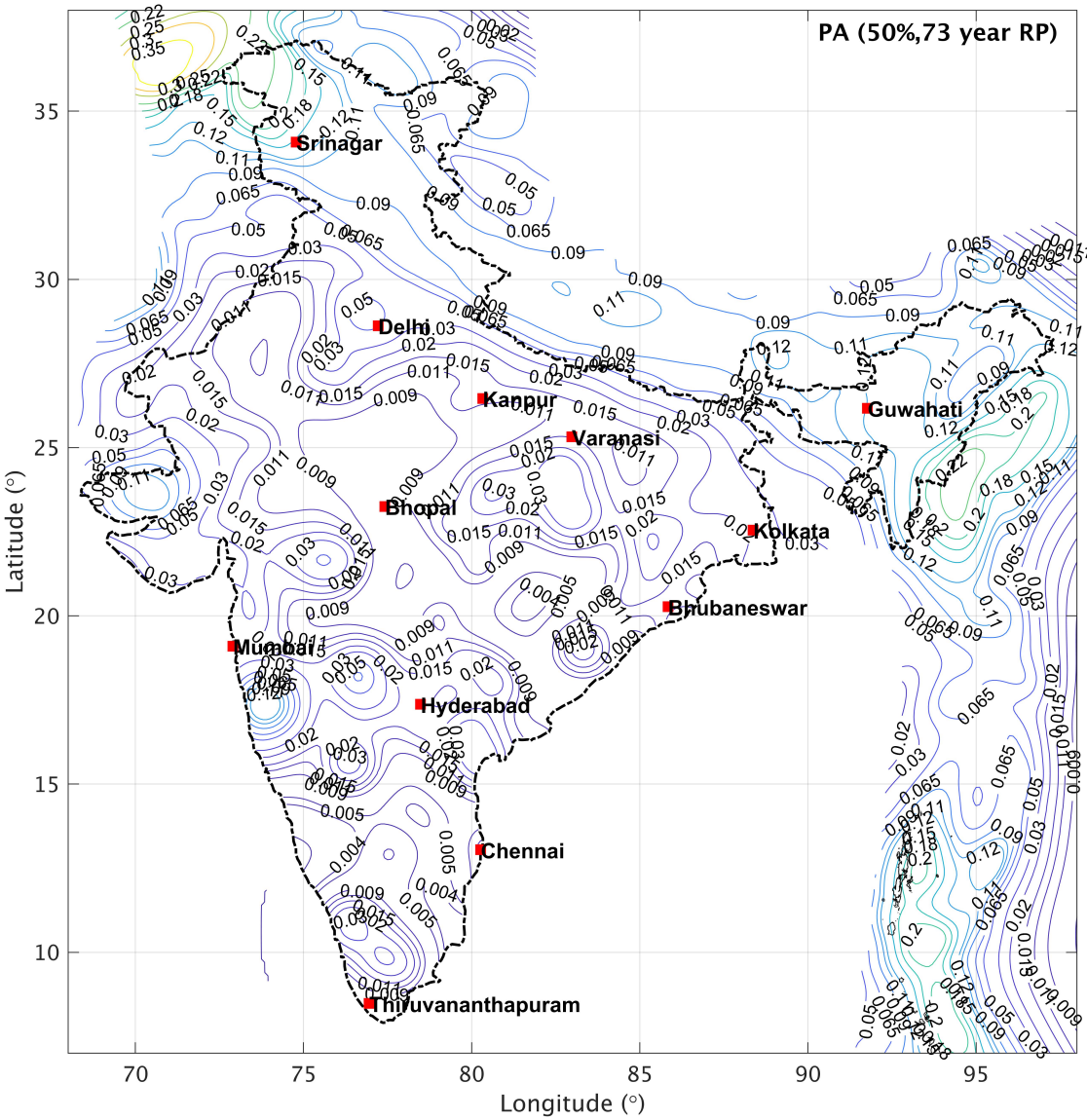

Figure 4.15: PA Contours (Units: g) with 50% probability of exceedence in 50 years (Return Period 73 years) on B-type Sites (V_{s30}=760m/s estimated using Elliptical Smoothing based approach. (Ranked weightage)

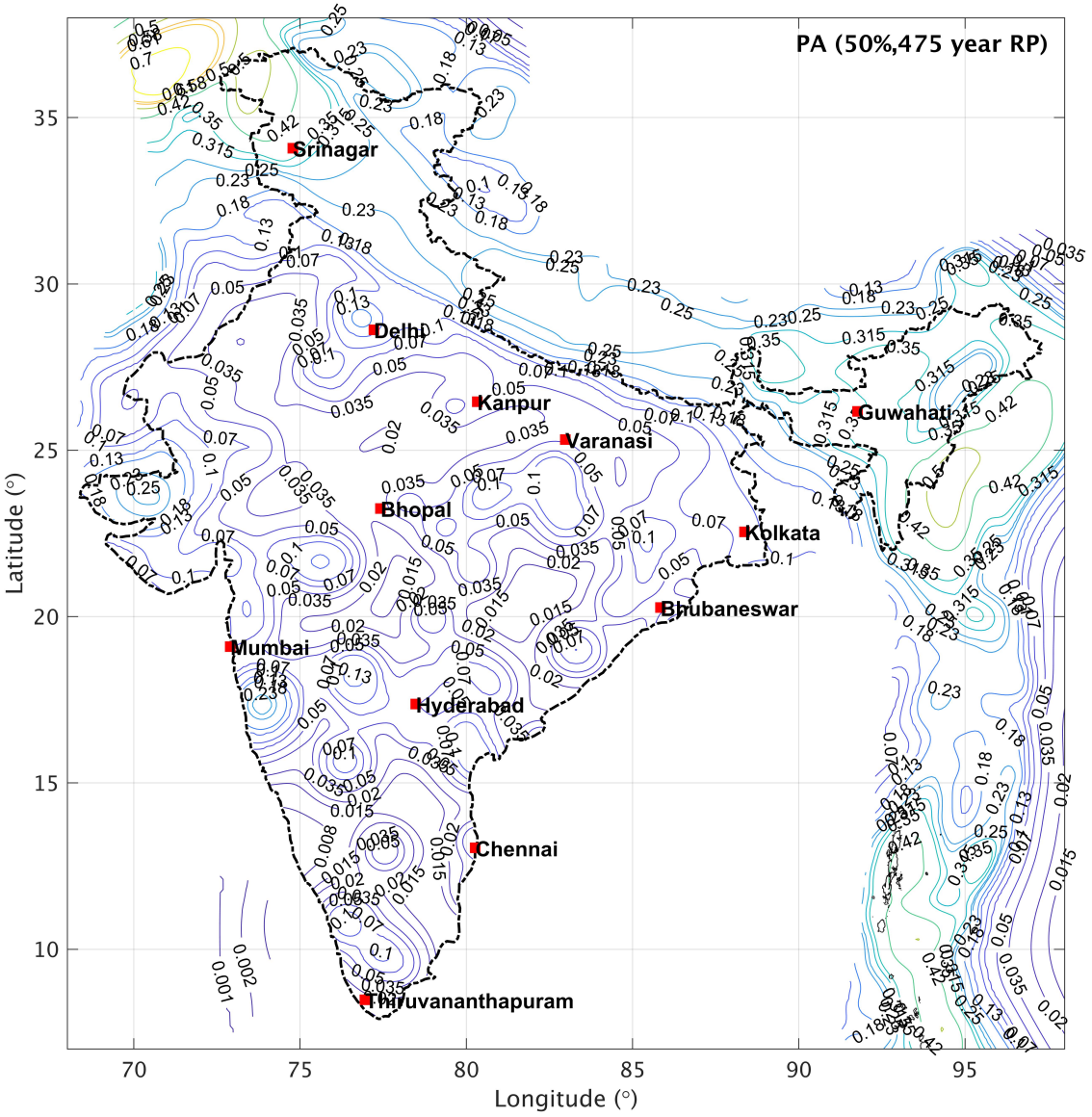

Figure 4.16: PA Contours (Units: g) with 10% probability of exceedence in 50 years (Return Period 475 years) on B-type Sites (V_{s30}=760m/s estimated using Elliptical Smoothing based approach. (Ranked weightage)

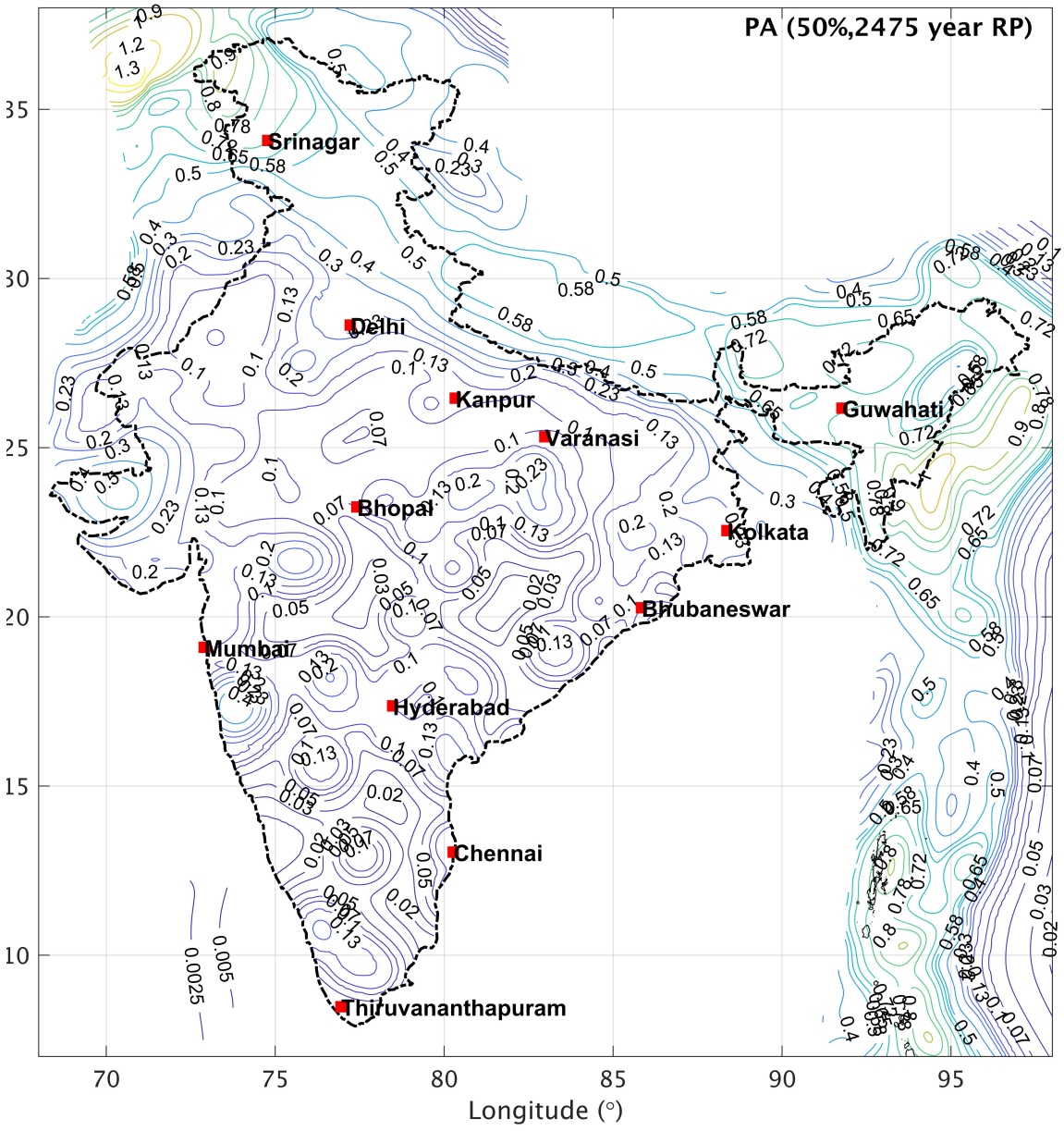

Figure 4.17: PA Contours (Units: g) with 2% probability of exceedence in 50 years (Return Period 2475 years) on B-type Sites (V_{s30}=760m/s estimated using Elliptical Smoothing based approach.(Ranked weightage)

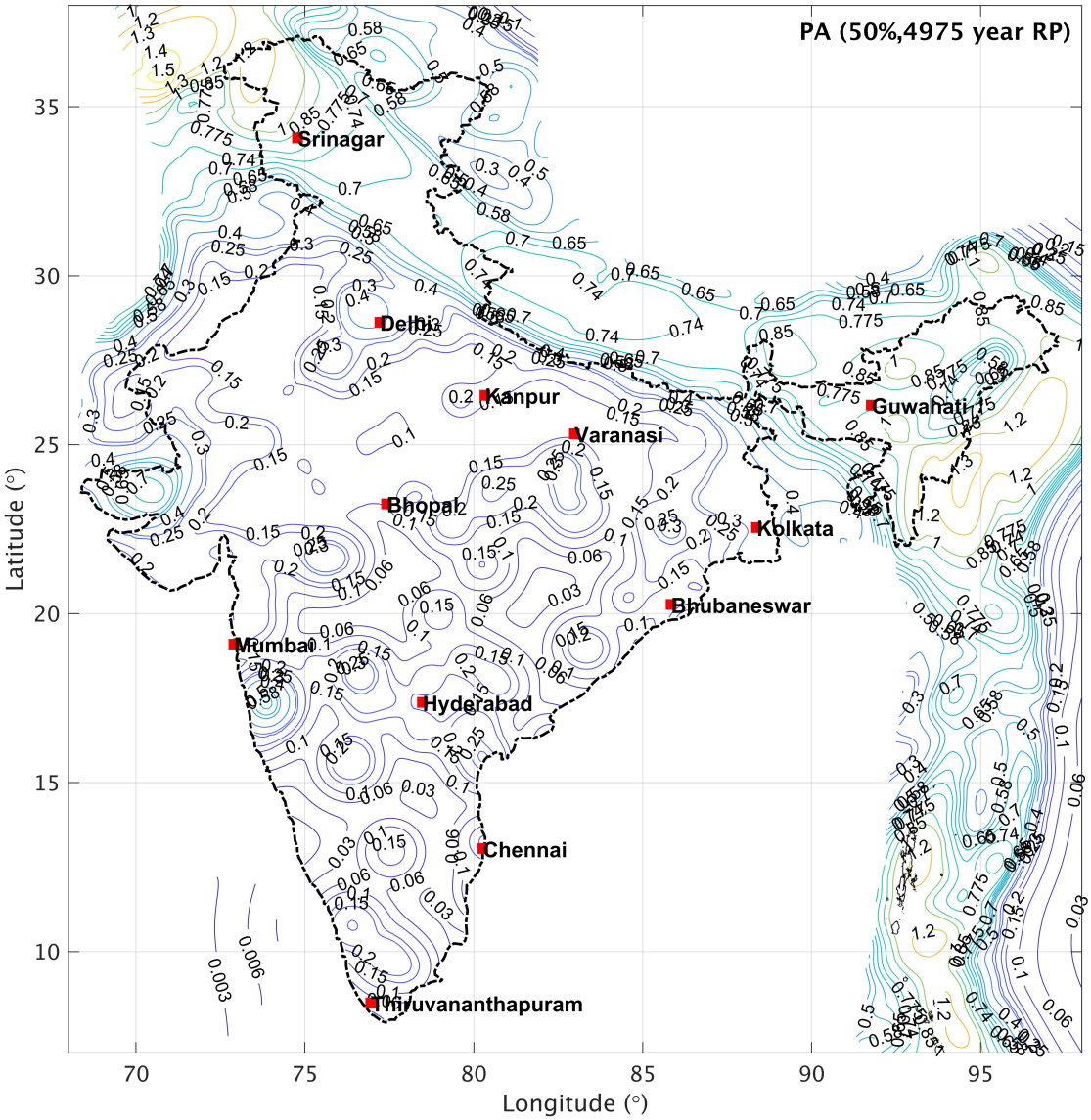

Figure 4.18: PA Contours (Units: g) with 1% probability of exceedence in 50 years (Return Period 4975 years) on B-type Sites (V_{s30}=760m/s estimated using Elliptical Smoothing based approach. (Ranked weightage)

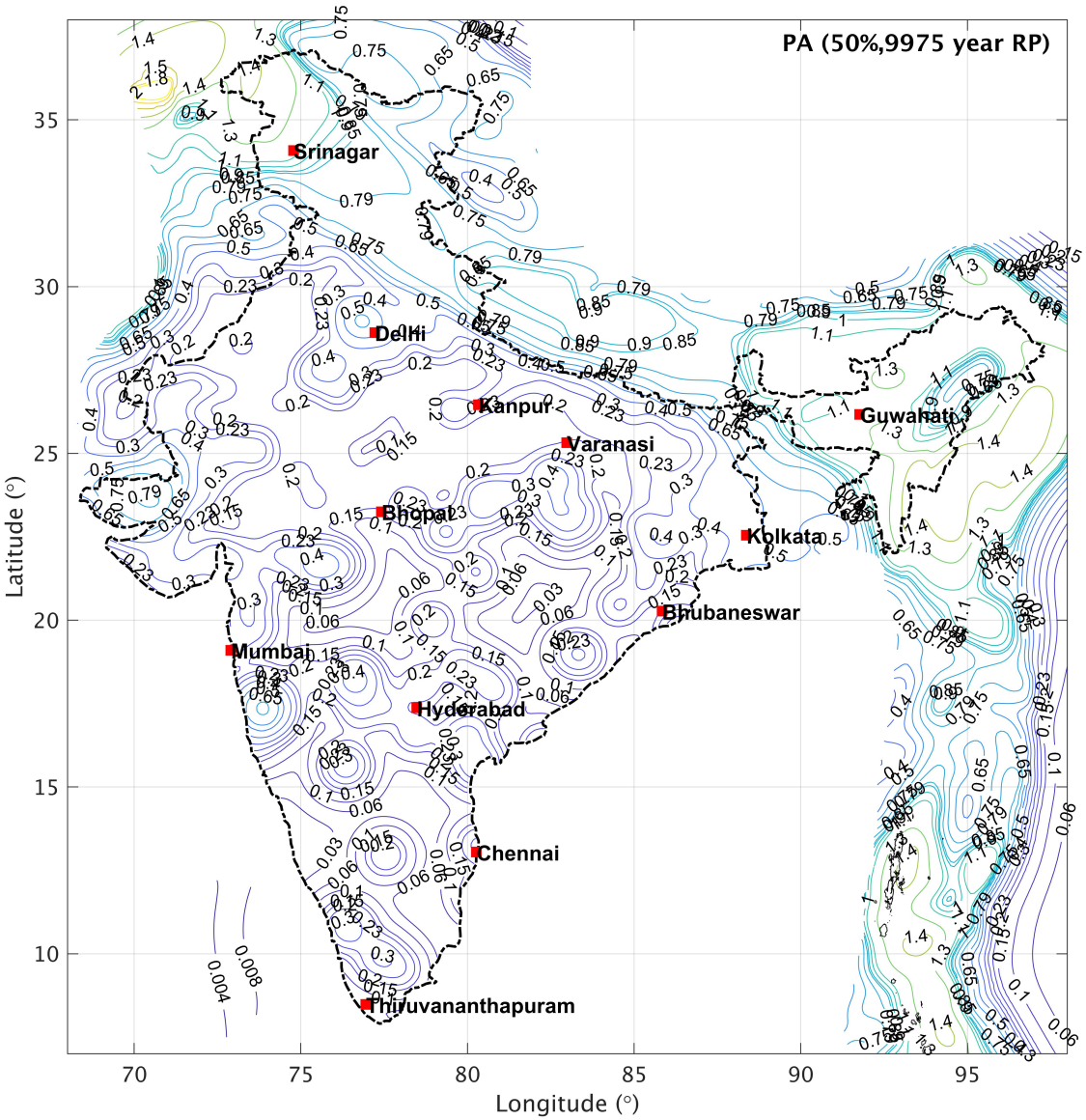

Figure 4.19: PA Contours (Units: g) with 0.5% probability of exceedence in 50 years (Return Period 9975 years) on B-type Sites (V_{s30}=760m/s estimated using Elliptical Smoothing based approach. (Ranked weightage)

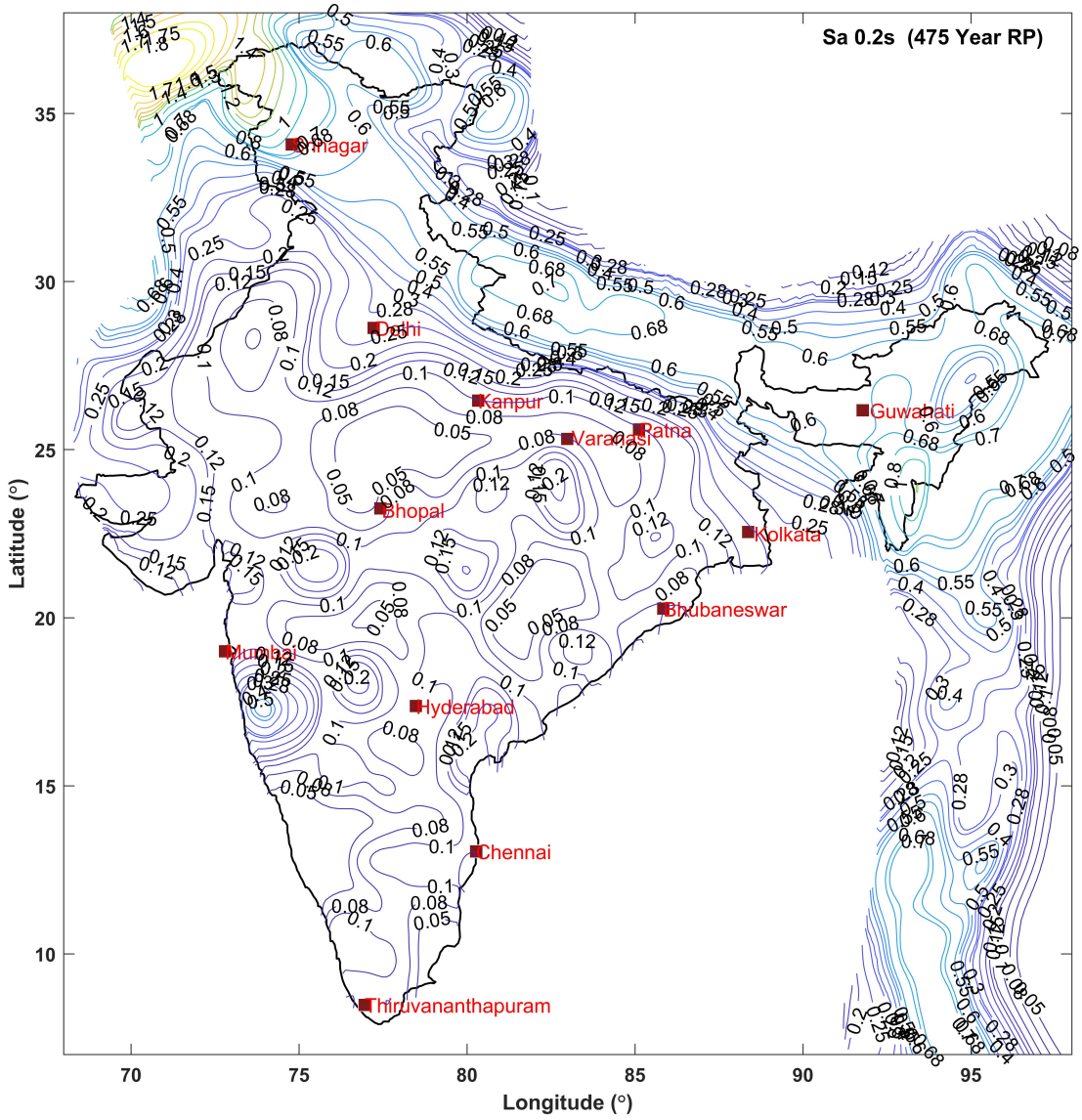

Figure 4.20: Spectral Acceleration at T = 0.2s and 5% damping Contours (Units: g) corresponding to 10% probability of exceedence in 50 years (Return Period 475 years) on B-type Sites (V_{s30}=760m/s estimated using Elliptical Smoothing based approach.

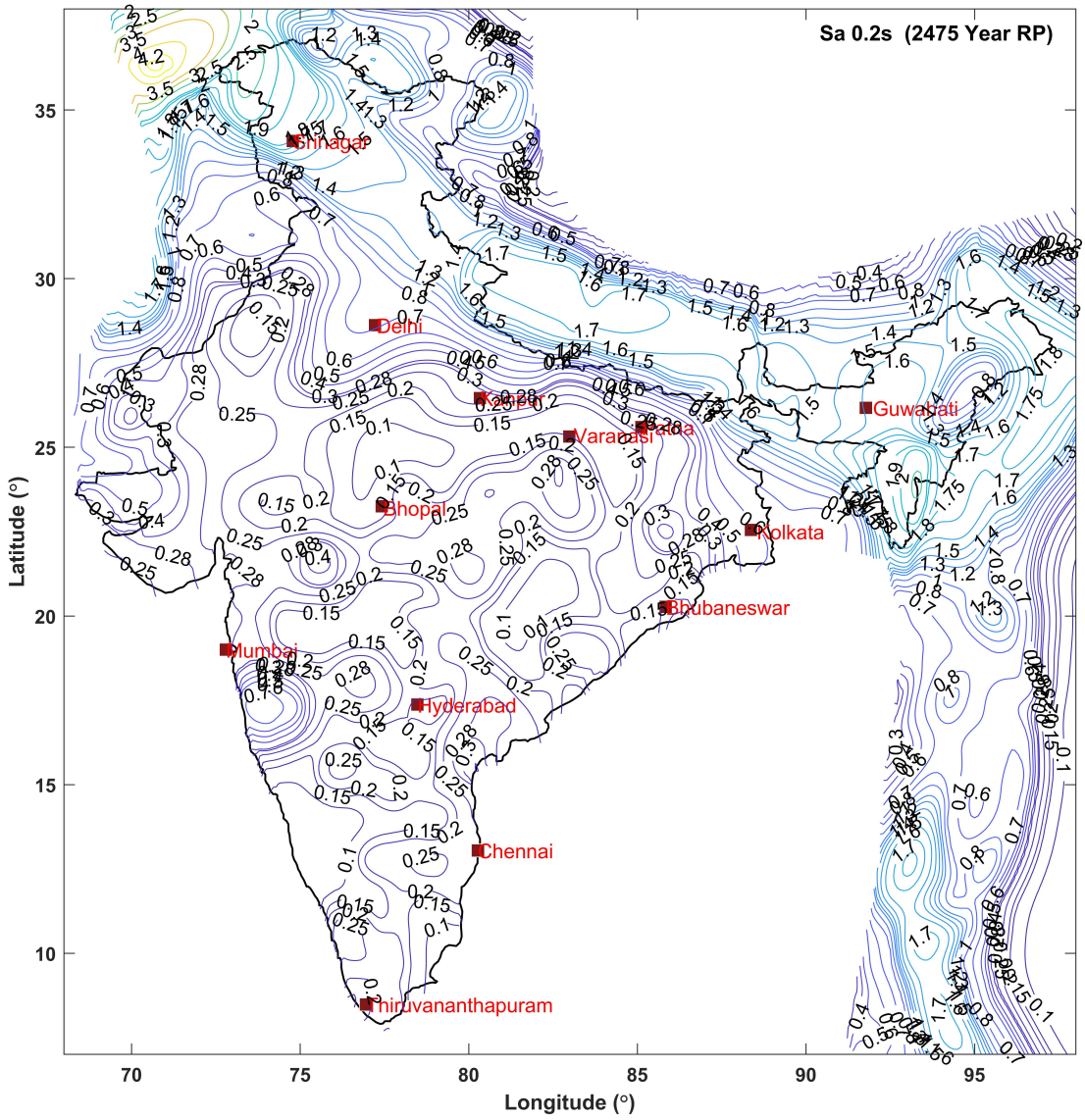

Figure 4.21: Spectral Acceleration at T = 0.2s and 5% damping Contours (Units: g) corresponding to 2% probability of exceedence in 50 years (Return Period 2475 years) on B-type Sites (V_{s30}=760m/s estimated using Elliptical Smoothing based approach.

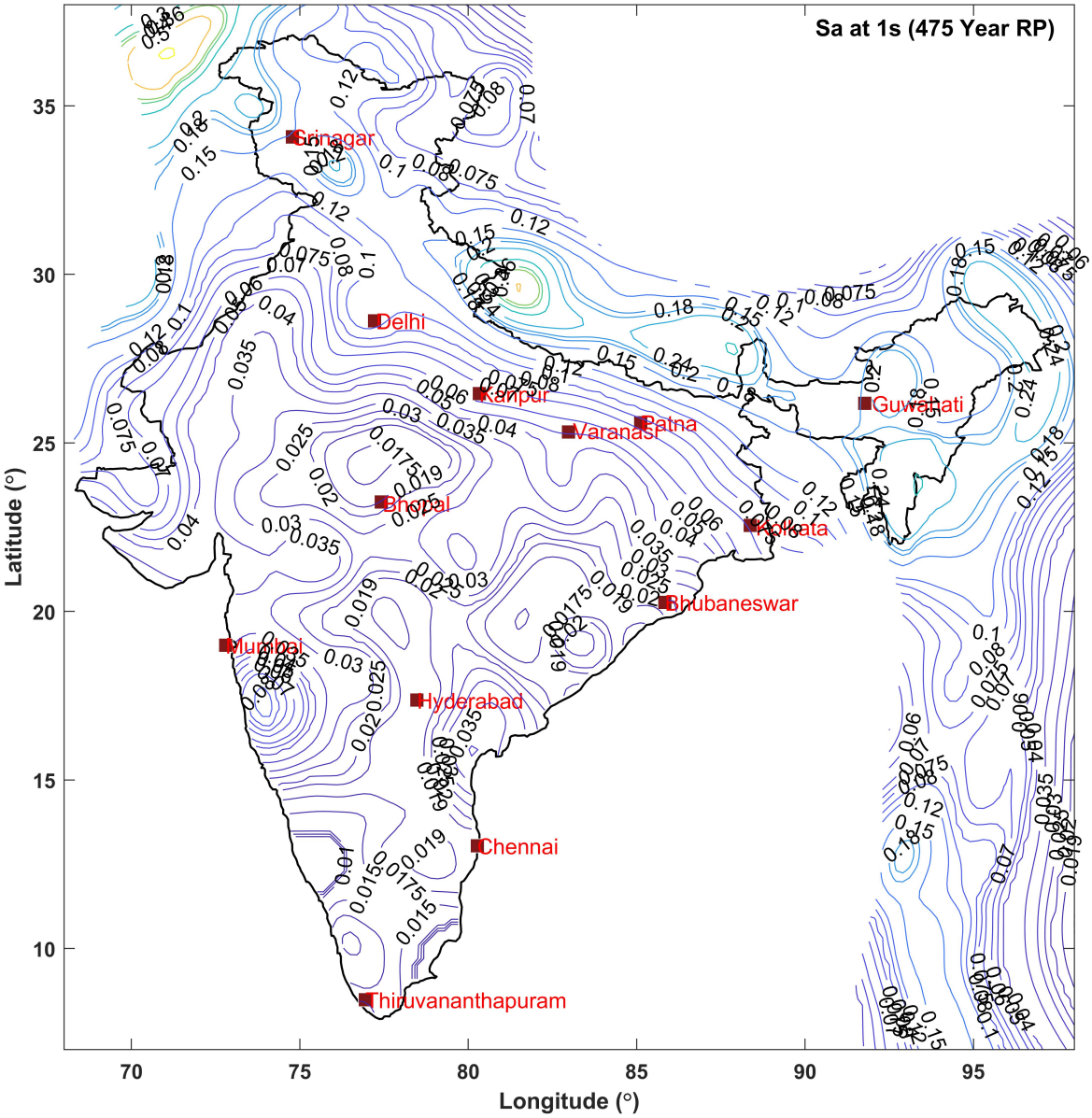

Figure 4.22: Spectral Acceleration at T = 1s and 5% damping Contours (Units: g) corresponding to 10% probability of exceedence in 50 years (Return Period 475 years) on B-type Sites (V_{s30}=760m/s estimated using Elliptical Smoothing based approach.

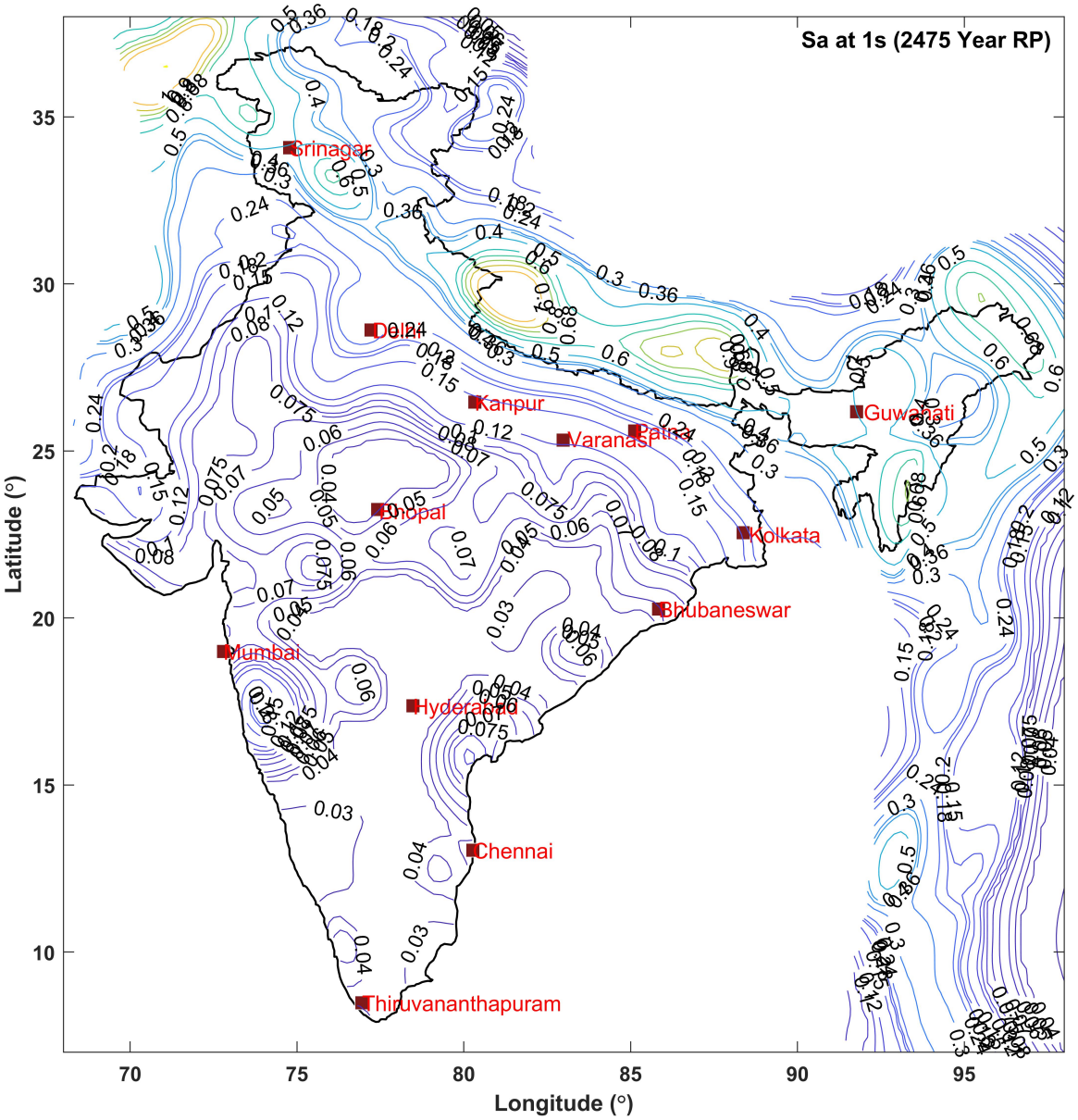

Figure 4.23: Spectral Acceleration at T = 1s and 5% damping Contours (Units: g) corresponding to 2% probability of exceedence in 50 years (Return Period 2475 years) on B-type Sites (V_{s30}=760m/s estimated using Elliptical Smoothing based approach.

Table 4.2: Relative Seismic Hazard of Indian Cities based on elliptically smoothed seismicity on B-type Sites (V_s30=760m/s) in terms of PA corresponding to 50 percentile value

Cities	Lat	Long	Return period					
			73year	475year	975year	2475year	4975year	9975year
Guwahati	26.2	91.8	0.121	0.348	0.433	0.701	0.800	1.175
Chandigarh	30.8	76.8	0.055	0.152	0.221	0.385	0.428	0.620
Kolkata	22.6	88.4	0.023	0.086	0.127	0.233	0.333	0.424
Mumbai	19.2	72.8	0.021	0.069	0.108	0.142	0.206	0.234
Jabalpur	23.2	79.8	0.020	0.080	0.117	0.177	0.221	0.272
Asansol	23.8	87.0	0.022	0.088	0.129	0.225	0.342	0.428
Delhi	28.6	77.2	0.052	0.148	0.217	0.236	0.413	0.545
Srinagar	34.0	74.8	0.141	0.377	0.479	0.720	0.801	1.159
Jaipur	26.8	75.8	0.023	0.085	0.124	0.207	0.265	0.376
Meerut	29.0	77.8	0.037	0.114	0.168	0.238	0.345	0.416
Agra	27.2	78.0	0.011	0.036	0.057	0.095	0.123	0.182
Ahmedabad	23.0	72.6	0.018	0.044	0.063	0.144	0.114	0.127
Vijayawada	16.4	80.6	0.021	0.066	0.098	0.126	0.181	0.220
Jamshedpur	22.8	86.2	0.019	0.068	0.110	0.184	0.229	0.333
Dhanbad	23.8	86.4	0.020	0.069	0.114	0.191	0.236	0.356
Pune	18.6	73.8	0.033	0.069	0.100	0.146	0.158	0.205
Kozhikode	11.4	75.8	0.013	0.048	0.068	0.111	0.129	0.189
Kolhapur	16.6	74.2	0.087	0.184	0.223	0.308	0.391	0.432
Rajkot	22.4	70.8	0.053	0.125	0.181	0.237	0.297	0.384
Vadodara	22.4	73.2	0.019	0.058	0.078	0.124	0.156	0.210
T'nanthapuram	8.4	77.0	0.007	0.020	0.030	0.037	0.059	0.068
Kochi	10.0	76.4	0.020	0.066	0.100	0.127	0.186	0.223
Ludhiana	30.8	75.8	0.032	0.088	0.122	0.274	0.235	0.346
Indore	22.4	75.6	0.020	0.065	0.098	0.127	0.181	0.219
Patna	25.6	85.2	0.017	0.049	0.068	0.116	0.158	0.216
Lucknow	26.8	80.8	0.016	0.051	0.074	0.151	0.190	0.234
Kanpur	26.6	80.4	0.012	0.046	0.070	0.122	0.184	0.231
Surat	21.2	72.8	0.034	0.104	0.127	0.200	0.230	0.314
Trichy	10.8	78.8	0.005	0.011	0.017	0.020	0.032	0.037
Ranchi	23.4	85.4	0.015	0.051	0.070	0.122	0.183	0.231
Allahabad	25.6	81.8	0.011	0.035	0.055	0.085	0.120	0.174
Amritsar	31.6	74.8	0.037	0.114	0.171	0.244	0.371	0.438
Coimbatore	11.0	77.0	0.018	0.060	0.087	0.114	0.160	0.210
Nagpur	21.2	79.2	0.007	0.023	0.035	0.055	0.068	0.093
Jodhpur	26.4	73.0	0.011	0.035	0.055	0.096	0.121	0.177
Nashir	20.0	73.8	0.021	0.070	0.110	0.129	0.204	0.232
Gwalior	26.2	78.2	0.008	0.029	0.045	0.076	0.117	0.171
Madurai	9.8	78.2	0.017	0.062	0.092	0.117	0.175	0.218
Varanasi	25.4	83.0	0.013	0.039	0.063	0.104	0.129	0.200
Bhopal	23.4	77.4	0.007	0.033	0.055	0.094	0.124	0.182
Hyderabad	17.4	78.6	0.016	0.053	0.070	0.103	0.131	0.195
Chennai	13.2	80.4	0.011	0.067	0.107	0.131	0.207	0.236
Solapur	17.8	75.8	0.033	0.089	0.119	0.130	0.214	0.236
Bhubaneswar	20.4	85.8	0.013	0.038	0.062	0.092	0.119	0.140
Bangalore	13.0	77.6	0.008	0.060	0.094	0.119	0.185	0.224
Aurangabad	19.8	75.4	0.009	0.019	0.027	0.034	0.042	0.058
Visakhapatnam	17.2	83.4	0.004	0.013	0.019	0.030	0.038	0.057
Raipur	21.2	81.6	0.005	0.012	0.018	0.024	0.033	0.037

Table 4.3: Comparison of maximum PA for 10% probability in 50 years as reported in literature for regions in India

Region	Nath and Thingbaijam (2012) Firm rock	Sitharam et al (2015) Bed rock	Jaiswal and Sinha (2007) hard-rock	NDMA (2010) A Type site	Present study (Elliptically Smoothed) Vs30 = 760m/s	IS:1893-1 (2016)
Himalayan	0.6-0.7g	0.2-0.3g	–	0.1-0.2g	0.2-0.65g	0.12-0.18g
Indo gangetic	0.3-0.35g	0.1-0.25g	–	0.1-0.15g	0.1 -0.2g	0.05-0.08g
North East India	0.5-0.9g	0.25-0.35g	–	0.2-0.35g	0.3-0.5g	0.18g
Koyna	0.3-0.4g	0.1-0.15g	0.2-0.36g	>0.25g	0.3-0.35g	0.12g
Central India	0.04-0.12g	<0.1g	0.1-0.15g	0.04-0.06g	0.05-0.10g	0.05-0.08g
Peninsular India	0.04-0.12g	0.05-0.2g	0.1-0.2g	0.04-0.06g	0.10-0.15g	0.05-0.08g
Gujarat	0.3-0.35g	0.1-0.15g	0.08-0.2g	0.05-0.3g	0.15-0.30g	0.12-0.18g
Andaman	–	–	–	–	0.3-0.36g	-

4.5 Spectral shape

As discussed in section 4.4, the PSHA has been carried out for all grid points spread over Indian land mass for spectral period 0 to 5s and the uniform hazard response spectra (UHRS) are derived for all these grid points. Based on the predetermined PA ranges (Zone A: <0.15g; Zone B: 0.15-0.3g; Zone C: 0.3-0.45g; Zone D: 0.45-0.6g; Zone E: >0.6g) by the map committee, the UHRS are grouped into five zones corresponding to the return period of 2,475 years (Figure 4.24).

Figure 4.25 shows the mean and $mean + 1.65\sigma$ shapes obtained separately for each zone by normalizing the computed spectra with corresponding PA. When compared with the normalized PSA spectra given in IS1893 (Part 1):2016, the peak amplitude of the $mean + 1.65\sigma$ spectral shapes is seen to be close to 2.5, but these spectra are observed to be narrower in all the five zones.

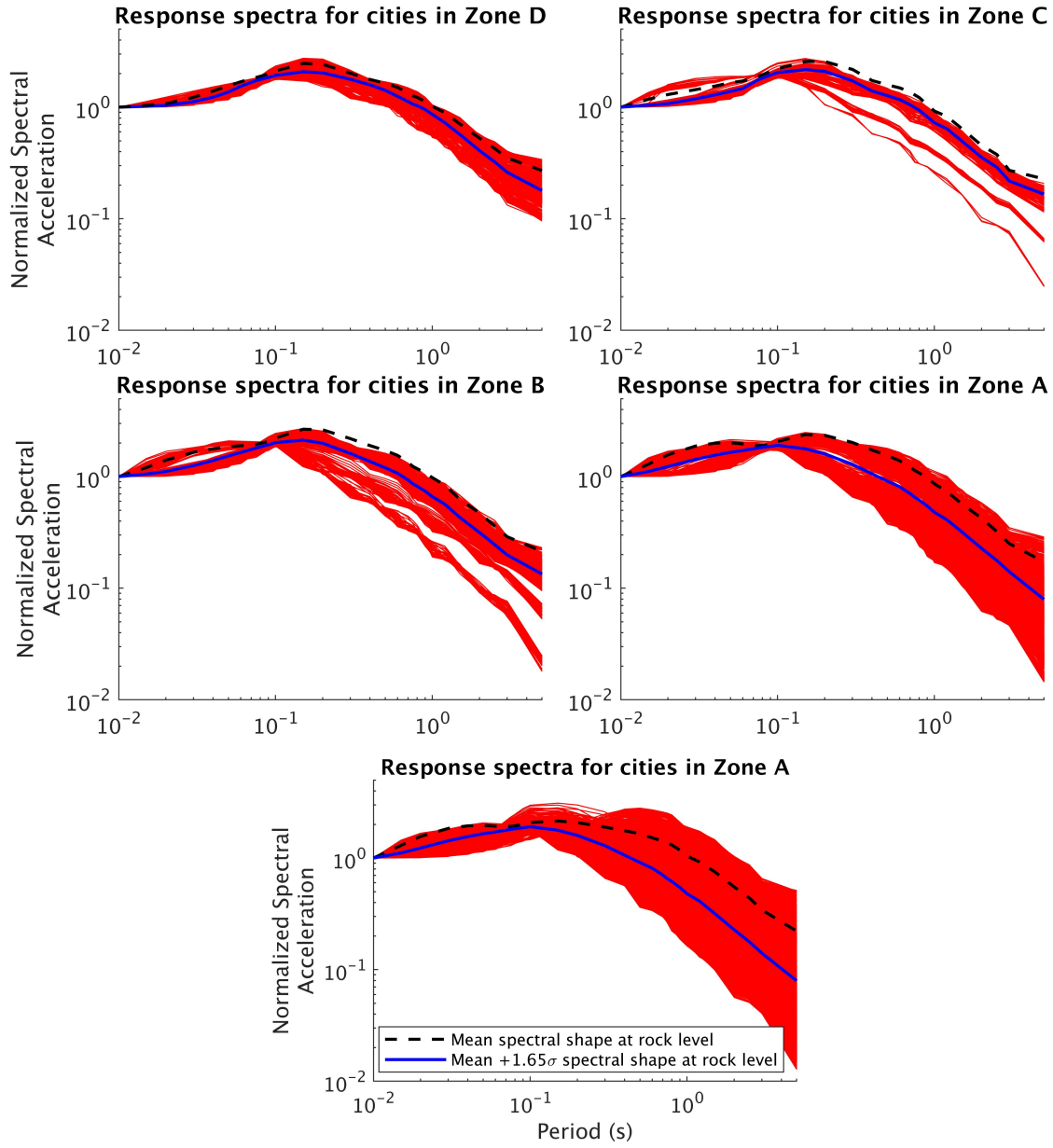

Figure 4.24: Normalized pseudo-spectral acceleration obtained from PSHA for all gridpoints with V_{s30}=760m/s

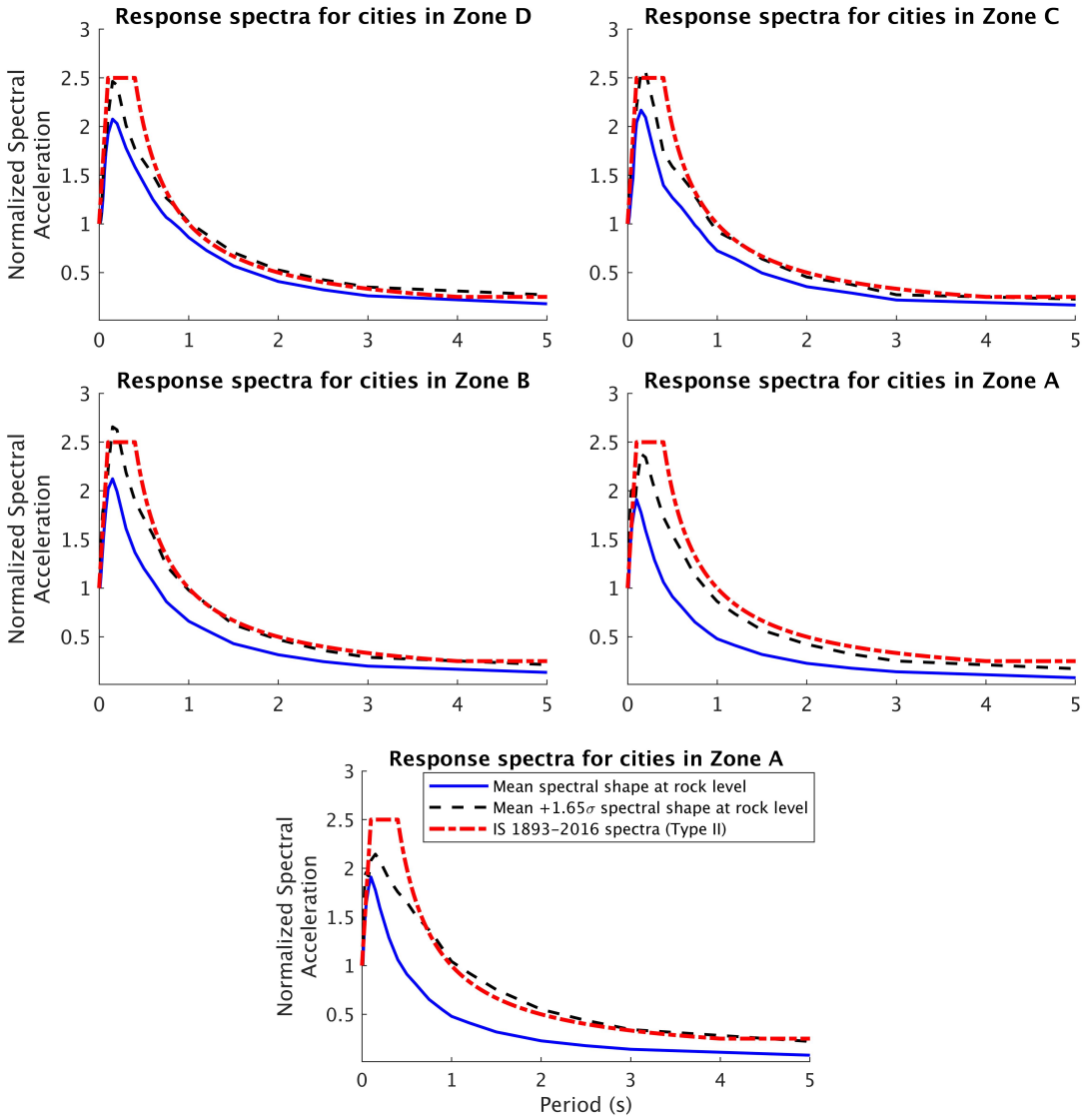

Figure 4.25: Mean and $mean + 1.65\sigma$ spectral shapes for all the five zones. Note that the spectral shape from IS 1893-2016 are also shown

REFERENCES

1. **Abrahamson, N.**, **N. Gregor**, and **K. Addo** (2016). Bc hydro ground motion prediction equations for subduction earthquakes. *Earthquake Spectra*, **32**(1), 23–44.

2. **Abrahamson, N. A.**, **W. J. Silva**, and **R. Kamai** (2014). Summary of the ask14 ground motion relation for active crustal regions. *Earthquake Spectra*, **30**(3), 1025–1055.

3. **Abrahamson, N. A.** and **R. Youngs** (1992). A stable algorithm for regression analyses using the random effects model. *Bulletin of the Seismological Society of America*, **82**(1), 505–510.

4. **Adhikari, L.**, **U. Gautam**, **B. Koirala**, **M. Bhattarai**, **T. Kandel**, **R. Gupta**, **C. Timsina**, **N. Maharjan**, **K. Maharjan**, **T. Dahal**, *et al.* (2015). The aftershock sequence of the 2015 april 25 gorkha–nepal earthquake. *Geophysical Supplements to the Monthly Notices of the Royal Astronomical Society*, **203**(3), 2119–2124.

5. **Ahmad, I.**, **M. H. El Naggar**, and **A. N. Khan** (2008). Neural network based attenuation of strong motion peaks in europe. *Journal of Earthquake Engineering*, **12**(5), 663–680.

6. **Alavi, A. H.** and **A. H. Gandomi** (2011). Prediction of principal ground-motion parameters using a hybrid method coupling artificial neural networks and simulated annealing. *Computers & Structures*, **89**(23-24), 2176–2194.

7. **Ambraseys, N.** and **R. Bilham** (2003). Earthquakes in afghanistan. *Seismological Research Letters*, **74**(2), 107–123.

8. **Ambraseys, N.** and **D. Jackson** (2003). A note on early earthquakes in northern india and southern tibet. *Current Science*, 570–582.

9. **Anbazhagan, P.**, **A. Kumar**, and **T. Sitharam** (2013). Seismic site classification and correlation between standard penetration test n value and shear wave velocity for lucknow city in indo-gangetic basin. *Pure and applied geophysics*, **170**(3), 299–318.

10. **Ancheta, T. D.**, **R. B. Darragh**, **J. P. Stewart**, **E. Seyhan**, **W. J. Silva**, **B. S.-J. Chiou**, **K. E. Wooddell**, **R. W. Graves**, **A. R. Kottke**, **D. M. Boore**, *et al.* (2014). Nga-west2 database. *Earthquake Spectra*, **30**(3), 989–1005.

11. **Anderson, J. G.** (1997). Nonparametric description of peak acceleration above a subduction thrust. *Seismological Research Letters*, **68**(1), 86–93.

12. **Ashish**, **C. Lindholm**, **I. Parvez**, and **D. Kühn** (2016). Probabilistic earthquake hazard assessment for Peninsular India. *J Seism.*, **20**, 629–653.

13. **Atkinson, G. M.** (2001). An alternative to stochastic ground-motion relations for use in seismic hazard analysis in eastern north america. *Seismological Research Letters*, **72**(2), 299–306.

14. **Atkinson, G. M.** and **D. M. Boore** (2003). Empirical ground-motion relations for subduction-zone earthquakes and their application to cascadia and other regions. *Bulletin of the Seismological Society of America*, **93**(4), 1703–1729.

15. **Atkinson, G. M.** and **D. M. Boore** (2006). Earthquake ground-motion prediction equations for eastern north america. *Bulletin of the seismological society of America*, **96**(6), 2181–2205.

16. **Bagchi, S.** and **S. Raghukanth** (2017). Seismic response of the central part of indo-gangetic plain. *Journal of Earthquake Engineering*, 1–25.

17. **Bajaj, K.** and **P. Anbazhagan** (2019). Regional stochastic gmpe with available recorded data for active region–application to the himalayan region. *Soil Dynamics and Earthquake Engineering*, **126**, 105825.

18. **Balakrishnan, T. S.**, **P. Unnikrishnan**, and **A. V. S. Murty** (2009). The Tectonic Map of India and Contiguous Areas. *J. Geol. Soc. India*, **74**(August), 158–170.

19. **Bapat, A.**, **R. Kulkarni**, and **S. K. Guha**, *Catalogue of earthquakes in India and neighbourhood: from historical period upto 1979*. Indian Society of Earthquake Technology, 1983.

20. **Bard, P.**, **M. Campillo**, **F. J. Cha´vez-Garcia**, and **F. Sa´nchez-Sesma** (1988). The mexico earthquake of september 19, 1985—a theoretical investigation of large- and small-scale amplification effects in the mexico city valley. *Earthquake Spectra*, **4**(3), 609–633. URL `https://doi.org/10.1193/1.1585493`.

21. **Bard, P.-Y.** and **M. Bouchon** (1985). The two-dimensional resonance of sediment-filled valleys. *Bulletin of the Seismological Society of America*, **75**(2), 519. URL `http://dx.doi.org/`.

22. **Baruah, S.**, **S. Baruah**, **P. Bora**, **R. Duarah**, **A. Kalita**, **R. Biswas**, **N. Gogoi**, and **J. Kayal** (2012). Moment magnitude (m w) and local magnitude (m l) relationship for earthquakes in northeast india. *Pure and applied geophysics*, **169**(11), 1977–1988.

23. **Basu, S.** and **N. Nigam**, Seismic risk analysis of Indian peninsula. *In Proc. 6th World Conf. Earthqu. Engg., New Delhi*. 1977.

24. **Berry, M. J.** and **G. Linoff**, *Data mining techniques: for marketing, sales, and customer support*. John Wiley & Sons, Inc., 1997.

25. **Bilham, R.** (2009). The seismic future of cities. *Bulletin of Earthquake Engineering*, **7**(4), 839.

26. **Bilham, R.** (2019). Himalayan earthquakes: a review of historical seismicity and early 21st century slip potential. *Geological Society, London, Special Publications*, **483**, SP483–16.

27. **Bommer, J.** and **J. E. Alarcon** (2006). The prediction and use of peak ground velocity. *J. Earthq. Eng.*, **10**(1), 1–31. ISSN 1363-2469.

28. **Boore, D. M.** (1983). Stochastic simulation of high-frequency ground motions based on seismological models of the radiated spectra. *Bulletin of the Seismological Society of America*, **73**(6A), 1865–1894.

29. **Boore, D. M.** (2003). Analog-to-Digital Conversion as a Source of Drifts in Displacements Derived from Digital Recordings of Ground Acceleration. *Bull. Seismol. Soc. Am.*, **93**(5), 2017–2024.

30. **Boore, D. M.** (2009). Comparing stochastic point-source and finite-source ground-motion simulations: Smsim and exsim. *Bulletin of the Seismological Society of America*, **99**(6), 3202–3216.

31. **Boore, D. M.** and **J. Boatwright** (1984). Average body-wave radiation coefficients. *Bull. Seismol. Soc. Am.*, **74**(5), 1615–1621.

32. **Boore, D. M.**, **J. P. Stewart**, **E. Seyhan**, and **G. M. Atkinson** (2014). Nga-west2 equations for predicting pga, pgv, and 5% damped psa for shallow crustal earthquakes. *Earthquake Spectra*, **30**(3), 1057–1085.

33. **Boore, D. M.** and **E. M. Thompson** (2015). Revisions to some parameters used in stochastic-method simulations of ground motion. *Bulletin of the Seismological Society of America*, **105**(2A), 1029–1041.

34. **Bradley, B. A.** (2012). Strong ground motion characteristics observed in the 4 september 2010 darfield, new zealand earthquake. *Soil Dynamics and Earthquake Engineering*, **42**, 32 – 46. ISSN 0267-7261. URL `http://www.sciencedirect.com/science/article/pii/S0267726112001315`.

35. **Bradley, B. A.** and **M. Cubrinovski** (2011). Near-source strong ground motions observed in the 22 february 2011 christchurch earthquake. *Seismological Research Letters*, **82**(6), 853. URL `http://dx.doi.org/10.1785/gssrl.82.6.853`.

36. **Brune, J.** (1970). Tectonic stress and the spectra of seismic shear waves from earthquakes. *J. Geophys. Res.*, **75**, 4997–5009.

37. **Campbell, K. W.** (2003). Prediction of strong ground motion using the hybrid empirical method and its use in the development of ground-motion (attenuation) relations in eastern north america. *B. Seismol. Soc. Am.*, **93**(3), 1012–1033.

38. **Campbell, K. W.** and **Y. Bozorgnia** (2014). Nga-west2 ground motion model for the average horizontal components of pga, pgv, and 5% damped linear acceleration response spectra. *Earthquake Spectra*, **30**(3), 1087–1115.

39. **Carlton, B.**, **E. Skurtveit**, **B. Bohloli**, **K. Atakan**, **E. Dondzila**, and **A. M. Kaynia** (2018). Probabilistic seismic hazard analysis for offshore bangladesh including fault sources. *Geotechnical Earthquake Engineering and Soil Dynamics V: Seismic Hazard Analysis, Earthquake Ground Motions, and Regional-Scale Assessment*.

40. **Cauzzi, C.**, **E. Faccioli**, **M. Vanini**, and **A. Bianchini** (2015). Updated predictive equations for broadband (0.01–10 s) horizontal response spectra and peak ground motions, based on a global dataset of digital acceleration records. *Bulletin of Earthquake Engineering*, **13**(6), 1587–1612.

41. **CEA** (2005). Training material on seismic hazard analysis for engineering sites (gb17741-2005). *China Earthquake Administration*.

42. **Chadha, R.**, **D. Srinagesh**, **D. Srinivas**, **G. Suresh**, **A. Sateesh**, **S. Singh**, **X. Pérez-Campos**, **G. Suresh**, **K. Koketsu**, **T. Masuda**, *et al.* (2015). Cign, a strong-motion seismic network in central indo-gangetic plains, foothills of himalayas: First results. *Seismological Research Letters*, **87**(1), 37–46.

43. **Chandra, U.** (1977). Earthquakes of peninsular india—a seismotectonic study. *Bulletin of the seismological Society of America*, **67**(5), 1387–1413.

44. **Chandra, U.** (1992). Seismotectonics of himalaya. *Current Science*, **62**, 40–71.

45. **Chiou, B. S.-J.** and **R. R. Youngs** (2014). Update of the chiou and youngs nga model for the average horizontal component of peak ground motion and response spectra. *Earthquake Spectra*, **30**(3), 1117–1153.

46. **Chopra, S.**, **V. Kumar**, **A. Suthar**, and **P. Kumar** (2012). Modeling of strong ground motions for 1991 uttarkashi, 1999 chamoli earthquakes, and a hypothetical great earthquake in garhwal–kumaun himalaya. *Natural hazards*, **64**(2), 1141–1159.

47. **Cornell, C. A.** (1968). Engineering seismic risk analysis. *Bulletin of the seismological society of America*, **58**(5), 1583–1606.

48. **De Natale, G.**, **E. Faccioli**, and **A. Zollo** (1988). Scaling of peak ground motions from digital recordings of small earthquakes at campi flegrei, southern italy. *pure and applied geophysics*, **126**(1), 37–53.

49. **Derras, B.**, **P. Y. Bard**, and **F. Cotton** (2014). Towards fully data driven ground-motion prediction models for europe. *Bulletin of earthquake engineering*, **12**(1), 495–516.

50. **Derras, B.**, **P.-Y. Bard**, and **F. Cotton** (2016). Site-condition proxies, ground motion variability, and data-driven gmpes: Insights from the nga-west2 and resorce data sets. *Earthquake spectra*, **32**(4), 2027–2056.

51. **Desai, S. S.** and **D. Choudhury** (2014). Spatial variation of probabilistic seismic hazard for mumbai and surrounding region. *Natural hazards*, **71**(3), 1873–1898.

52. **Dhanya, J.**, **M. Gade**, and **S. Raghukanth** (2016). Ground motion estimation during 25th april 2015 nepal earthquake. *Acta Geodaetica et Geophysica*, **52**.

53. **Dhanya, J.** and **S. Raghukanth** (2018). Ground motion prediction model using artificial neural network. *Pure and Applied Geophysics*, **175**(3), 1035–1064.

54. **Dhanya, J.** and **S. T. G. Raghukanth** (2019). A non-gaussian random field model for earthquake slip. *Journal of Seismology*, 1–24.

55. **Douglas, J.** (2016). Ground motion prediction equations 1964–2016, report. *Accessible on http://www. gmpe. org. uk/gmpereport2014. pdf*.

56. **Douglas, J.** (2018). Ground motion prediction equations 1964–2018. *Review, University of Strathclyde, Glasgow*.

57. **Esteva, L.** (1963). Regionalizacion sismica de la Republica Mexicana. *Rev. Soc. Mex. do Ing. Sismica*, **1**(1), 31–35.

58. **Esteva, L.** and **E. Rosenblueth** (1964). Espectros de temblores a distancias moderadas y grandes. *Boletin Sociedad Mexicana de Ingenieria Sesmica*, **2**(1), 1–18.

59. **Fletcher, J. B.** and **K.-L. Wen** (2005). Strong ground motion in the taipei basin from the 1999 chi-chi, taiwan, earthquake. *Bulletin of the Seismological Society of America*, **95**(4), 1428–1446.

60. **Frankel, A.** (1995). Mapping seismic hazard in the central and eastern united states. *Seismological Research Letters*, **66**(4), 8–21.

61. **Gamage, P.** and **S. Venkatesan** (2019). Evaluation of seismic hazard in low to moderate seismic regions, sri lanka—a case study. *Journal of Seismology*, **23**(3), 579–611.

62. **Gangrade, B. K.**, **A. Prasad**, **M. Kumar**, **E. Unnikrishnan**, and **C. Nagaraja** (2012). Seismicity of peninsular india and earthquake catalogue based on gauribidanur seismic array data. Technical report, Bhabha Atomic Research Centre.

63. **Gansser, A.** (1974). Himalaya. *Geological Society, London, Special Publications*, **4**(1), 267–278.

64. **Gardner, J.** and **L. Knopoff** (1974). Is the sequence of earthquakes in Southern California, with aftershocks removed, Poissonian? *Bull. Seismol. Soc. Am.*, **64**, 1363–1367.

65. **Geological Survey of India (GSI)** (2000). Seismotectonic Atlas of India and its Environs.

66. **Goulet, C.**, **Y. Bozorgnia**, **N. Abrahamson**, **N. Kuehn**, **L. Al Atik**, **R. Youngs**, **R. Graves**, and **G. Atkinson** (2018). Central and eastern north america ground. motion characterization: Nga. east final report, pacific earthquake engineering research center, berkeley, ca. Technical report, PEER Report.

67. **GSI**, *Seismotectonic atlas of India and its environs*. Geological Survey of India, 2000.

68. **Guha, S.** and **P. Basu** (1993). Catalogue of earthquakes (=> m 3.0) in peninsular india. Technical report, Atomic Energy Regulatory Board.

69. **Güllü, H.** and **E. Erçelebi** (2007). A neural network approach for attenuation relationships: An application using strong ground motion data from turkey. *Engineering Geology*, **93**(3-4), 65–81.

70. **Günaydın, K.** and **A. Günaydın** (2008). Peak ground acceleration prediction by artificial neural networks for northwestern turkey. *Mathematical Problems in Engineering*, **2008**.

71. **Gupta, I.** (2018). Uniformly processed strong motion database for himalaya and northeast region of india. *Pure Appl. Geophys.*, **175**(3), 829–863.

72. **Gupta, I.** and **M. Trifunac** (2018a). Attenuation of strong earthquake ground motion–i: Dependence on geology along the wave path from the hindu kush subduction to western himalaya. *Soil Dynamics and Earthquake Engineering*, **114**, 127–146.

73. **Gupta, I.** and **M. Trifunac** (2018b). Attenuation of strong earthquake ground motion–ii: Dependence on geology along the wave paths from the burmese subduction zone to northeastern india. *Soil Dynamics and Earthquake Engineering*, **112**, 256–276.

74. **Herrmann, R. B.** and **M. J. Goertz** (1981). A numerical study of peak ground motion scaling. *Bulletin of the Seismological Society of America*, **71**(6), 1963–1979.

75. **Hole, J.** (1992). Nonlinear high-resolution three-dimensional seismic travel time tomography. *Journal of Geophysical Research: Solid Earth*, **97**(B5), 6553–6562.

76. **Hough, S. E.**, **S. Martin**, **R. Bilham**, and **G. M. Atkinson** (2002). The 26 january 2001 m 7.6 bhuj, india, earthquake: Observed and predicted ground motions. *Bulletin of the Seismological Society of America*, **92**(6), 2061–2079.

77. **Hough, S. E.** and **B. Roger** (2008). Site response of the ganges basin inferred from re-evaluated macroseismic observations from the 1897 shillong, 1905 kangra, and 1934 nepal earthquakes. *Journal of Earth System Science*, **117**(2), 773–782.

78. **IBC** (2009). International building code. *International Code Council, Inc.(formerly BOCA, ICBO and SBCCI)*, **4051**, 60478–5795.

79. **IBC, I.** (2015). International building code. *International Code Council, Inc.(formerly BOCA, ICBO and SBCCI)*.

80. **Irikura, K.** and **K. Kamae** (1994). Estimation of strong ground motion in broad-frequency band based on a seismic source scaling model and an empirical green's function technique. URL `http://hdl.handle.net/2122/1859`.

81. **IS:1893-1** (2016). Criteria for Earthquake Resistant Design of Structures, Part 1: General Provisions and Buildings.

82. **Iyengar, R.** and **S. Ghosh** (2004*a*). Microzonation of earthquake hazard in greater delhi area. *Current Science*, **87**(9), 1193–1202.

83. **Iyengar, R.** and **S. T. G. Raghukanth** (2004). Attenuation of strong ground motion in peninsular india. *Seismol. Res. Lett.*, **75**(4), 530–540.

84. **Iyengar, R.**, **D. Sharma**, and **J. Siddiqui** (1999). Earthquake history of india in medieval times. *Indian Journal of history of science*, **34**, 181–238.

85. **Iyengar, R. N.** and **S. Ghosh** (2004*b*). Microzonation of earthquake hazard in Greater Delhi area. *Curr. Sci.*, **87**(9), 1193–1202.

86. **Jaiswal, K.** and **R. Sinha** (2007). Probabilistic seismic-hazard estimation for peninsular india. *Bulletin of the Seismological Society of America*, **97**(1B), 318–330.

87. **Jayalakshmi, S.**, **J. Dhanya**, **S. T. G. Raghukanth**, and **P. M. Mai** (2020). 3d seismic wave amplification in the indo-gangetic basin from spectral element simulations. *Soil Dynamics and Earthquake Engineering*, **129**, 105923.

88. **Jayalakshmi, S.** and **S. Raghukanth** (2016). Regional ground motion simulation around delhi due to future large earthquake. *Natural Hazards*, **82**(3), 1479–1513.

89. **Kaila, K.**, **V. Gaur**, and **H. Narain** (1972). Quantitative seismicity maps of india. *Bulletin of the Seismological Society of America*, **62**(5), 1119–1132.

90. **Kale, Ö.** (2019). Some discussions on data-driven testing of ground-motion prediction equations under the turkish ground-motion database. *Journal of Earthquake Engineering*, **23**(1), 160–181.

91. **Kale, Ö.** and **S. Akkar** (2013). A new procedure for selecting and ranking ground-motion prediction equations (gmpes): The euclidean distance-based ranking (edr) method. *Bulletin of the Seismological Society of America*, **103**(2A), 1069–1084.

92. **Kanno, T.**, **A. Narita**, **N. Morikawa**, **H. Fujiwara**, and **Y. Fukushima** (2006). A new attenuation relation for strong ground motion in japan based on recorded data. *Bulletin of the Seismological Society of America*, **96**(3), 879–897.

93. **Khattri, K.**, **A. Rogers**, **D. Perkins**, and **S. Algermissen** (1984*a*). A seismic hazard map of India and adjacent areas. *Tectonophysics*, **108**(1-2), 93–134.

94. **Khattri, K.**, **A. Rogers**, **D. Perkins**, and **S. Algermissen** (1984*b*). A seismic hazard map of india and adjacent areas. *Tectonophysics*, **108**(1-2), 93–134.

95. **Kijko, A.** (2004). Estimation of the maximum earthquake magnitude, mmax. *Pure Appl. Geophys.*, **161**, 1655–1681.

96. **Kijko, A.** and **G. Graham** (1998). Parametric-historic procedure for probabilistic seismic hazard analysis: Part I - estimation of maximum regional magnitude mmax,. *Pure Appl. Geophys.*, **152**, 413–442.

97. **Kiureghian, A. D.** and **A. H. Ang** (1977). A fault-rupture model for seismic risk analysis. *Bulletin of the Seismological Society of America*, **67**(4), 1173–1194.

98. **Knopoff, L.** (1964). The statistics of earthquakes in southern california. *Bulletin of the Seismological Society of America*, **54**(6A), 1871–1873.

99. **Knopoff, L.** and **Y. Kagan** (1977). Analysis of the theory of extremes as applied to earthquake problems. *J. Geophys. Res.*, **82**, 5647–5657.

100. **Kolathayar, S.**, **T. G. Sitharam**, and **K. S. Vipin** (2012). Deterministic seismic hazard macrozonation of India. *J. Earth Syst. Sci.*, **121**(5), 1351–1364.

101. **Komatitsch, D.**, **Q. Liu**, **J. Tromp**, **P. Suss**, **C. Stidham**, and **J. H. Shaw** (2004). Simulations of ground motion in the los angeles basin based upon the spectral-element method. *Bulletin of the Seismological Society of America*, **94**(1), 187–206.

102. **Komatitsch, D.** and **J. Tromp** (1999). Introduction to the spectral element method for three-dimensional seismic wave propagation. *Geophysical journal international*, **139**(3), 806–822.

103. **Kramer, S. L.** (1996). Geotechnical earthquake engineering. in prentice–hall international series in civil engineering and engineering mechanics. *Prentice-Hall, New Jersey*.

104. **Kumar, N.**, **I. A. Parvez**, and **H. Virk** (2005). Estimation of coda wave attenuation for nw himalayan region using local earthquakes. *Physics of the earth and planetary interiors*, **151**(3-4), 243–258.

105. **Kumar, S.**, **S. G. Wesnousky**, **T. K. Rockwell**, **D. Ragona**, **V. C. Thakur**, and **G. G. Seitz** (2001). Earthquake recurrence and rupture dynamics of himalayan frontal thrust, india. *Science*, **294**(5550), 2328–2331.

106. **Lapajne, J.**, **B. S. Motnikar**, and **P. Zupancic** (2003). Probabilistic seismic hazard assessment methodology for distributed seismicity. *Bulletin of the Seismological Society of America*, **93**(6), 2502–2515.

107. **Lavé, J.**, **D. Yule**, **S. Sapkota**, **K. Basant**, **C. Madden**, **M. Attal**, and **R. Pandey** (2005). Evidence for a great medieval earthquake (˜ 1100 ad) in the central himalayas, nepal. *Science*, **307**(5713), 1302–1305.

108. **Mai, P. M.** and **G. Beroza** (2003). A hybrid method for calculating near-source, broadband seismograms: application to strong motion prediction. *Physics of the Earth and Planetary Interiors*, **137**(1), 183 – 199. ISSN 0031-9201. URL `http://www.sciencedirect.com/science/article/pii/S0031920103000141`. The quantitative prediction of strong-motion and the physics of earthquake sources.

109. **Mai, P. M.**, **P. Spudich**, and **J. Boatwright** (2005). Hypocenter locations in finite-source rupture models. *Bulletin of the Seismological Society of America*, **95**(3), 965. URL `http://dx.doi.org/10.1785/0120040111`.

110. **Maiti, S. K.**, **S. K. Nath**, **M. D. Adhikari**, **N. Srivastava**, **P. Sengupta**, and **A. K. Gupta** (2016). Probabilistic Seismic Hazard Model of West Bengal, India. *J. Earthq. Eng.*, **preprint**, 1–45.

111. **McGuire, R. K.** (1974). Seismic structural response risk analysis, incorporating peak response regressions on earthquake magnitude and distance. *Report R74-51, Structures Publication*, (399).

112. **Milne, J.** (1911). A catalogue of destructive earthquakes: A.D. 7 to A.D. 1899. *Br. Assoc. Adv. Sci. London*, 92.

113. **Motazedian, D.** and **G. M. Atkinson** (2005). Stochastic finite-fault modeling based on a dynamic corner frequency. *Bull. Seismol. Soc. Am.*, **95**(3), 995–1010.

114. **Nath, S.** and **K. Thingbaijam** (2012). Probabilistic seismic hazard assessment of india. *Seismological Research Letters*, **83**(1), 135–149.

115. **NDMA** (2010). Development of probabilistic seismic hazard map of india. *The National Disater Management Authority*, 86.

116. **NHUD**, *National urban housing and habitat policy*. Government of India Ministry of Housing & Urban Poverty Alleviation, New Delhi, 2007.

117. **Oldham, T.** (1883*a*). A catalogue of Indian earthquakes from the earliest times to the end of 1869 A.D. *Mem. Geol. Surv. Indai*, **XIX**(3), 163–242.

118. **Oldham, T.** (1883*b*). A catalogue of indian earthquakes from the earliest times to the end of 1869 ad mem geol surv india. *XIX, Part*, **3**.

119. **Ornthammarath, T.**, **P. Warnitchai**, **K. Worakanchana**, **S. Zaman**, **R. Sigbjörnsson**, and **C. G. Lai** (2011). Probabilistic seismic hazard assessment for thailand. *Bulletin of Earthquake Engineering*, **9**(2), 367–394.

120. **Pallav, K.**, **S. T. G. Raghukanth**, and **K. D. Singh** (2012). Probabilistic seismic hazard estimation of Manipur, India. *J. Geophys. Eng.*, **9**(5), 516–533.

121. **Paolucci, R.** (1999). Shear resonance frequencies of alluvial valleys by rayleigh's method. *Earthquake Spectra*, **15**(3), 503–521. URL `https://doi.org/10.1193/1.1586055`.

122. **Parvez, I. A.**, **F. Vaccari**, and **G. F. Panza** (2003). A deterministic seismic hazard map of India and adjacent areas. *Geophys. J. Int.*, **155**(2), 489–508.

123. **Petersen, M. D.**, **M. P. Moschetti**, **P. M. Powers**, **C. S. Mueller**, **K. M. Haller**, **A. D. Frankel**, **Y. Zeng**, **S. Rezaeian**, **S. C. Harmsen**, **O. S. Boyd**, *et al.* (2015). The 2014 united states national seismic hazard model. *Earthquake Spectra*, **31**(S1), S1–S30.

124. **Pezeshk, S.**, **A. Zandieh**, and **B. Tavakoli** (2011). Hybrid empirical ground-motion prediction equations for eastern north america using nga models and updated seismological parameters. *B. Seismol. Soc. Am.*, **101**(4), 1859–1870.

125. **Quittmeyer, R.** and **K. Jacob** (1979). Historical and modern seismicity of Pakistan, Afghanistan, north-western India and south-eastern Iran. *Bull. Seismol. Soc. Am.*, **69**, 773–823.

126. **Raghukanth, S.** (2010). Estimation of seismicity parameters for india. *Seismological Research Letters*, **81**(2), 207–217.

127. **Raghukanth, S.** (2011). Seismicity parameters for important urban agglomerations in india. *Bulletin of Earthquake Engineering*, **9**(5), 1361–1386.

128. **Raghukanth, S.** and **R. Iyengar** (2007). Estimation of seismic spectral acceleration in peninsular india. *Journal of Earth System Science*, **116**(3), 199–214.

129. **Raghukanth, S.**, **C. Murthy**, **P. Muthuganeisan**, and **J. Dhanya** (2017). Development of earthquake displacement and velocity hazard maps of india, (cie1213195dstxstgr).

130. **Raghukanth, S. T. G.** and **R. N. Iyengar** (2006). Seismic hazard estimation for mumbai city. *Current Science*, **91**(11), 1486–1494.

131. **Raghukanth, S. T. G.** and **B. Kavitha** (2014). Ground motion relations for active regions in india. *Pure Appl. Geophys.*, **171**(9), 2241–2275.

132. **Rahman, M. M.** and **L. Bai** (2018). Probabilistic seismic hazard assessment of nepal using multiple seismic source models. *Earth and Planetary Physics*, **2**(4), 327–341.

133. **Rajendran, C.**, **K. Rajendran**, **B. Duarah**, **S. Baruah**, and **A. Earnest** (2004). Interpreting the style of faulting and paleoseismicity associated with the 1897 shillong, northeast india, earthquake: Implications for regional tectonism. *Tectonics*, **23**(4).

134. **Ram, T. D.** and **G. Wang** (2013). Probabilistic seismic hazard analysis in nepal. *Earthquake Engineering and Engineering Vibration*, **12**(4), 577–586.

135. **Rao, B.** (2005). Monograph on history of indian earthquakes from earliest to 2005.

136. **Rao, B. R.**, *Seismic Activity Of Indian Scenario*. Buddha Publishers, 2015.

137. **Rao, B. R.** and **P. S. Rao** (1984). Historical seismicity of peninsular india. *Bulletin of the Seismological Society of America*, **74**(6), 2519–2533.

138. **Reasenberg, P.** (1985). Second-order moment of central california seismicity, 1969–1982. *Journal of Geophysical Research: Solid Earth*, **90**(B7), 5479–5495.

139. **Rout, M. M.**, **J. Das**, **Kamal**, and **R. Das** (2015). Probabilistic seismic hazard assessment of NW and central Himalayas and the adjoining regions. *J. Earth Syst. Sci.*, **124**(3), 577–586.

140. **Sangeetha, S.**, **J. Dhanya**, and **S. Raghukanth** (2018). 3d crustal velocity model for ground motion simulations in north-east india. *Journal of Earthquake Engineering*, 1–37.

141. **Saragoni, G.** and **G. Hart** (1974). Simulation of artificial earthquakes. *Eq. Engg. Str. Dyn.*, **2**, 249–267.

142. **Scherbaum, F.**, **F. Cotton**, and **P. Smit** (2004). On the use of response spectral-reference data for the selection and ranking of ground-motion models for seismic-hazard analysis in regions of moderate seismicity: The case of rock motion. *Bulletin of the seismological society of America*, **94**(6), 2164–2185.

143. **Scherbaum, F.**, **E. Delavaud**, and **C. Riggelsen** (2009). Model selection in seismic hazard analysis: An information-theoretic perspective. *Bulletin of the Seismological Society of America*, **99**(6), 3234–3247.

144. **Schnabel, P. B.** and **H. Bolton Seed** (1973). Accelerations in rock for earthquakes in the western united states. *Bulletin of the Seismological Society of America*, **63**(2), 501–516.

145. **Scordilis, E. M.** (2006). Empirical global relations converting M_S and m_b to moment magnitude. *J. Seismol.*, **10**(2), 225–236.

146. **Seeber, L.**, **J. Armbruster**, and **K. Jacob** (1999). Probabilistic assessment of earthquake hazard for the state of maharashtra. *Report to Government of Maharashtra Earthquake Rehabilitation Cell, Mumbai*.

147. **Shanker, D.** and **M. Sharma** (1998). Estimation of seismic hazard parameters for the himalayas and its vicinity from complete data files. *Pure and applied geophysics*, **152**(2), 267–279.

148. **Sharma, M. L.**, **J. Douglas**, **H. Bungum**, and **J. Kotadia** (2009). Ground-motion prediction equations based on data from the himalayan and zagros regions. *J. Earthq. Eng.*, **13**(8), 1191–1210.

149. **Sil, A.** and **T. G. Sitharam** (2015). Site specific design response spectrum proposed for the capital city of Agartala , Tripura. *Geomatics , Nat. Hazards Risk*.

150. **Singh, S.**, **D. Srinagesh**, **D. Srinivas**, **D. Arroyo**, **X. Pérez-Campos**, **R. Chadha**, **G. Suresh**, and **G. Suresh** (2017). Strong ground motion in the indo-gangetic plains during the 2015 gorkha, nepal, earthquake sequence and its prediction during future earthquakes. *Bulletin of the Seismological Society of America*, **107**(3), 1293–1306.

151. **Sitharam, T.** and **S. Kolathayar** (2012). Probabilistic evaluation of seismic hazard in india: Comparison of different methodologies. *15th World Conference in Earthquake Engineering*.

152. **Somerville, P.**, **K. Irikura**, **R. Graves**, **S. Sawada**, **D. Wald**, **N. Abrahamson**, **Y. Iwasaki**, **T. Kagawa**, **N. Smith**, and **A. Kowada** (1999). Characterizing crustal earthquake slip models for the prediction of strong ground motion. *Seismological Research Letters*, **70**(1), 59–80.

153. **Somsa-Ard, N.** and **S. Pailoplee** (2013). Seismic hazard analysis for myanmar. *Journal of Earthquake and Tsunami*, **7**(04), 1350029.

154. **Srinagesh, D.**, **S. Singh**, **R. Chadha**, **A. Paul**, **G. Suresh**, **M. Ordaz**, and **R. Dattatrayam** (2011). Amplification of seismic waves in the central indo-gangetic basin, india. *Bulletin of the Seismological Society of America*, **101**(5), 2231–2242.

155. **Srinivas, D.**, **D. Srinagesh**, **R. Chadha**, and **M. Ravi Kumar** (2013). Sedimentary thickness variations in the indo-gangetic foredeep from inversion of receiver functions. *Bulletin of the Seismological Society of America*, **103**(4), 2257–2265.

156. **Stepp, J.** (1972). Analysis of Completeness of the Earthquake Sample in the Puget sound area and its effect on statistical estimates of earthquake hazard. *Int. Conf. Microzonat.*, **II**, 897–909.

157. **Stewart, J. P.**, **G. A. Parker**, **G. M. Atkinson**, **D. M. Boore**, **Y. M. Hashash**, and **W. J. Silva** (2019). Ergodic site amplification model for central and eastern north america. *Earthquake Spectra*, 8755293019878185.

158. **Styron, R.**, **M. Taylor**, and **K. Okoronkwo** (2010). Database of active structures from the indo-asian collision. *Eos, Transactions American Geophysical Union*, **91**(20), 181–182.

159. **Sukhija, B.**, **B. Lakshmi**, **M. Rao**, **D. Reddy**, **P. Nagabhushanam**, **S. Hussain**, and **H. Gupta** (2006). Widespread geologic evidence of a large paleoseismic event near the meizoseismal area of the 1993 latur earthquake, deccan shield, india.

160. **Tavakoli, B.** and **S. Pezeshk** (2005). Empirical-stochastic ground-motion prediction for eastern north america. *B. Seismol. Soc. Am.*, **95**(6), 2283–2296.

161. **Tezcan, J.** and **Q. Cheng** (2012). Support vector regression for estimating earthquake response spectra. *Bulletin of Earthquake Engineering*, **10**(4), 1205–1219.

162. **Thingbaijam, K. K. S.**, **P. M. Mai**, and **K. Goda** (2017). New empirical earthquake source-scaling laws. *Bulletin of the Seismological Society of America*. ISSN 0037-1106. URL `http://hdl.handle.net/10754/626418`.

163. **Thomas, S.**, **G. Pillai**, **K. Pal**, and **P. Jagtap** (2016). Prediction of ground motion parameters using randomized anfis (ranfis). *Applied Soft Computing*, **40**, 624–634.

164. **Tinti, S.** and **F. Mulargia**, Completeness analysis of a seismic catalog. *In Annales geophysicae (1983)*, volume 3. 1985.

165. **Tromans, I.** (2004). *Behaviour of buried water supply pipelines in earthquake zones*. Ph.D. thesis, University of London.

166. **Uhrhammer, R.** (1986). Characteristics of northern and southern Californai seismicity. *Earthq. Notes*, **57**, 21.

167. **Valdiya, K.** (1976). Himalayan transverse faults and folds and their parallelism with subsurface structures of north indian plains. *Tectonophysics*, **32**(3-4), 353–386.

168. **Van Stiphout, T.**, **J. Zhuang**, and **D. Marsan** (2012). Seismicity declustering, community online resource for statistical seismicity analysis, doi: 10.5078/corssa-52382934.

169. **Waseem, M.**, **C. G. Lai**, and **E. Spacone** (2018). Seismic hazard assessment of northern pakistan. *Natural Hazards*, **90**(2), 563–600.

170. **Waseem, M.**, **A. Lateef**, **I. Ahmad**, **S. Khan**, and **W. Ahmed** (2019). Seismic hazard assessment of afghanistan. *Journal of Seismology*, **23**(2), 217–242.

171. **Weichert, D. H.** (1980). Estimation of the earthquake recurrence parameters for unequal observation periods for different magnitudes. *Bulletin of the Seismological Society of America*, **70**(4), 1337–1346. ISSN 0037-1106.

172. **Wells, D. L.** and **K. J. Coppersmith** (1994*a*). New Empirical Relationships among Magnitude, Rupture Length, Rupture Width, Rupture Area, and Surface Displacement. *Bull. Seismol. Soc. Am.*, **84**(4), 974–1002.

173. **Wells, D. L.** and **K. J. Coppersmith** (1994*b*). New empirical relationships among magnitude, rupture length, rupture width, rupture area, and surface displacement. *Bulletin of the seismological Society of America*, **84**(4), 974–1002.

174. **Xu, W.-J.** (2019). Probabilistic seismic hazard assessment using spatially smoothed seismicity in north china seismic zone. *Journal of Seismology*, **23**(3), 613–622.

175. **Yenier, E.**, **O. Erdoğan**, and **S. Akkar**, Empirical relationships for magnitude and source-to-site distance conversions using recently compiled turkish strong-ground motion database. *In The 14th world conference on earthquake engineering*. 2008.

176. **Youngs, R.**, **S.-J. Chiou**, **W. Silva**, and **J. Humphrey** (1997). Strong ground motion attenuation relationships for subduction zone earthquakes. *Seismological Research Letters*, **68**(1), 58–73.

177. **Zeng, Y.** (1993). Theory of scattered p-and s-wave energy in a random isotropic scattering medium. *Bulletin of the Seismological Society of America*, **83**(4), 1264–1276.

178. **Zeng, Y.**, **F. Su**, and **K. Aki** (1991). Scattering wave energy propagation in a random isotropic scattering medium: 1. theory. *Journal of Geophysical Research: Solid Earth*, **96**(B1), 607–619.

179. **Zhao, J. X.**, **F. Jiang**, **P. Shi**, **H. Xing**, **H. Huang**, **R. Hou**, **Y. Zhang**, **P. Yu**, **X. Lan**, **D. A. Rhoades**, *et al.* (2016). Ground-motion prediction equations for subduction slab earthquakes in japan using site class and simple geometric attenuation functions. *Bulletin of the Seismological Society of America*, **106**(4), 1535–1551.

180. **Zhao, J. X.**, **J. Zhang**, **A. Asano**, **Y. Ohno**, **T. Oouchi**, **T. Takahashi**, **H. Ogawa**, **K. Irikura**, **H. K. Thio**, **P. G. Somerville**, *et al.* (2006). Attenuation relations of strong ground motion in japan using site classification based on predominant period. *Bulletin of the Seismological Society of America*, **96**(3), 898–913.

181. **Zuccolo, E.**, **M. Corigliano**, and **C. G. Lai** (2013). Probabilistic seismic hazard assessment of italy using kernel estimation methods. *Journal of seismology*, **17**(3), 1001–1020.

LIST OF PAPERS BASED ON THIS REPORT

Papers in Refereed Journals

1. Dhanya, J., and Raghukanth, S. T. G., (2020). Neural Network based hybrid Ground Motion Prediction Equations for Western Himalayas and North-Eastern India, *Acta Geophysica* DOI:10.1007/s11600-019-00395-y.

2. Dhanya, J., Sreejaya K. P., and Raghukanth, S. T. G.,(2022) Seismicity Parameters for India and Adjoined Regions, *Journal of Seismology* (Accepted).

3. Sreejaya K P., S T G Raghukanth., ID Gupta., C V R Murty., and D Srinagesh.,(2022) Seismic Hazard Map of India and Neighbouring Regions, *Soil dynamics and earthquake engineering* (Under review).